REGULATION OF TGF-β SIGNALING BY NUCLEAR RECEPTOR CO-REPRESSOR (N-CoR) IN GASTRIC CANCER CELLS

NORLIZAN BINTE ABDOL MALEK

(B. Sc. (Hons.), NUS)

A THESIS SUBMITTED

FOR THE DEGREE OF DOCTOR OF PHILOSOPHY

DEPARTMENT OF PHYSIOLOGY

YONG LOO LIN SCHOOL OF MEDICINE

NATIONAL UNIVERSITY OF SINGAPORE

2013

DECLARATION

I hereby declare that this thesis is my original work and it has been written by me in its entirety. I have duly acknowledged all the sources of information which have been used in the thesis.

This thesis has also not been submitted for any degree in any university previously.

Norlizan Binte Abdol Malek

13 August 2013

ACKNOWLEDGEMENTS

My PhD candidature has been a fulfilling but challenging experience for me, and there are a number of people without whom this thesis might not have been written. To my supervisor, Dr Matiullah Khan, I would like to express my deepest gratitude for his guidance and encouragement throughout all this time. I could not have wished for a more patient and kind mentor. His unwavering optimism and enthusiasm for research has greatly inspired me in my own work. Had he not kindly given me this opportunity, I might have never pursued this line of study.

Special thanks to both my co-supervisors: A/Prof. Prakash Hande, who contributed constructive advice and valuable input during my PhD qualifying exam, and for kindly taking me in as a student in this last year of my candidature. My deepest gratitude also goes to A/Prof. Chng Wee Joo, for his kindness in providing me with the research facilities and materials needed for the completion of my research. My sincere gratitude also goes towards my thesis advisory committee advisor, A/Prof. Go Mei Lin, for her kindness and understanding in my time of need. I would also like to thank our collaborator, Prof. Richard Haynes, for his generous contribution of the artemisinin derivatives used in this project.

I have been blessed with so many wonderful lab mates, past and present, some of whom have become dear friends to me. Working with such brilliant scientists had widened the scope of my knowledge and added value to my work. Many thanks to Su Yin, Dawn, Angie, Leo, Pei Li, Seow Ching, Jess, Angela, Fen Yee, Li Feng, John, Adawiyah, Azhar, Bee Keow, Li Ren and

Meg for their delightful companionship, stimulating conversations, and all the fun times in the lab. I am especially grateful towards Dr. Azhar, whose constant encouragement and advice kept me going all this time. His passion and flair for research never fails to inspire me. Also to Li Ren, who has always found time to encourage me and help me in my times of need.

I would also have never done it without the friendship and support of my two best friends, Kay and Santhi, who have always been there for me, through thick and thin. A very big thank you also goes out to Isa and his lovely family, whose tremendous help and support have been instrumental in the final leg of my PhD journey. To my family members, I owe them more thanks that I can ever put into words. I am extremely grateful for their relentless care and support in my academic pursuit all these years.

Last but not least, many thanks to NUS, for awarding me the NUS Research Scholarship, for which all of this have been made possible.

Thank you.

Norlizan A. Malek

August 2013

TABLE OF CONTENTS

SUMMARY

Transforming growth factor-beta (TGF-β) signaling plays an important role in cell-fate determination by dynamically regulating the transcription of genes involved in cell proliferation, differentiation and apoptosis. Many of these processes are regulated by precise transcriptional control imparted by factors like nuclear hormone receptor co-repressor (N-CoR). Acquired resistance to TGF-β-induced apoptosis is an important feature of many human malignancies including gastric cancer. The molecular mechanism underlying TGF-β-resistance in gastric cancer cells is presently not known. Preliminary findings from our laboratory suggested that the recently identified N-CoR misfolding pathway might be linked to TGF-β-resistance in gastric cancer. Therefore, identification and characterization of agents that can sensitize gastric cancer cells to TGF-β-induced apoptosis could lead to better therapeutic management in gastric cancer. One such promising compound is artemisinin, which blocked the growth of colorectal cells through inhibiting the hyperactive Wnt/β-catenin pathway. Since TGF-β is known to antagonize the growth promoting signal of Wnt pathway, it was hypothesized that growth suppressive effect of artemisinin might also involve the activation of TGF-β signaling. Based on this hypothesis, screening of a selected group of synthetic artemisinin analogues was carried out on various gastric cancer derived cell lines and it was found that an artemisinin derivative designated as GC011 selectively inhibited the growth and promoted apoptosis of TGF-β sensitive gastric cancer cells.

The pro-apoptotic effect of GC011 was apparently mediated through the activation of Smad3 and up-regulation of proapoptotic TGF-β target genes

PAI-1 and p21. GC011 also imparted a TGF-β-like effect on IgCα promoter that contains a consensus TGF-β-responsive element. Moreover, it promoted a selective dose- and time-dependent downregulation of N-CoR/HDAC1 in TGF-β sensitive cells, suggesting that the GC011-induced up-regulation of TGF-β target genes was caused by an abrogation of N-CoR transcriptional control. These findings identify GC011 as a possible inhibitor of N-CoR/HDAC1 function and highlight the therapeutic potential of GC011 as a TGF-β analogue in TGF-β sensitive gastric cancer cells.

However, majority of gastric cancer cells are not sensitive to TGF-β-induced growth inhibitory function. Consistent with this characteristic, almost all the TGF-β resistant gastric cancer cells displayed lack of sensitivity to GC011. This prompted a need to design and develop a novel therapeutic approach that could break the barrier of TGF-β resistance and sensitized the TGF-β resistant gastric cancer cells to apoptosis by targeting the N-CoR misfolding pathway. Our laboratory has previously demonstrated how a misfolded conformation dependent loss (MCDL) of N-CoR protein contributed to the pathogenesis of APL, AML-M5 and NSCLC cells, suggesting the involvement of generic N-CoR misfolding pathway in a diverse group of human tumors, including gastric cancer. As such, it was hypothesized that an APL-like loss of N-CoR due to misfolding might be prevalent in gastric cancer as well, since normal N-CoR is already recognized to play an important role in the normal development of gastric cells. Based on this hypothesis, N-CoR status was analyzed in various gastric cancer cells and patient-derived primary gastric cancer tissue. N-CoR consistently demonstrated post-transcriptional loss in primary and secondary gastric cancer cells. The N-CoR which was subjected

to loss in majority of gastric cancer cells displayed the characteristics of misfolded N-CoR as seen previously in APL, including aberrant cytosolic localization, detergent insolubility, and amplification of ER stress. Cellular response to the accumulation of misfolded proteins involves the activation of the unfolded protein response (UPR) pathway, whereby components of the ER folding machinery and ER-associated degradation (ERAD) are upregulated, which eventually refolds the misfolded proteins to their native conformation or degrades the misfolded proteins that cannot be refolded. Proteasome inhibition is thought to cause an accumulation of misfolded proteins which overwhelm the ERAD pathway resulting in ER stress-induced apoptosis. Therefore, it was postulated that blocking the loss of misfolded N-CoR with proteasome inhibitor would sensitize the gastric cancer cells to ER-stress induced apoptosis. Based on this hypothesis, the effects of bortezomib, a clinical grade protease inhibitor, was investigated in gastric cancer cells. Interestingly, bortezomib effectively sensitized the gastric cancer cells to ER stress-induced apoptosis by promoting the accumulation of misfolded N-CoR via inhibition of its proteosomal degradation by the ERAD pathway. These findings suggest that gastric cancer cells have a low threshold for proteosomal inihibitor-induced UPR activation and ER stress-induced apoptosis due to the loss of misfolded N-CoR protein, and also demonstrate the therapeutic potential of proteasome inhibitors such as bortezomib in the treatment of gastric cancer.

LIST OF TABLES

LIST OF FIGURES

LIST OF ABBREVIATIONS

AML	acute myeloid leukemia
APL	acute promyelotic leukemia
BSA	bovine serum albumin
cDNA	complementary deoxyribonucleic acid
CMA	chaperone-mediated autophagy
DAPI	4.6-diamidino-2-phenylindole
DHA	Dihydroartemisinin
DMSO	dimethyl sulfoxide
DNA	deoxyribonucleic acid
ER	endoplasmic reticulum
ERAD	ER-associated degradation
FDA	Food and Drug Administration
HDAC1	histone deacetylase 1
HMW	high molecular weight
IgG	Immunoglobulin G
kb	kilo base
kDa	kilo dalton
MCDL	Misfolded Conformation Dependent Loss
MM	multiple myeloma
mRNA	messenger RNA
mTOR	mammalian target of rapamycin
N-CoR	nuclear receptor corepressor
NR	nuclear receptor
NSCLC	non-small-cell lung cancer
PBS	phosphate buffered saline

PI	propidium iodide
PI3K	phosphatidyl-inositol 3 kinase
PML	Promyelocytic leukemia
PML-RAR	PML-retinoic acid receptor
RT-PCR	reverse transcription polymerase chain reaction
SDS	Sodium dodecyl sulphate
SDS-PAGE	SDS-polyacrylamide gel electrophoresis
siRNA	small interfering RNA
SMRT	Silencing mediator of retinoic and thyroid receptors
UPP	ubiquitin-proteosome pathway
UPR	unfolded protein response

CHAPTER 1

Introduction

1.1 Gastric Cancer

1.1.1 Epidemiology

Although the incidence of gastric cancer has decreased in the last few years, it remains a major health problem. Worldwide, almost one million patients are newly diagnosed with gastric cancer annually, making it the fourth most common malignancy (9% of all cancers). It is also the second leading cause of cancer-related mortality, with more than 700,000 patients succumbing to this disease every year (10% of all cancer deaths). On the whole, age-standardised incidence rates of gastric cancer are higher in men than in women, especially more so in middle-aged and elderly groups, with a male to female ratio ranging from 1.5 to 3.[1] Significant geographical variation in incidence also exists. More than two thirds of all cases occur in developing countries - over half of the cases occur in East Asia, with China and Japan accounting for roughly 41% and 11% of the cases.[2]

The two major classification systems used for gastric cancer are the World Health Organization (WHO)[2] and the Laurén classifications.[3] Histologically, adenocarcinoma of the stomach is the most common form of all gastric malignancies (90-95%). Gastric adenocarcinoma is generally located at two main tumor sites, namely proximal (cardia) and distal (noncardia). The Laurén classification further divides gastric adenocarcinomas into two categories: (1) undifferentiated or diffuse types, and (2) well-differentiated or intestinal types.[4] These two histological variants appear to have distinctive clinicopathological characteristics and are thought to develop via distinct molecular pathways. Diffuse type gastric cancers are more prevalent among

females and young patients than in males and elderly patients, may be multifocal, is not often accompanied by intestinal metaplasia, and can be hereditary. It is also more prevalent in low-risk areas. In contrast, intestinal type gastric cancers occur more frequently in males and elderly patients, predominate in the high-risk areas, and often develop following multifocal gastritis accompanied by intestinal metaplasia.[2] Other histologies are varied and rare, and these include lymphomas (MALToma, 1-5%), gastrointestinal stromal tumors (also known as leiomyosarcomas, 2%), carcinoids (1%), adenocanthomas (1%), and squamous cell carcinomas (1%).[4]

1.1.2 Etiology

Several factors have been shown to play a contributory role in the etiology of this disease. The considerable geographic variability in gastric cancer incidences has been attributed to regional dietary practice, where high salt and nitrates intake and low fresh fruits and vegetables consumption have been associated with increased risk of gastric cancer.[5-7] *Helicobacter pylori* infection has also emerged as an important contributing factor, especially in the development of intestinal-type adenocarcinoma. In such cases, a sequence of prolonged precancerous steps precedes carcinogenesis: chronic gastritis, multifocal atrophy, intestinal metaplasia, and intraepithelial neoplasia. *H. pylori* is reported to be the most frequent cause of chronic gastritis.[8] Effective primary preventive strategies such as improved sanitation, dietary and lifestyle changes have resulted in a downward trend of gastric cancer worldwide but incidence of proximal gastric cancer has been steadily increasing since the 1970s. Gastro-esophageal reflux and obesity have been shown to play more significant roles in proximal gastric cancer.[9]

However, while *H. pylori* infection is a well-established risk factor for gastric carcinogenesis, only a fraction of infected individuals develop gastric cancer. This variable phenotypic expression of infection can be attributed to the combined effects of environmental factors, host factors and bacterial virulence factors. Several host genetic factors are associated with increased gastric cancer risk in patients infected with *H. pylori*. Human genetic polymorphisms in inflammation-related genes, such as interferon-γ receptor 1 (*IFNGR1*), interleukin-1β (*IL-1β*), interleukin-1 receptor antagonist (*IL-RN*), toll-like receptor 4 (*TLR4*), and tumor-necrosis factor-α (*TNF-α*), modulate host inflammation response to infection, and thus progression of the disease.[10-13] The presence of bacterial virulence factors, including cytotoxin-associated gene (cagA) and vacuolating cytotoxin (vacA), is also associated with gastric cancer risk.[14]

While most gastric cancer presentations are sporadic, familial aggregation of the disease is observed in approximately 10% of the cases, suggesting that inherited conditions may also increase risk of gastric cancer. Hereditary diffuse gastric cancer (HDGC) is a rare, autosomal dominant inherited form of gastric cancer (1-3%), in which approximately 30% of the cases have been attributed to germline mutations in the E-cadherin gene (*CDH1*).[15] The estimated life-time gastric cancer risk in individuals carrying this mutation is as high as 67% in men and 83% in women[16]. Familial disorders such as Lynch syndrome (germline mutations in DNA mismatch repair genes)[17] and Peutz-Jeghers syndrome (germline mutation in *STK11* gene)[18] may also raise gastric cancer risk, although to a lesser extent. In the absence of germline mutations in such high penetrance genes, familial clustering of gastric cancer is thought

to be a result of the cumulative effect of dietary and environmental risk factors, and the genetic susceptibility of these individuals associated with low penetrance genes. These unknown genetic defects may include inactivation of tumor suppressor genes such as *RUNX3*[19] and *SMAD4,*[20] which have been implicated in gastric cancer.

1.1.3 Molecular pathology

Malignant transformation of gastric cells is a multi-step process which, in addition to the host genetic background and environmental exposures, involves various genetic and epigenetic alterations in numerous genes. This in turn, affects cellular functions that promote cancer cell survival, such as apoptosis evasion, sustained angiogenesis, self-sufficiency in growth signals, and insensitivity to antigrowth signals.

Majority of gastric carcinomas are characterized by two distinct genomic pathways, chromosomal instability (CIN) and microsatellite instability (MSI). Most of the sporadic gastric carcinomas demonstrate CIN, resulting in aberrations of chromosome copy number (gains/loss/amplification)[21,22] or structural chromosome anomalies (translocations/inversions),[23,24] which is probably the result of failures in either mitotic chromosome transmission or the spindle mitotic checkpoint.[25]

The remaining gastric carcinomas (10-25%) have defective DNA mismatch repair (MMR) systems, presenting with MSI phenotype characterized by widespread somatic mutations at coding and non-coding mononucleotide repeats.[26,27] The human MMR system consists of the proteins hMLH1, hMLH3, hMSH2, hMSH3, hMSH6, hPMS1 and hPMS2, and is responsible

for repairing DNA replication errors or physico-chemical induced damage. Hypermethylation of *hMLH1* gene promoter has been associated with silencing of hMLH1 protein and microsatellite instability in gastric cancer.[28] As microsatellite regions are particularly susceptible to mutation due to slippage of DNA polymerase during DNA replication, a defective MMR system may lead to frameshift mutations or protein truncations in genes that include or are linked to these microsatellite regions, such as transforming growth factor β receptor II (*TGFβRII)*, insulin-like growth factor II receptor (*IGF-IIR*), and *BAX*.[29,30]

1.1.4 Current treatment modalities

Presently, there is no standard treatment or worldwide consensus for treatment of gastric cancer. Different therapeutic strategies are employed in the Western and Eastern countries. In western countries, preoperative chemotherapy or adjuvant chemoradiotherapy is preferred, whereas Asia favours surgery followed by adjuvant chemotherapy. Opinions on lymphadenectomy also vary; where D2 lymph node dissection is routine and standardised in Asia, it is often not implemented in western countries.[31] Surgical resection is the only potentially curative treatment at present, where high survival rates have been reported in early-stage gastric cancer.[32] However, prognosis for gastric cancer remains poor as most gastric cancer patients are usually asymptomatic in the early stage and are usually undiagnosed until at an advanced stage.[33] In such cases, surgical resection as a single treatment modality for gastric cancer seems to have reached its optimum limit for control and survival of the disease.[34,35] Preoperative or postoperative strategies which include radiotherapy, chemotherapy or both, have been assessed and are currently

evaluated in several clinical studies, but median survival is still yet to exceed one year in phase III studies.[36,37]

Prevention and early detection of the disease are currently not achievable in gastric cancer. There are no reliable serum tumor markers recommended for use in the diagnosis of gastric cancer, due to the low sensitivity of such markers, especially at early stage gastric cancer.[38] At present, preventive surgery is only limited to individuals with a mutation in the *CDH1* gene which predisposes them to HDGC,[39] as no other genetic markers for gastric cancer has been determined. Large, population-based endoscopy screenings implemented in high risk incidence areas such as Japan has led to diagnosis at an early stage for approximately a third of its gastric cancer patients, but its implememtation may be impractical in low risk areas.

At present, many studies are currently underway to define the biology and molecular features of gastric cancer that will help customize treatment. Molecular targeting strategies currently investigated include apoptosis promoters, cell cycle inhibitors, antiangiogenic agents, and matrix metalloproteinases. The number of trials investigating these agents is at present limited, but some have shown promising results. While the use of gefitinib, an epidermal growth factor receptor (EGFR) inhibitor, has shown little clinical activity, promising results have been demonstrated with bevacizumab, an anti-VEGF monoclonal antibody, in a small multicenter phase II study for the treatment of metastatic disease.[40,41] The clinical response of another drug, imatinib, a highly selective inhibitor of the receptor tyrosine kinase family which targets the platelet-derived growth factor receptor (PDGFR), has been demonstrated in metastatic or unresectable gastrointestinal

stromal tumors (GIST)[42]. It is increasingly clear however, that the understanding of the underlying biology of gastric cancer may give rise to better molecular targets or elucidation of signalling pathways that can be modified or blocked by therapeutic intervention.

1.2 TGF-β signalling pathway

One of the molecular pathways that may be involved in gastric carcinogenesis is the TGF-β pathway. The TGF-β signaling pathway is considered by many to be a tumor suppressive pathway, owing to its functions in cell growth inhibition and apoptosis. Any alterations or aberration in this pathway results in the dysregulation of cellular growth in vivo, which may contribute to carcinogenesis. The transforming growth factor-β (TGF-β) family constitutes a variety of ubiquitous growth and differentiation factors, which control cell-fate determination by dynamically regulating the transcription of genes involved in cell proliferation, differentiation, migration and apoptosis. This family includes the TGF-βs, bone morphogenetic proteins (BMPs), Nodals, Activins, and Anti-Müllerian hormone. There are three isoforms of TGF-β termed TGF-β1, β2 and β3 in mammals, encoded by different genes but yet employ the same receptor signaling systems.[43] Of note, TGF-β1 is most frequently up-regulated in tumor cells and its role in cancer has been frequently studied.[44-47]

1.2.1 The canonical TGF-β/Smad signaling pathway

TGF-βs are synthesized as inactive, latent high-molecular-weight complexes which are released as mature, bioactive ligands upon proteolytic cleavage. The TGF-β superfamily signals are conveyed through a heteromeric cell-surface

complex of two types of transmembrane serine/threonine kinase receptors, type I and type II receptors. The type II and type I receptors form hetero-tetramers composed of two identical TβRII/TβRI receptor heterodimers. The bioactive dimeric form of the TGF-β cytokine binds to this hetero-tetramic complex, triggering the transphosphorylation of specific serine and threonine residues of TβRI by the TβRII kinase. This phosphorylation results in the activation of the TβRI kinase that mediates its autophosphorylation and phosphorylation of downstream target proteins. With the activation of type I receptor kinase, TGF-β initiates various intracellular signaling pathways, including the Erk and p38 mitogen-activated protein (MAP) kinase pathways. The most established signalling effector pathway triggered by activated TGF-β receptors however, is the Smad pathway. Smads belong to a conserved family of signal transducers, and consists of conserved N-terminal Mad-homology 1 (MH1), intermediate linker and C-terminal MH2 domains. The MH1 domain drives nuclear translocalization, and contains DNA-binding and protein–protein interacting sites. The linker domain contains multiple phosphorylation sites which allows regulatory phosphorylation by other signaling kinases (e.g. mitogen activated protein kinases (MAPKs) or cyclin-dependent kinases (CDKs)), and a PY motif, which mediates interaction with Smurf1 and Smurf2, E3 ubiquitin ligases that target Smads and Smad-associated TGF-β receptors for degradation by the 26S proteasome. The MH2 domain is a major protein–protein interaction domain, including phospho-serine-binding activity (Fig. 1.1). Activated TβRI specifically recognizes receptor-regulated Smads (R-Smads), Smad2 and Smad3, resulting in the phosphorylation of the C-terminus, which then relieves the inhibition on both N-terminal MH1 domain

and C-terminal MH2 domain, resulting in translocation of the Smads to the nucleus. En route to the nucleus, Smad2/3 recruits the Co-Smad, Smad4, to form heterotrimeric complexes. In the nucleus, activated Smad complex associates with DNA binding cofactors, and various coactivators or corepressors that will determine the transcriptional effect on a diverse array of target genes. Smad6 and Smad7, the inhibitory or I-Smads, can also interact with activated type I receptors and therefore function as competitive inhibitors of R-Smads activation by the receptors. Also, Smad6 interacts with activated R-Smads and inhibits their complex formation with Smad4. The E3 ubiquitin ligases, Smurf1 and Smurf2, support the inhibitory activities of I-Smads on TGF-β superfamily signalling by mediating the ubiquitination and subsequent degradation of R-Smads. Smurfs can also interact with I-Smads and induce their nuclear export, therefore enhancing the degradation of TGF-β receptors (Fig. 1.2)[43,48-52].

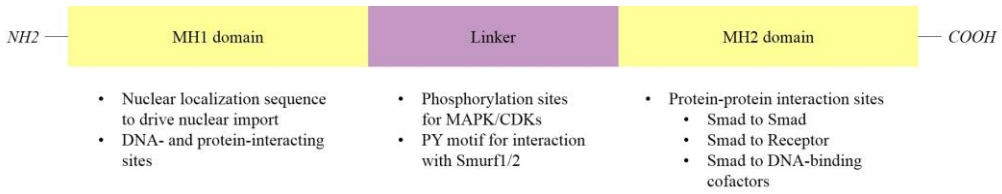

Figure 1.1. Domain structure of Smads. The general structure-function relationships of the different domains of Smads are depicted. The N-terminal and C-terminal domains (termed as MH1 and MH2 domains respectively), are conserved between receptor-regulated Smads and Co-Smads. The MH2 domain is also conserved in the inhibitory Smads, but not the MH1 domain.

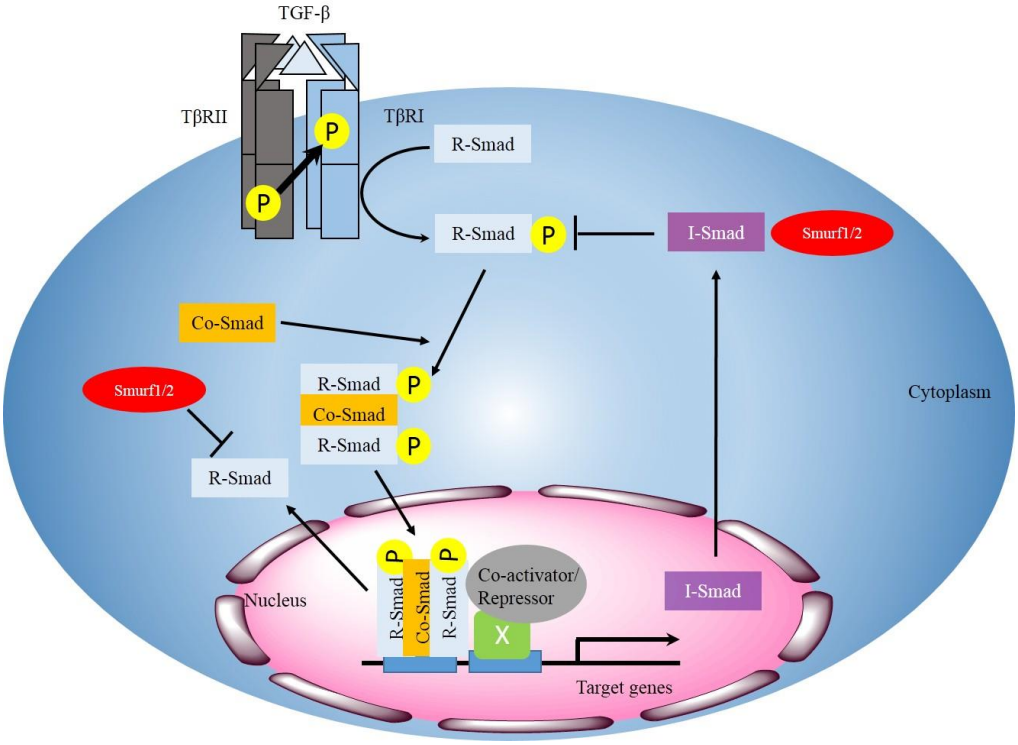

Figure 1.2. Schematic representation of the TGF-β signal transduction pathway. TGF-β binds to the TβRII/TβRI hetero-tetrameric receptor complex. TβRII trans-phosphorylates TβRI, which then phosphorylates R-Smads that forms heterotrimeric complexes with Co-Smad, Smad4, and translocates to the nucleus. In the nucleus, this heterotrimeric Smad complex regulates the transcription of target genes, by binding to DNA-binding co-factors (X), and co-activators or co-repressors. With TGF-β signaling, I-Smads and Smurfs are also exported from the nucleus to form complexes with Smads and receptors, leading to their degradation. I-Smads also inhibit phosphorylation of the receptor complex.

1.2.2 Role of TGF-β signalling pathway in gastric cancer

Dysregulation of the TGF-β signaling pathway has been documented in gastric cancer. TGF-β signaling pathway controls a diverse set of cellular processes, including cell proliferation, differentiation, migration, and apoptosis.[50] Accordingly, it plays a complex role in the development of cancer, and is involved in essentially all six cardinal hallmarks of cancer.[53] In general, TGF-β is known to be a tumor suppressor in the early stage of cancer due to its cytostatic and pro-apoptotic effects. On the other hand, TGF-β exerts a pro-tumorigenic role at advanced stages of cancer, by promoting tumor cell

invasion and metastasis through remodeling of tumor matrix, and induction of epithelial-to-mesenchymal transition (EMT), tumor angiogenesis, and immune suppression.[54-57]

Recent studies have demonstrated a strong role for the TGF-β signaling pathway in gastric carcinogenesis. Smad2 and Smad4 have been established as tumor suppressors in humans, and inactivation of Smad4 is frequently observed in human gastrointestinal tumors.[58,59] Haploid loss of Smad4 initiated gastric polyposis and cancer in mice, indicating that loss of heterozygosity (LOH) of the SMAD4 locus contributes to the development of gastric cancer.[20,60] This LOH of the human SMAD4 gene, located on chromosome 18q21.1, is frequently demonstrated in not only gastric adenocarcinomas, but also in other tumors, including pancreatic and colon carcinomas.[61] Smad proteins interact with various transcriptional factors downstream of the TGF-β signaling pathway, such as Runx, which has shown to play a significant role in gastric cancer. Runx3-null mice exhibit gastric hyperplasia, and approximately half of human cancers lack Runx expression due to hemizygous deletion and DNA methylation of the Runx promoter.[19,62] The role of RUNX3 in gastric carcinogenesis will be discussed further in Section 1.3. Structural alterations of the TβRII gene have also been identified in gastric cancer cells,[63] as well as CpG hypermethylation of its promoter.[64]

1.3 RUNX3

Recently, runt-related (RUNX) genes have also been implicated in gastric cancer.[62] There are three mammalian *runt*-related genes; *RUNX1*, *RUNX2*, and *RUNX3*, all of which are involved in major developmental pathways, and in

cell proliferation and differentiation.[65-67] Data from various studies suggest that RUNX3 is a gastric cancer tumor suppressor,[19,62,68] but it still remains to be elucidated how Runx3 exerts its tumor suppressor function.

These runt domain transcription factors are also targets of transforming growth factor-β (TGF-β) superfamily signaling, and the RUNX proteins form complexes with SMAD2 and SMAD3 that transmit TGF-β signals.[69] As discussed in Section 1.2.2, various components of the TGF-β pathway have been observed to be defective in many human tumors, [55,70] and the pathway is considered to be a tumor suppressive pathway in the early stages of tumorigenesis, in its dual roles as an inhibitor of cell proliferation and promoter of apoptosis.[57]

1.3.1 RUNX3 in Gastric Cancer

The function of RUNX3 as a tumor suppressor was initially reported in gastric cancer cells and molecular studies of its function in carcinogenesis had its roots in gastric cancer. In April 2002, Li and coworkers reported Runx3 as a candidate tumor suppressor in gastric carcinogenesis. Genetic ablation of *Runx3* displayed profound effects. *Runx3*$^{-/-}$ mice died soon after birth and the gastric epithelia displayed hyperplasia, reduced apoptosis and reduced sensitivity to TGF-β-mediated growth inhibition. There was also significant correlation between loss of Runx3 and gastric cancer progression stage, from 40% of *Runx3* silencing at early cancer stages to almost 90% as the cancer stage progressed. Li et al. only identified one mutation within the conserved Runt domain among 116 tumor samples analyzed, but they found that *Runx3* was silenced frequently by hypermethylation of CpG islands in the exon 1

region. When they injected gastric cancer cells that overexpressed wild type or Runt domain mutated Runx3 into nude mice, they observed that while wild type Runx3 mediated a significant reduction in tumorigenicity, the Runt domain mutant exacerbated tumor formation. Additionally, cell lines isolated from *p53* knockout mice were only tumorigenic in nude mice when *Runx3* was also deleted.[62]

Taken together, the above findings strongly suggest that RUNX3 is a tumor suppressor whose inactivation is strongly involved in gastric carcinogenesis. While the mechanisms underlying the tumor suppressive activity of RUNX3 is still far from being fully elucidated, recent studies have thrown up several possible mechanisms, among which the TGF-β signaling pathway has emerged as a major player.

1.3.2 Role of RUNX3 in the Tumor Suppressive Effect of TGF-β Signaling Pathway in Gastric Cancer

Hints of a meaningful association between RUNX3 and the TGF-β signaling pathway first emerged when it was demonstrated that RUNX3 forms complexes with receptor-regulated Smads (R-Smads) that regulate TGF-β target gene expression; RUNX3 contacts with the MH2 domains of Smads present in their C-terminal conserved region, and Smads appear to interact with RUNX3 at two regions of its C-terminal region. It was also shown that Smads and RUNX3 work synergistically to regulate TGF-β target genes such as the germline IgCα promoter, which contains a TGF-β responsive element. These findings strongly suggested that RUNX3 is a downstream target of the TGF-β signaling pathway.[69]

The above finding spurred subsequent studies which aimed to elucidate the functional relationship between the two. In 2004, Fukumachi et al. reported a phenotype of *Runx3* knockout mice which provides a tight link between Runx3 and TGF-β; hyperplasia and increased proliferation of the gastric epithelial cells were observed, and this phenomenon is attributed to the reduction in sensitivity to the growth suppressive effect and the apoptotic-inducing activity of TGF-β. They also showed that RUNX3 expression was frequently lost in gastric cancer cells and that exogenous expression of RUNX3 in these cells exhibited an inhibition of growth both *in vivo* and *in vitro*. Through this study, the authors thus demonstrated the involvement of *RUNX3* in the transmission of signals initiated by TGF-β, as disruption of *RUNX3* in their experimental model inhibits the action of TGF-β on gastric epithelial growth.[71]

In 2005, Ito and coworkers studied the expression pattern of RUNX3 in human gastric epithelial cells and gastric cancer cell lines and discovered a novel cytoplasmic localization of a substantial fraction of RUNX3 in chief cells. As a signal transducer, RUNX3 in the cytoplasm is presumed to be in an inactive state, and its nuclear import is an essential element in gaining access to their target genes. In their studies, Ito et al identified TGF-β as an agent that stimulates the nuclear import of RUNX3. Furthermore, in cells that demonstrated a cytoplasmic localization of RUNX3, it is known that the components of TGF-β signaling pathway are impaired, prompting the postulation that perhaps this cascade is primarily involved in regulating the nuclear import of RUNX3.[19]

Also in 2005, Chi et al. succeeded in demonstrating that RUNX3 inhibits gastric epithelial cell growth by up-regulating p21 gene expression in response to TGF-β[72]. Exogenous RUNX3 expression increased endogenous p21 expression in response to TGF-β, whereas RUNX3 suppression reduced TGF-β-induced p21 expression. The p21 promoter was activated by RUNX3, and mutations of the Runx-binding sites decreased this activity, thereby indicating that p21 is a direct target of RUNX3. RUNX3 was also shown to transactivate p21 expression, in cooperation with SMADs. As p21 is one of the downstream targets of TGF-β which plays a central role in CDK inhibition and cell cycle control, as well as apoptosis, their findings suggested that RUNX3 acts as an upstream regulator of *p21* expression, through which it inhibits cell growth in response to TGF-β.[72]

Another group, Yano et al (2006), demonstrated yet another link between Runx3 and another TGF-β target gene, *Bim.* RUNX3 was shown to bind to the *Bim* promoter and physically interacts with a transcription factor FoxO3a/FKHLR1, which is involved in apoptosis and cell cycle, to activate the expression of the proapoptotic *Bim.* The gastric epithelia of Runx3$^{-/-}$ mice had reduced levels of Bim expression, and of apoptosis, similar to that found in *Bim*$^{-/-}$ mice. Furthermore, in TGF-β−/− mice, levels of Bim expression was reduced in the stomach. Their results demonstrated that RUNX3 is responsible for transcriptional regulation of Bim in TGF-β-induced apoptosis.[73]

Most recently in 2007, a group led by Saeki found that the highly apoptotic GASDERMIN (GSDM) was found to be expressed in gastric pit epithelial cells but not in gastric cancer cell lines. Its expression is regulated by Lim domain only 1 (LMO1), a transcription factor, through a sequence through

which RUNX3 binds to in the *GSDM* promoter. Additionally, they observed that TGF-β up-regulated both the expression of *LMO1* and *GSDM* in the gastric epithelial cell lines, and apoptosis was induced. Taken together, their findings again pointed out the involvement of RUNX3 in the induction of TGF-β-induced apoptosis.[74]

As such, there is a significant amount of data that demonstrates strong functional cooperation between RUNX3 and the TGF-β signaling pathway in gastric cancer. However, even with the current existing data, the mechanism of action of RUNX3 in the tumor suppressive activity of the TGF-β pathway still remains to be clarified.

Association	**Proposed Functional Cooperation**	**Reference**
RUNX3 contacts the MH2 domains of Smad 1 and Smad3 present in their conserved C-terminal regions; interaction synergistically activates germline promoter IgCα.	RUNX3 is a downstream target of TGF-β signaling pathway.	[69]
In $Runx3^{-/-}$ mice, hyperplasia of glandular stomach epithelial cells observed, due to a reduced sensitivity to the cell growth inhibitory and apoptosis-inducing activity of TGF-β.	RUNX3 is a possible tumor suppressor, and contribute to the tumor suppressive effect of TGF-β pathway.	[62]
$Runx3^{-/-}$ gastric epithelial cells resistant to apoptosis-inducing action of TGF-β; exogenous expression of RUNX3 caused growth inhibition *in vitro* and *in vivo.*	RUNX3 plays an essential role in transmitting signals initiated by TGF-β, as disruption of RUNX3 inhibits the action of TGF-β on gastric epithelial growth.	[71]
A substantial fraction of RUNX3 was found to reside in the cytoplasm in chief cells, as an apparently nonfunctional form; and TGF-β was found to stimulate nuclear translocation of RUNX3.	The non-functional, cytoplasmic state of RUNX3 observed in many gastric cancer cells may be due to an impaired TGF-β signaling pathway.	[19]

RUNX3 binds to and activates *p21* promoter; RUNX3 is required for TGF-β-dependent induction of *p21* expression in stomach epithelial cells; RUNX3 induces *p21* expression in cooperation with TGF-β specific SMADs.	RUNX3 is the upstream regulator of *p21* expression, through which it inhibits cell growth in response to TGF-β.	[72]
RUNX3 binds to *Bim* promoter, and interacts with FoxO3a to activate Bim expression; Runx3$^{-/-}$ gastric epithelia had reduced levels of Bim expression, and apoptosis, similar to Bim$^{-/-}$ mice; levels of Bim reduced in TGF-β$^{-/-}$ mice.	RUNX3 is responsible for the transcriptional up-regulation of *Bim* in TGF-β-induced apoptosis.	[73]
Proapoptotic GASDERMIN (GSDM) was found to be suppressed in gastric cancer cell lines and primary gastric cancers; Lim domain only one (LMO1) regulates GSDM expression through a sequence to which RUNX3 binds in GSDM promoter region; TGF-β up-regulates LMO1 and GSDM expression and induces apoptosis.	RUNX3 is involved in the induction of TGF-β-induced apoptosis.	[74]

Table 1.1. Functional cooperation between RUNX3 and TGF-β-induced tumor suppressive pathway

1.4 The nuclear receptor co-repressor (N-CoR)

1.4.1 The nuclear receptor co-repressor (N-CoR) is a key component of the generic multi-protein complex involved in transcriptional control.

Nuclear receptors such as thyroid-hormone and retinoic-acid receptors (TR, RAR) are ligand-dependent transcription factors that play an essential role in the regulation of growth, development and homeostasis by regulating gene expression. Nuclear receptors interact with a wide array of co-regulator molecules termed as co-activators and co-repressors. While co-activators are generally recruited to nuclear receptors upon ligand binding to promote gene transcription, co-repressors mainly bind to un-liganded nuclear receptors and repress gene transcription of targets.[75] One of the first nuclear receptor co-

repressors identified is nuclear receptor co-repressor (N-CoR), a 270-kDa protein which interacts with both thyroid hormone and retinoic-acid receptors and mediates ligand-independent transcriptional repression.[76] N-CoR can also interact with steroid hormone receptors, estrogen receptor (ER) and progesterone receptor (PR), in the presence of their antagonists, suggesting a role for N-CoR in mediating the antagonist-associated effects of steroid hormone receptors.[77,78]

N-CoR contains multiple repression domains (RDs), nuclear receptor interaction domains (NRIDs) and Swi2/Ada2/N-CoR/TFIIID (SANT) motifs (Fig. 1.3). This large protein serves as a large docking surface for various components of the repression machinery to tether to for transcriptional repression. As such, N-CoR exists in large assemblies with an apparent molecular weight of between 1.5 to 2 MDa.[79] N-CoR complexes are associated with multiple histone deacetylase (HDAC) enzymes, suggesting that N-CoR-mediated transcriptional repression involves chromatin remodeling via the deacetylation of nucleosomal histones.[79-82] N-CoR also forms a complex with mammalian Sin3 orthologs, which together with HDACs, forms a complex which is required for transcriptional repression by thyroid hormone receptor and tumor suppressor Mad.[80,83]

Several studies have also implicated N-CoR in repression by its interaction with unrelated transcription factors, which regulate diverse cellular processes. One such factor is ETO, the fusion partner of t(8:21) acute myeloid leukemia (AML). The interaction of the fusion AML1/ETO with the N-CoR complex results in the disruption of normal hematopoiesis by the transcriptional repression of the AML1-responsive genes.[84] Kaiso, a methyl binding CpG

protein belonging to the BTB/POZ family of transcription factors, has also been shown to bind to the N-CoR repressor complex, demonstrating the involvement of N-CoR in DNA methylation-mediated biological functions.[85] It was also demonstrated that BCL6 (B-cell lymphoma-6) transcriptional repressor modulates survival of tumor cells in diffuse large B-cell lymphomas (DLBCLs) via the recruitment of the N-CoR repressor complex to BCL6 target genes involved in survival and proliferation such as *ATR* and *TP53*.[86,87]

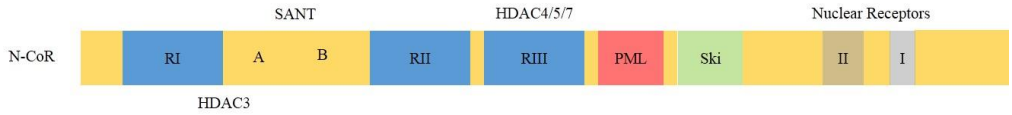

Figure 1.3. The domains of N-CoR. The interaction domains for HDAC lie within the repression domains (RI, RII, RIII) of N-CoR. The histone-binding SANT domains (A and B), and interaction domains for nuclear receptors (I and II), PML, Ski and other transcription factors are highlighted.

N-CoR play important physiological roles in development, differentiation, and carcinogenesis. Studies with N-CoR knockout mice demonstrated the importance of N-CoR in early embryonic development. Murine knockouts of N-CoR are embryonically lethal and observed phenotypes in N-CoR-deficient mice include defects in T cell development and lower thymocyte counts, smaller livers and overall size, defects in neural development, and anemia due to defects in erythrocyte development.[88,89] N-CoR also regulates neural stem cell differentiation as cytoplasmic translocation of N-CoR leads to astrocytic differentiation.[90] Also, N-CoR plays a role in myogenesis by regulating differentiation and MyoD-dependent repression.[91]

1.4.1 N-CoR plays a role in carcinogenesis

A well-established oncogenic role for N-CoR has been elucidated in acute promyelocytic leukaemia (APL). APL, which is caused by a block in myeloid differentiation, is associated with rearrangements of RAR-α, which results in fusion between the RAR-α gene and the promyelocytic leukemia gene (PML) or the promyelocytic leukemia zinc finger gene (PLZF).[92] Both RAR-α fusion proteins recruit the N-CoR repressor complex which blocks differentiation of hematopoietic precursors.[93]

In acute myeloid leukemias (AML) which result from the t(8;21) translocation between AML1 and ETO, the AML1-ETO fusion protein also recruits the N-CoR-histone complex resulting in the transcriptional repression of AML1 target genes involved in normal hematopoiesis.[84]

Dysregulation of N-CoR and its subsequent loss of function as a repressor also contribute to carcinogenesis. Phosphorylation of N-CoR by IKKα in colorectal cancer cells results in a nuclear export of N-CoR, relieving its repressive effects and thereby promoting the survival of these cells.[94] Also, loss of N-CoR protein expression in thyroid tumor cells has been shown to promote PI3K signaling pathway, thus contributing to tumor progression.[95]

1.4.2 N-CoR and its involvement in TGF-β signaling pathway

It was first established that Ski/SnoN (Ski-related novel protein N) directly binds to N-CoR and mSin3A to form a complex with HDAC.[83] It was later shown that Ski/SnoN also physically interacts with Smad3 and Smad4, displacing the co-activator p300/CBP from the Smad proteins and recruiting the N-CoR/HDAC complex. This repressor complex is then recruited to

Smad-binding elements (SBE) in the promoters of TGF-β-responsive genes in a ligand-dependent manner, resulting in the repression of TGF-β target genes (Fig. 1.4).[96-98] N-CoR thus plays a role in the negative regulation of TGF-β signaling.

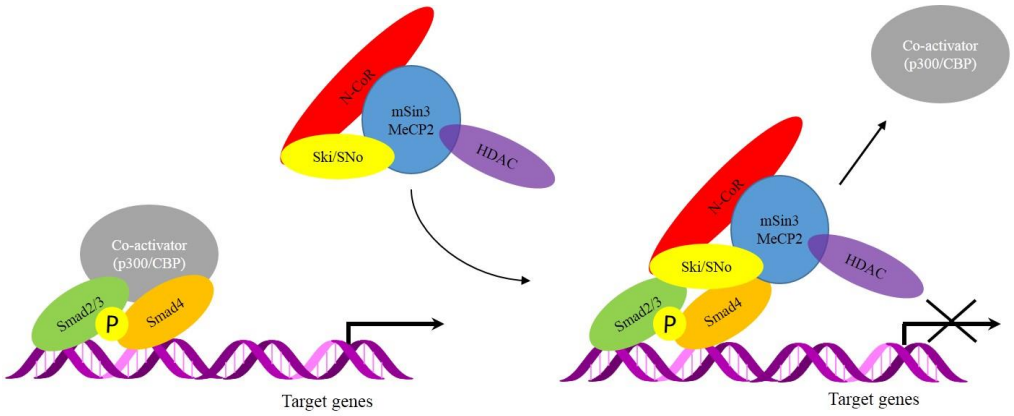

Figure 1.4. Mode of action of N-CoR-mediated repression on Smad target genes. It has been shown that Ski/SnoN directly binds to N-CoR, MeCP2 and mSin3A to form a complex with HDAC. Upon binding of Ski/SnoN to Smads, Ski/SnoN displaces the activator complex p300/CBP and recruits the repressor complex containing N-CoR to Smad target genes, thereby repressing transcription of these genes.

1.5 Artemisinin

Artemisinin (Fig. 1.5) is a sesquiterpene lactone containing a 1,2,4-trioxane structural motif. This endoperoxide compound is isolated from the Chinese plant *Artemisia annua* (more commonly known as qinghaosu or sweet wormwood) and has been used by Chinese traditional medicine practitioners for over two millennia for the treatment of fever and malaria.[99,100] Artemisinin, and its bioactive derivatives such as artesunate (ART) and dihydroartemisinin (DHA) are newer generation FDA-approved anti-malarial drugs used in the clinical management of malaria, including multidrug-resistant strains. The peroxide group within the trioxane bestows potent antimalarial activity on

these compounds, by its cleavage in the presence of iron leading to generation of free-radical reactive oxygen species (ROS)[99]. These compounds demonstrate excellent parasiticidal activity at plasma concentrations well-tolerated by the host cells.[99-103]

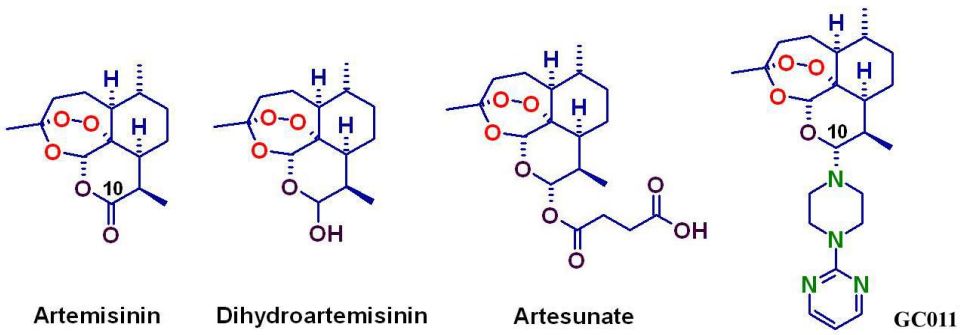

Figure 1.5. Artemisinin and its derivatives dihydroartemisinin and artesunate. The active pharmacophore is the peroxide bridge that bestows antimalarial activity, and the derivatives are now widely used for treatment of malaria. GC011 is a newer derivative prepared from dihydroartemisinin that possesses potent antimalarial activity in *in vitro* screens. The pyrimidinylpiperazinyl unit attached to C10 in GC011 confers enhanced lipophilicity as compared to artemisinin and the derivatives dihydroartemisinin and artesunate.

1.5.1 Anticancer properties of Artemisinin

In addition to anti-malarial activity, artemisinin and its derivatives also demonstrate remarkable anti-tumor activity against a variety of tumor cells.[104-107] An analysis of 55 cancer cell lines by the Developmental Therapeutics Program of the National Cancer Institute (NCI), USA, showed that artesunate displays strong inhibitory activity against leukemia and colon cancer cells, and intermediate activities on melanoma, breast, ovarian, prostate, central nervous system (CNS), and renal cancer cells.[108] Antitumor activity has also been reported in cancer patients[109,110] and a phase II study with advanced non-small cell lung cancer (NSCLC) patients reported improved short-term survival rate

and time-to-progression rates of patients with artemisinin combination treatments.[111]

In general, cancer cells exposed to these derivatives demonstrate decreased proliferation, induction of apoptosis, and inhibition of angiogenesis and migratory properties. Studies have identified several mechanisms by which artemisinins exert their antitumor activities. One study showed that both ART and DHA inhibited cell proliferation in hepatoma cells by inducing G_1-phase arrest, via their action on key cell cycle regulatory proteins such as cyclin D1, cyclin E, and p21.[112] DHA treatment also promoted apoptosis in acute promyeloid leukemia cells and Jurkat T-lymphoma cells via its regulation of pro-apoptotic proteins Bax and Bak, and anti-apoptotic protein Bcl-2.[113-115] DHA also demonstrated antiangiogenic properties by targeting vascular endothelial growth factor (VEGF) in human umbilical vein endothelial cells (HUVEC) via the NF-kB pathway.[116,117] Another group reported the inhibitory effects of artemisinin on migratory abilities of metastatic melanoma cells by downregulating metalloproteinase-2 (MMP-2) and αVβ3 integrin expression.[118]

However, little is known of the mechanism underlying its pharmacological activity in cancer. One proposed mechanism is cleavage of the endoperoxide bridge by iron in the cancer cells, which possess higher influx of iron via transferrin receptors, resulting in generation of ROS and other free radicals.[112] This is similar to the action of artemisinins on malarial parasites. Generation of radicals may therefore play a role in the antitumor effects reported in artemisinin-treated cancer cells, such as enhanced apoptosis, growth arrest, inhibition of angiogenesis, and DNA damage. However, studies show that the

lack of the endoperoxide moiety does not completely diminish anticancer activity of artemisinin, suggesting that not all of its anticancer activities may be caused by the global toxic effects of oxidative damage.[119] Alternative peroxide-independent mechanisms may contribute to its activities.

1.6 ER stress and the unfolded protein response

1.6.1 Protein folding and modification in the endosplamic reticulum (ER)

The ER is the entry site for proteins destined for secretion or insertion into cellular membranes. The lumen of the ER provides an oxidative environment containing high calcium levels for the early steps in the maturation of these proteins to take place in the ER - the folding of the nascent polypeptide chains and posttranslational modifications of the proteins important for correct folding of proteins, such as N-linked glycosylation and disulphide bond formation. Proteins destined for translocation to the ER are usually recognized by a cytosolic ribonucleoprotein complex, the signal recognition particle (SRP), typically via amino terminal signal sequences on the nascent proteins. The resulting ribosome-nascent chain-SRP complex then binds to the SRP receptor on the ER membrane, whereby the SRP dissociates and the ribosome-nascent chain is then directed to a proteinaceous core in the membrane called Sec61 translocon, which allows the translocation of the growing polypeptide chain across the membrane and into the ER.[120-122]

As the polypeptide enters the lumen of the ER, its proper folding is mediated by a range of ER resident chaperones and folding enzymes. These folding factors include heat shock proteins acting as chaperones such as glucose-

regulated protein of molecular weight 78 kDa (GRP78), oxidoreductases such as protein disulphide isomerase (PDI) and ERp57, and glycan-binding proteins such as calnexin and calreticulin. GRP78 is a highly expressed ER resident chaperone which binds to the ER through an N-terminal cleaved signal peptide and a C terminal ER retention motif (KDEL). The C-terminal domain of GRP78 binds to exposed hydrophobic regions of protein folding intermediates with low affinity in an ATP-bound state, which becomes more stable upon ATP hydrolysis. GRP78 returns to a low-affinity peptide-binding state upon exchange of ATP for bound ADP. As such, protein binding is coupled to cellular energy expenditure in this manner.[123]

The ER lectins calnexin and calreticulin bind to partially folded monoglucosylated N-linked glycans together with ER-resident oxidoreductase, ERp57.[124] Binding and release from the calnexin/calreticulin is determined by monoglucosylation of the glycans, and proteins only leave this cycle once the side chains are no longer monoglucosylated. This on-and-off cycle is mediated by two independent ER enzymes; glucosidase II and UP-glucose glycoprotein glucosyl transferase (UGGT). Glucosidase II hydrolyses the glucose from the monoglucosylated core glycan for dissociation from calnexin/calreticulin, whereas UGGT glucosylates the incompletely folded proteins for reassociation with calnexin and calreticulin. This cycle of glucosylation and deglucosylation continues until the glycoprotein has reached its native conformation or is targeted for degradation. Only correctly folded proteins are exported to the Golgi, whereas incompletely folded proteins are either retained in the ER or targeted for degradation. PDI binds to unfolded proteins with high affinity and targets them for export to the cytosol via the Sec61 translocon, for refolding or

degradation.[125] For degradation, a single mannose residue is removed by the ER α1,2-mannosidase I, and associates with ER degradation-enhancing α-mannosidase-like protein (EDEM).[121]

Physiological conditions prevailing in the cell and changing environmental factors may interrupt the protein folding process of newly synthesized chains or promote loss of native conformation in mature polypeptides, leading to the problem of misfolded protein aggregration. To counteract this problem, cells evolved a sophisticated system of molecular chaperones, which protects nascent proteins during folding. These cytosolic chaperones include heat shock protein 70 (Hsp70), Hsp100, small heat shock proteins (sHSPs), and chaperonins such as TRiC (TCP-1 ring complex), with roles in protein refolding and aggregation prevention.[126,127] Another two chaperones, HSC70 and HSP90 work as a single multichaperone system which, in addition to a role in protein folding, also function in protein sorting to intracellular organelles, or proteasome for degradation. This system removes misfolded proteins through interactions with co-chaperones CHIP (carboxyl terminal of HSC70-interacting protein), which promotes ubiquitylation and degradation of HSC70-HSP90 substrate polypeptides, and BAG1 (BCL2-associated athanogene-1), which mediates contact with the proteasome.[128]

1.6.2 ER stress and the Unfolded Protein Response (UPR)

In cases where demands on the ER protein folding machinery exceeds its capacity, resulting in the accumulation of unfolded or misfolded proteins in the ER, a condition called “ER stress” occurs. Multiple pathologic stimuli can cause the accumulation of proteins in the ER, such as hypoxia, glucose

deprivation, oxidative stress, expression of mutant proteins and overexpression of some wild-type proteins.[129] To alleviate ER stress and re-establish ER homeostasis, a group of signal transduction pathways collectively called the unfolded protein response (UPR) is activated. The UPR has two primary functions: 1) to restore homeostasis by downregulating transcription and translation of proteins, activating signalling pathways to increase production of molecular chaperones involved in protein folding and increasing the removal of misfolded proteins via the ER-associated degradation (ERAD) pathway[130] or autophagy[131,132] and 2) to initiate apoptotic pathways if ER stress persists or is prolonged.[133] The latter reflects the cytotoxic branch of UPR while the former represents the cytoprotective branch of UPR.

UPR generally involves three signalling pathways originating from the ER, the inositol requiring kinase 1 (IRE-1) pathway, the PKR-like ER kinase (PERK) pathway, and the activating transcription factor 6 (ATF6) pathway (Fig. 1.6). IRE-1, PERK and ATF6 are integral ER proteins and function as ER stress sensors, and are activated upon dissociation with GRP78. As misfolded proteins accumulate in the ER, sequestration of GRP78 from these proximal sensors allows their dimerization and activation.[134]

The most immediate response to the accumulation of unfolded or misfolded proteins is the activation of PERK. PERK, a type I transmembrane kinase, upon release from GRP78, autophosphorylates itself following oligomerization, thereby triggering its serine-threonine kinase activity. Activated PERK then phosphorylates eukaryotic initiating factor 2 subunit α (eIF2α), which shuts off general protein translation. Phosphorylated eIF2α promotes the translation of some mRNAs however, such as ATF4, which then

induces expression of ER chaperones to alleviate ER stress. Under prolonged or severe ER stress, ATF4 also induces GADD34 and C/EBP homologous protein (CHOP), proteins involved in ER stress-induced apoptosis.[130]

Upon dissociation from GRP78, IRE-1, a type I transmembrane protein containing both a serine-threonine kinase domain and an endoribonuclease domain, homodimerizes and autophosphorylates itself, activating its endoribonuclease activity. This results in its cleavage of X-box-binding protein 1 (XBP1) mRNA, and due to a frameshift, produces a spliced form of XBP1, a functional 41-kDa basic leucine zipper (bZIP) family transcription factor that induces transcription of UPR- and ERAD-related genes. IRE1 also binds the RING finger protein TRAF2, leading to phosphorylation and activation of apoptosis signal-regulating kinase 1 (ASK1). This in turn leads to phosphorylation and activation of JNK, which has been reported to inhibit anti-apoptotic BCL2 by phosphorylation.[135]

ATF6 is a type II transmembrane protein which, upon dissociation from GRP78, translocates to the Golgi, where it is cleaved by Golgi-resident serine proteases, site 1 and site 2 proteases (S1P and S2P) to release its cytosolic domain. This cytosolic domain moves into the nucleus and induces expression of gene targets including ER chaperones such as GRP78, calnexin and calreticulin, foldases such as PDI, and ERAD components.[123,136] ATF6 can also induce CHOP mRNA expression, although no link to ER stress-induced apoptosis has been established, suggesting that the ATF6 pathway is primarily cytoprotective.[137]

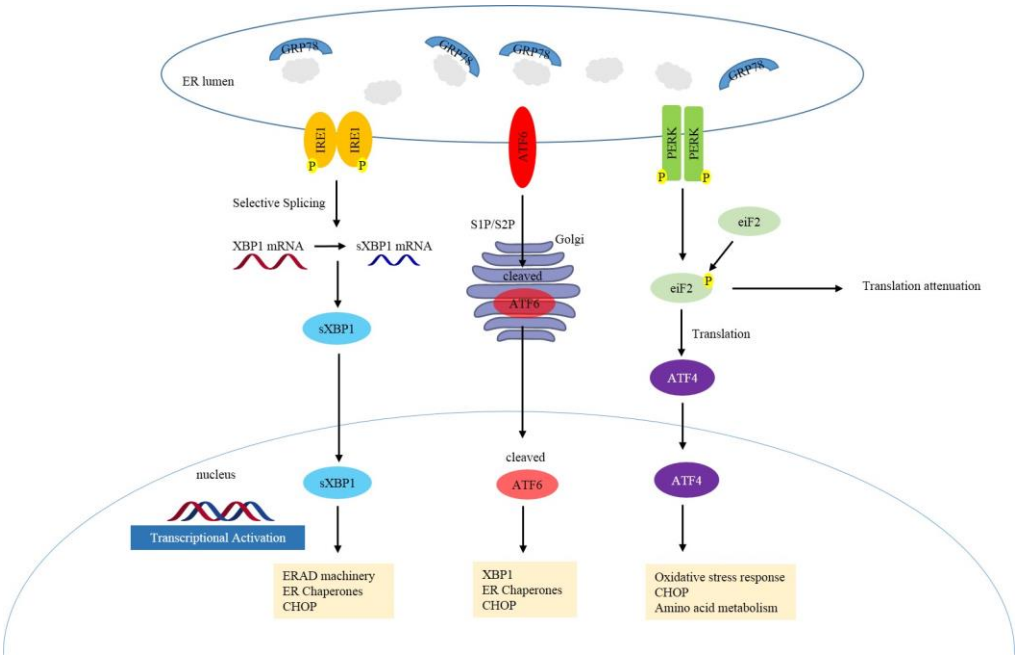

Figure 1.6. The Unfolded Protein Response (UPR). Upon ER stress due to accumulation of misfolded proteins results, GRP78 dissociates from the proximal ER sensors, thereby triggering UPR via the activation of the PERK, ATF6 and IRE-1 pathways.

1.6.3 UPR-induced apoptosis

It is apparent that the UPR has both cytoprotective and cytotoxic effects. Under chronic ER stress conditions where the cytoprotective pathway of UPR fails to correct the folding defect, UPR-induced apoptosis may occur. The IRE1-ASK1-JNK pathway has been implicated in ER stress–induced cell death, by promoting the activation of proapoptotic BCL-2 family protein BIM and inhibiting anti-apoptotic BCL-2 family protein BCL2.[135] Additionally, the PERK pathway, via its activation of ATF4, and the ATF6 pathway, upregulates proapoptotic CHOP.[135] While the PERK and the IRE-1 pathways can initiate pro-apoptotic signal during prolonged ER stress, it is the activation of downstream molecules that commit the cells to ER stress-induced apoptosis. CHOP-induced apoptosis involves the activation of BIM and

GADD34, and downregulation of BCL-2.[138,139] GADD34, a protein phosphatase 1 (PP1)-interacting protein, induces PP1 to dephosphorylate eIF2α, thus relieving the translational block mediated by PERK. Although GADD34 has been shown to correlate with apoptosis, the underlying mechanism is still unknown. GADD34 might induce apoptosis through its inhibition of eIF2α phosphatases.[137]

The execution phase of ER stress-induced apoptosis is caspase activation. There are two major pathways of apoptosis. The intrinsic (mitochondrial) pathway is regulated by a balance between proapoptotic BH3-only proteins such as BAK and BAX and antiapoptotic proteins, such as BCL2. Bak and Bax oligomerize and are inserted into the outer mitochondrial membrane, forming a pore for the release of cytochrome c. Cytochrome c then promotes the formation of the apoptosome between Apaf-1 and procaspase-9, leading to caspase-9 activation, and ultimately, caspase 3. The extrinsic (death receptor) pathway on the other hand, responds to extracellular stimuli, involves clustering of death receptors, recruitment of procaspase-8 and formation of a death-inducing signalling complex (DISC), resulting in the activation of caspase-8 and subsequent caspase cascade leading to apoptosis. ER stress-induced apoptosis appears to act via the intrinsic pathway, although some recent studies have implicated the involvement of the extrinsic pathway. The relative importance of either pathway in ER stress still remains to be elucidated.[137,140]

1.6.4 UPR as a possible target in cancer therapy

Tumor cells are constantly under stressful stimuli such as hypoxia, glucose deprivation, insufficient ER energy supply, pH changes, and viral infection. Additionally, they can express mutant proteins. All of these can cause ER stress and UPR has been shown to provide survival pathways for tumor growth.[141-143] Increased expression of UPR components in various cancers were reported, such as XBP1, ATF6, CHOP, GRP78/BiP.[143,144] On the other hand, most normal cells are not subject to stress and their UPR pathway are in a quiescent state. This discrepancy between normal and tumor cells raises the possibility of specifically targeting tumor cells by UPR targeting agents. One therapeutic approach is to induce the accumulation of misfolded protein in the ER to overwhelm the UPR, and promote the switch from cytoprotective UPR to cytotoxic UPR. This may be achieved by inhibition of the proteosomal or autophagic degradation of misfolded proteins retrotranslocated from ER to the cytosol. Another approach is to inhibit components of the UPR so that tumor cells cannot cope with the stressful conditions, ultimately leading to cell death (Fig. 1.7).

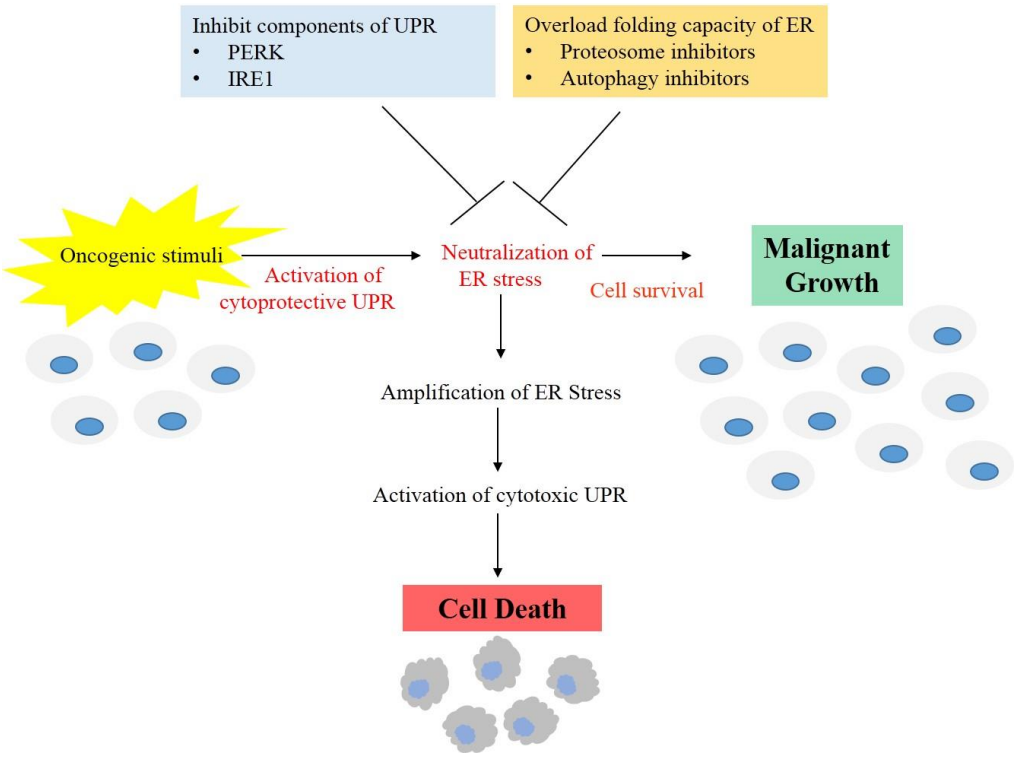

Figure 1.7. Targeting the UPR for anticancer therapeutics. The UPR is an attractive target for cancer therapeutics. Activation of cytoprotective UPR pathway promotes survival of tumor cells whereas strong ER stress activates cytotoxic UPR, leading to cell death. Modulation of the activation of UPR pathways to drive the cells towards the death pathway could be achieved by inhibiting components of the UPR so that cancer cells cannot cope with the stressful environment which then results in cell death. Another approach is to increase the stress on the tumor cells by inhibiting the clearance of misfolded or unfolded proteins in the ER, either via inhibiting proteosomal degradation or autophagic degradation. As a result, ER stress is amplified, thereby driving the cells towards the death pathway.

1.7 Inhibition of proteasome degradation as a therapeutic strategy in cancer

1.7.1 The Ubiquitin-Proteosome Pathway (UPP)

Degradation of proteins plays an important role in regulation of cellular functions and homeostasis. In eukaryotic cells, this role is carried out by the ubiquitin-proteasome pathway (UPP), which is comprised of an ubiquitin conjugating system and a 26S proteasome.[145] UPP substrates include cellular proteins involved in cell-cycle regulation,[146] oncogenesis,[147] and apoptosis.[148] The UPP also selectively removes mutant, misfolded, damaged or obsolete proteins for the maintenance of cellular homeostasis.[149]

The 26S proteasome is a proteolytic complex comprised of a multi-catalytic 20S core flanked by two 19S regulatory caps. The 20S catalytic core contains the proteolytic activities of the proteasome, namely the chymotrypsin-like, trypsin-like, and caspase-like activities. The 19S subunits regulate entry of ubiquitinated proteins into the hollow chamber of the 20S core.[150] Briefly, proteosomal degradation of proteins proceeds as follows: 1) Tagging of target proteins with polyubiquitin molecules in an ATP-dependent manner through E1, E2, and E3 ligases. 2) Polyubiquitinated proteins are recognized by the 19S regulatory caps and directed into the 20S catalytic core for degradation, generating peptides 3-25 amino acids in length. 3) Ubiquitin molecules are released to be recycled (Fig. 1.8).[150,151]

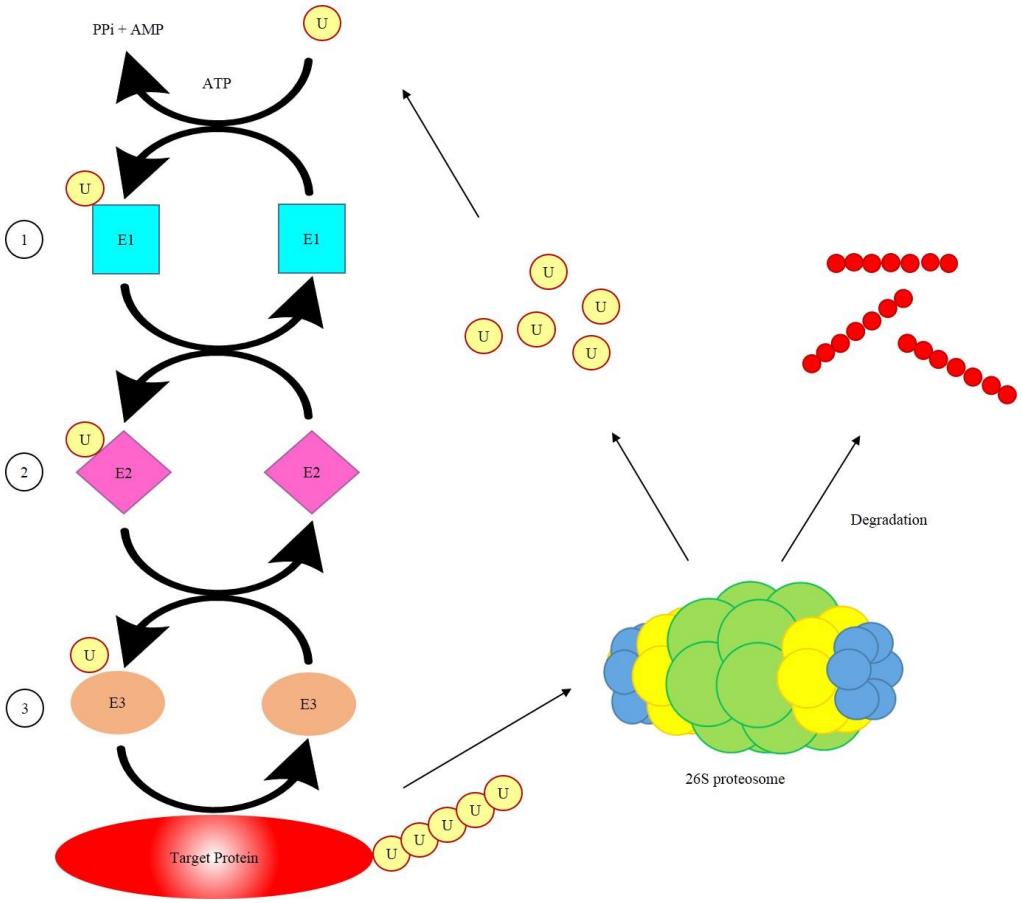

Figure 1.8. The UPP pathway. The attachment of ubiquitin to the target proteins requires involves a series of ATP-dependent enzymatic steps by E1 (ubiquitin activating enzyme), E2 (ubiquitin conjugating enzyme) and E3 (ubiquitin ligating enzyme). E1 binds ubiquitin, which is transferred to E2. E3 then transfers ubiquitin to target protein. The 26S proteosome recognizes polyubiquitinated protein, which leads to its subsequent degradation. The ubiquitin molecules are then removed to be recycled.

1.7.2 Proteosome inhibition as an anticancer therapy

As mentioned earlier, one of the functions of the UPP is the degradation of misfolded or unfolded proteins. Detection of misfolded proteins trigger the ER stress and the induction of the UPR pathway, resulting in the degradation of the proteins by the 26S proteasome via the ERAD pathway.[152] Inhibition of the proteolytic activity of the proteasome may cause the accumulation of misfolded or unfolded proteins, and results in constitutive ER stress that switches on the cytotoxic UPR pathways leading to cell death.[153]

It was reported in several studies that proteasome inhibitors are more cytotoxic in cancer cells than normal cells.[153-156] As cancer cells are more likely to have defective or mutant proteins and thus increased accumulation of misfolded proteins, it may be more dependent on the proteosomal degradation process. Addtionally, as many proteins involved in cell cycle control and apoptosis are degraded by the proteosome, it follows that these cellular processes may be affected by proteasome inhibition. As such, proteosome inhibition presents an attractive strategy for anticancer therapy.

Proteosome inhibitors can exist as naturally-occurring compounds, such as lactacystin and epoxyketones, or as synthetic compounds, such as the peptide aldehyde MG132.[157] These synthetic compounds generally target the chymotrypsin-like activity of the proteasome.[158] However, as these compounds are not sufficiently selective inhibitors of proteosome, dissociate quickly from the proteasome, or are removed by the multi-drug transporter system, they may not be suitable for clinical use.[159]

To circumvent this problem, the aldehyde group of synthetic inhibitors was replaced with boronic acid. Bortezomib (N-pyrazinecarbonyl-L-phenylalanine-L-leucine boronic acid, originally known as PS-341 and marketed as Velcade by Millennium Pharmaceuticals), a boronic acid dipeptide, has been found to be a potent and specific inhibitor of the 26S proteasome. This specificity is due to the bond formation between the boronic acid moiety of bortezomib and the nucleophilic hydroxyl side chain of Thr1 in the S1 pocket of the β5 subunit of the proteasome.[160] It is the first and only proteasome inhibitor that has been U.S Food and Drug Administration (FDA)-approved as treatment for cancer, that is of newly diagnosed multiple

myeloma, relapsed/refractory multiple myeloma, and mantle cell lymphoma.[161-163] Bortezomib, either on its own or in combination with other drugs, has an overall positive clinical response.[164,165]

1.7.3 Mechanism of action of Bortezomib

Bortezomib has demonstrated anticancer properties in a variety of cancer cells including multiple myeloma, prostate cancer, pancreatic cancer, renal cell carcinoma, gastric cancer and squamous cell carcinoma.[164,166-170] Several possible mechanisms of action has been proposed for the anticancer properties of bortezomib. In myeloma cell lines, it was found that bortezomib induced gene expression of components of the UPR such as HSP70, calreticulin and BAG3. The induction of ER stress results in calcium release, leading to cytochrome c release from the mitochondria and activation of caspases, followed by cleavage of Bid to tBid.[171] Another group reported that bortezomib-triggered apoptosis in multiple myeloma cells is dependent on caspase-2 activation. Caspase-2, which is associated with ER stress, can serve as a proximal caspase that functions upstream of mitochondrial signalling during ER stress-induced apoptosis by bortezomib in multiple myeloma cells.[172] Another study described the suppression of the pro-survival nuclear factor-κB pathway by the inhibition of proteasome by bortezomib in multiple myeloma cells.[173,174] The molecular sequelae of proteasome inhibition by bortezomib in multiple myeloma cells was also investigated, revealing a shift of balance between proapoptotic and antiapoptotic genes to induce or increase sensitivity to apoptosis, up-regulation of heat-shock proteins and ubiquitin/proteasome pathway members, and the triggering of both extrinsic and intrinsic apoptotic pathways.[175] As multiple myeloma cells produce and

secrete abundant immunoglobulins (Igs), it is very likely that they are more susceptible to ER stress induction and proapoptotic UPR. This might explain its sensitivity to the proteasome inhibitor bortezomib.[176]

Other than proteasome inhibition, other mechanisms by which bortezomib may exert its anticancer activity have been proposed. For example, bortezomib has been reported to induce pro-apoptotic NOXA,[177] and reduce pro-survival hypoxia-inducible factor-1α (HIF-1α).[178]

With the FDA approval of bortezomib as a front-line treatment for cancer, it is increasingly clear that the UPP is a viable therapeutic target. Although other mechanisms may be also be responsible for the antitumor effects of bortezomib, the proteasome inhibitory effect of bortezomib may prove to be highly efficacious in malignant cells in which the ER is already predisposed to aberrant protein load.

1.8 Hypotheses and Objectives

Artemisinin, a sesquiterpene lactone isolated from the plant *Artemisia annua*, is recognized as a newer generation of anti-malarial drugs which demonstrates excellent larvicidal activity at plasma concentrations that are well-tolerated by the host cells. In addition to the anti-malarial activity, artemisinin also demonstrated remarkable anti-tumor activity against a variety of tumor cells. The molecular mechanism underlying its anti-tumor effect is thought to be similar to its anti-malarial activity, which is based on the endoperoxide bridge that reacts with haem molecules and generates potentially cytotoxic free radicals that promote cell death. Artemisinin has recently been shown to arrest the growth of human colorectal carcinoma cells through attenuating the hyperactive Wnt/β-catenin pathway. Since TGF-β acts as a natural antagonist of Wnt signaling, therefore, it is likely that artemisinin-induced growth inhibition may also involve an activation of genes regulated by TGF-β pathway. Based on this hypothesis, the aims of this project are to investigate whether artemisinin could induce any growth suppressive effect on gastric cancer cells, and elucidate the mechanism underlying such effect, if any.

Our laboratory has previously demonstrated how a misfolded conformation dependent loss (MCDL) of N-CoR protein contributed to the pathogenesis of APL cells. It is hypothesized that an APL-like MCDL of N-CoR might be prevalent in gastric cancer as well. In eukaryotes, the accumulation of misfolded proteins in the endoplasmic reticulum typically results in the induction of a stress signalling pathway known as the unfolded protein response (UPR). To prevent the accumulation of misfolded protein, UPR induction includes the downregulation of general protein synthesis and

increased transcription of components of both ER folding machinery and degradative machinery. Misfolded proteins which cannot be properly refolded are targeted for ER-associated degradation (ERAD), which involves the retrograde translocation of the proteins from the ER and subsequent degradation by the 26S proteasome, a large ATP-dependent protease. When the stress is prolonged, the cytotoxic UPR is activated instead, eventually leading to UPR-induced apoptosis. Thus, treatment with proteosome inhibitors would result in the accumulation of misfolded proteins within the ER, which would then elicit ER stress response and UPR, eventually leading to the induction of apoptosis. With these hypotheses in mind, this project also aims to evaluate the potential of proteasome inhibition, specifically that of bortezomib, as an anticancer strategy in gastric cancer.

CHAPTER 2

Materials and Methods

2.1 Materials

2.1.1 General Reagents and Kits

Chemicals/Reagents/Kits	Company	Country
2-Mercaptoethanol	Bio-Rad	CA, USA
4',6-diamidino-2-phenylindole (DAPI)	Sigma Aldrich	MO,USA
1 kb DNA ladder	Promega	WI,USA
100 bp DNA ladder	Promega	WI, USA
30% Acrylamide-Bis Solution	Bio-Rad	CA, USA
Agarose	Bio-Rad	CA,USA
Ammonium Persulfate	Bio-Rad	CA,USA
Ampicillin	Sigma Aldrich	MO,USA
Annexin V-FITC Apoptosis Detection Kit	BD Pharmingen	CA,USA
Bovine Serum Albumin (BSA)	Sigma Aldrich	MO,USA
Bromophenol Blue	Sigma Aldrich	MO,USA
Cell Proliferation Kit I [3-(4,5-dimethylthiazol-2-yl)-2,5-diphenyltetrazolium bromide; (MTT)	Roche	Germany
CellTiter 96® AQueous One Solution Cell Proliferation Assay (MTS)	Promega	WI, USA
Chemiluminescent HRP Substrates	PerkinElmer Life Sciences	MA, USA
cOmplete, mini protease inhibitor cocktail tablet	Roche	Germany
Diethylpyrocarbonate (DEPC)	Sigma Aldrich	MO,USA
Dimethyl sulfoxide (DMSO)	Sigma Aldrich	MO,USA
Dual-Luciferase Reporter Assay System	Promega	WI, USA
Dulbucco's Modified Eagle's Medium (DMEM)	Sigma Aldrich	MO,USA
Ethanol	Merck	Darmstadt, Germany
Fetal Bovine Serum (FBS)	Hyclone Laboratories	Logan, UT
Fugene 6	Roche	Germany
GelRed™ Nucleic Acid gel stain	Biotium	CA, USA
Glacial Acetic Acid	Merck	Darmstadt, Germany
Glycine	Bio-Rad	CA,USA
Goat ImmunoCruz™ Staining System	Santa Cruz Biotechnologies	CA, USA
Isopropanol	Merck	Darmstadt, Germany
Kanamycin	Sigma Aldrich	MO,USA
Lipofectamine® 2000	Invitrogen	CA,USA
Lipofectamine® RNAiMAX	Invitrogen	CA, USA
Luciferase Assay System (Dual)	Promega	WI,USA
Methanol	Sigma Aldrich	MO,USA
Murine Reverse Transcriptase, MMLV	Promega	WI,USA
Normal Goat IgG	Santa Cruz Biotechnologies	CA,USA
Normal Mouse IgG	Santa Cruz	CA,USA

	Biotechnologies	
Normal Rabbit IgG	Santa Cruz Biotechnologies	CA,USA
Nuclear Extract Kit	Active Motif	CA, USA
Paraformaldehyde	Sigma Aldrich	MO,USA
Penicillin/Streptomycin	PAA Laboratories	Austria
Phophatase Inhibitor Cocktails 1 and 2	Sigma Aldrich	MO,USA
Pierce® BCA Protein Assay kit	ThermoFisher Scientific	IL, USA
Precision Dual Colour Standard Protein Marker	Bio-Rad	CA,USA
Prolong Gold Antifade Reagent	Invitrogen	CA,USA
Protein G Sepharose Breads	Roche	Germany
Proteosome-Glo™ Chymotrypsin-like, Trypsin-like and Caspase-like Cell Based Assay	Promega	WI, USA
PVDF Membrane	Bio-Rad	CA,USA
Qiagen plasmid DNA purification Kit (maxi and miniprep kit)	Qiagen GmBH	Hilden, Germany
Qiagen RNasey RNA extraction Kit (RNA miniprep kit)	Qiagen GmBH	Hilden, Germany
Recombinant human TGF-β1	R & D Systems	Abingdon, UK
RPMI 1640	Life Technologies	Gaithersburg, MD
Skim Milk powder	Sigma Aldrich	MO,USA
Sodium Dodecyl Sulfate (SDS)	Bio-Rad	CA,USA
Sodium Fluoride	Sigma Aldrich	MO,USA
TaqMan Gene Expression Assay (Real time PCR)	ABI systems	CA,USA
Tetramethylethylenediamine (TEMED)	Bio-Rad	CA,USA
Tris-Base	Bio-Rad	CA,USA
Trizol	Sigma Aldrich	CA,USA
Tween 20	Sigma Aldrich	MO,USA

Table 2.1. List of chemicals, reagents, and kits

2.1.2. Antibodies

2.1.2.1 Antibodies for Western Blotting

Target	Company	Reactivity	Dilution	Incubation Period
β-Actin	Sigma Aldrich	Mouse Monoclonal	1:10000	Overnight at 4^0C
ATF6	Santa Cruz Biotechnologies	Goat Polyclonal	1:1000	Overnight at 4^0C
ASK1	Cell Signaling Technology	Rabbit Polyclonal	1:1000	Overnight at 4^0C
Bcl2	Santa Cruz Biotechnologies	Rabbit Polyclonal	1:1000	Overnight at 4^0C
Caspase-3	Cell Signaling Technology	Rabbit Polyclonal	1:2000	Overnight at 4^0C

Caspase-9	Cell Signaling Technology	Rabbit Polyclonal	1:2000	Overnight at 4^0C
Cleaved Caspase-3	Cell Signaling Technology	Rabbit Polyclonal	1:1000	Overnight at 4^0C
EIF2α	Cell Signaling Technology	Rabbit Polyclonal	1:1000	Overnight at 4^0C
HDAC1	Santa Cruz Biotechnologies	Goat Polyclonal	1:500	Overnight at 4^0C
HSP60	Santa Cruz Biotechnologies	Rabbit Polyclonal	1:5000	Overnight at 4^0C
Flag	Sigma Aldrich	Mouse Monoclonal	1:10000	Overnight at 4^0C
GRP 78	Santa Cruz Biotechnologies	Goat Polyclonal	1:1000	Overnight at 4^0C
JNK	Cell Signaling Technology	Rabbit Polyclonal	1:1000	Overnight at 4^0C
N-CoR	Santa Cruz Biotechnologies	Goat Polyclonal	1:500	Overnight at 4^0C
p21	Cell Signaling Technology	Mouse Monoclonal	1:500	Overnight at 4^0C
PAI-1	Santa Cruz Biotechnologies	Mouse Monoclonal	1:250	Overnight at 4^0C
PARP	Cell Signaling Technology	Rabbit Polyclonal	1:2000	Overnight at 4^0C
PDI	Santa Cruz Biotechnologies	Rabbit Polyclonal	1:1000	Overnight at 4^0C
PERK	Santa Cruz Biotechnologies	Rabbit Polyclonal	1:1000	Overnight at 4^0C
Phospho-ASK1	Cell Signaling Technology	Rabbit Polyclonal	1:1000	Overnight at 4^0C
Phospho-Bcl2	Cell Signaling Technology	Rabbit Polyclonal	1:1000	Overnight at 4^0C
Phospho-EIF2α	Cell Signaling Technology	Rabbit Polyclonal	1:1000	Overnight at 4^0C
Phospho-JNK	Cell Signaling Technology	Rabbit Polyclonal	1:2000	Overnight at 4^0C
Phospho-PERK	Cell Signaling Technology	Rabbit Polyclonal	1:1000	Overnight at 4^0C
Phospho-Smad2	Cell Signaling Technology	Rabbit Polyclonal	1:1000	Overnight at 4^0C
Phospho-Smad3	Cell Signaling Technology	Rabbit Polyclonal	1:1000	Overnight at 4^0C
Runx1	Active Motif	Rabbit Polyclonal	1:1000	Overnight at 4^0C
Runx3	Santa Cruz Biotechnologies	Mouse Monoclonal	1:1000	Overnight at 4^0C
Smad2	Cell Signaling Technology	Rabbit Polyclonal	1:1000	Overnight at 4^0C
Smad3	Cell Signaling Technology	Rabbit Polyclonal	1:1000	Overnight at 4^0C
TGF-β	Cell Signaling Technology	Rabbit Polyclonal	1:1000	Overnight at 4^0C
TBRI	Santa Cruz Biotechnologies	Rabbit Polyclonal	1:1000	Overnight at 4^0C
TBRII	Santa Cruz Biotechnologies	Mouse Monoclonal	1:1000	Overnight at 4^0C

Table 2.2. List of primary antibodies

Target	Company	Dilution	Incubation Period
HRP Goat Anti-Rabbit	Zymed Laboratories	1:10000	1h, room temperature
HRP Goat Anti-Mouse	Zymed Laboratories	1:10000	1h, room temperature
HRP Rabbit Anti-Goat	Zymed Laboratories	1:10000	1h, room temperature

Table 2.3. List of secondary antibodies

2.1.2.2 Antibodies for Immunostaining

Target	Company	Reactivity	Dilution	Incubation Period
Flag	Sigma	Mouse	1:1000	2h, room temperature
Runx3	Santa Cruz Biotechnologies	Monoclonal Goat Polyclonal	1:100	2h, room temperature
N-CoR	Santa Cruz Biotechnologies	Goat Polyclonal	1:100	2h, room temperature
PDI	Santa Cruz Biotechnologies	Rabbit Polyclonal	1:100	2h, room temperature

Table 2.4. List of primary antibodies used in immunofluorescent staining

Description	Company	Dilution	Incubation Conditions
Alexa Flour Chicken Anti-Goat 488	Invitrogen	1:200	1hr, Room Temperature
Alexa Flour Chicken Anti-Goat 594	Invitrogen	1:200	1hr, Room Temperature
Alexa Flour Chicken Anti-Mouse 488	Invitrogen	1:200	1hr, Room Temperature
Alexa Flour Chicken Anti-Mouse 594	Invitrogen	1:200	1hr, Room Temperature
Alexa Flour Chicken Anti-Rabbit 488	Invitrogen	1:200	1hr, Room Temperature
Alexa Flour Chicken Anti-Rabbit 594	Invitrogen	1:200	1hr, Room Temperature

Table 2.5. List of secondary antibodies used in immunofluorescent staining

2.1.3 Primer Sequences

2.1.3.1 Semi-quantitative RT-PCR primers

Target gene	Sequence (5'-3')	Annealing temperature (°C)	# Cycles
B2M	Forward: ATCCAGCGTACTCCAAAGAT Reverse: TTACATGTCTCGATCCCACT	58	30
GAPDH	Forward: TGATGACATCAAGAAGGTGG Reverse: TTTCTTACTCCTTGGAGGCC	60	30
NCoR1	Forward: GACTCTGATATGGCAGCTGCTCAG	60	30

	Reverse: GCTGAGCATCCGCATAGTCAGAG		
SMAD2	Forward: GTTCCTGCCTTTGCTGAGAC	60	30
	Reverse: TCTCTTTGCCAGGAATGCTT		
SMAD3	Forward: TGCTGGTGACTGGATAGCAG	60	30
	Reverse: CTCCTTGGAAGGTGCTGAAG		
TGFβ1	Forward: ACCTGCCACAGATCCCCTAT	62	30
	Reverse: CTCCCGGCAAAAGGTAGGAG		
TGFβ2	Forward: TCTTCCCCTCCGAAAATGCC	62	30
	Reverse: ATCGAAGGAGAGCCATTCGC		
TGFβ3	Forward: CGAGCAGAATTCCGGGTCTT	62	30
	Reverse: ATCAAAGGACAGCCACTCGG		
TGFBRI	Forward: CATTTTTCCCAAGTGCCAGT	60	30
	Reverse: ACACCCCTAAGCATGTGGAG		
TGFBRII	Forward: CCATGTCTCACAGCCAGCTA	60	30
	Reverse: CCAGGAGAAATAAGGGCACA		

Table 2.6. List of semi-quantitative RT-PCR primers

2.1.3.2 Real-time PCR Primer Assays (Taqman)

Target gene	Taqman Gene Expression Array ID
HPRT1	Hs02800695_m1
NCoR	Hs01094540_m1
p21	Hs00355782_m1
PAI-1	Hs01126606_m1

Table 2.7. List of Taqman Assays used in Real-Time PCR analysis

2.1.3.3 siRNA sequences

Target gene	Sequence (5'-3')
Luciferase	CGTACGCGGAATACTTCGA
NCoR	AATGCTACTTCTCGAGGAAACA
Smad2 (1)	GCCACAUGUUAUAUAUUGCCGAUUA
Smad2 (2)	UAAUCGGCAAUAUAUAACAUGUGGC
Smad2 (3)	UCUGGAUGACUAUACUCACUCCAUU
Smad3	CCACCAGGAUGCAACCUGAAGAUCU
	AGAUCUUCAGGUUGCAUCCUGGUGG
	AGGACGAGGUCUGCGUGAAUCCCUA
TGFBRI	GCAUCUCACUCAUGUUGAUGGUCU
	UAGACCAUCAACAUGAGUGAGAUG
	GCCAAAUGAAGAGGACCCUUCAUUA
TGFBRII	UCCUGACUUGUUGCUAGUCAUAUUU
	AAAUAUGACUAGCAACAAGUCAGGA
	UCAUCUUCUACUGCUACCGCGUUAA

Table 2.8. List of siRNA sequences used in siRNA mediated knockdown

2.1.4 Gastric Cancer Tissue

2.1.4.1 Human Samples

Gastric cancer tissues were obtained from 10 patients diagnosed with stomach carcinoma. Tissues were collected from the tissue repository of National University Hospital (Singapore) and the use of these samples has been approved by the NUS Institutional Review Board (IRB). Paired tissues were obtained from each patient, one from the tumour region of the resected stomach and the other matching control from adjacent non-tumour (normal) region.

2.1.4.2 Tissue Microarray

The stomach cancer tissue array from US Biomax (ST811) was selected for immunohistochemistry (IHC) studies. It consists of 80 cores - 70 cases of stomach tumor and 10 normal tissue.

2.1.5 Plasmids

2.1.5.1 pACT-NCoR-FLAG

The pACT vector (Promega, USA) is a non-viral mammalian expression vector containing CMV promoter and carries the ampicillin bacterial resistance gene. pACT-NCoR-FLAG consists of 2 tandem repeats of Flag sequence, linked in frame to the C-terminus of mouse N-CoR sequence and cloned into the vector at *Nco*1 and *Xba*1 sites.

2.1.5.2 IgCα promoter construct

The TGF-β-responsive element (TβRE) promoter reporter construct, generously provided by Dr. Ko Tun Kiat (Cancer Science Institute, Singapore), was derived from the mouse germline Ig Cα promoter and contained three tandemly repeated wild-type TβREs of the Ig Cα promoter fused to a heterologous c-Fos and luciferase reporters. All of the polymerase chain reaction products were sequenced [69].

2.1.5.3 pACT-RUNX1/RUNX2/RUNX3

pACT-RUNX plasmids were kindly provided by Professor Yoshiaki Ito (National University of Singapore), and were constructed as previously described [68].

2.1.6 Cell Lines

2.1.6.1 Human Gastric Cancer Cell Lines

SNU-5 and SNU-16 cell lines were generous gifts from Dr Ayumi Yamada. All other human gastric carcinoma cell lines (SNU-1, SNU-620, SNU-719, SCH, MKN1, MKN7, MKN28, MKN74, TMK1, NUGC3 and AZ52) were kindly provided by A/Prof Richie Soong (Cancer Science Institute, National University of Singapore, Singapore).

2.1.6.2 Non-gastric Cancer Cell Lines

HEK 293T (Human Embryonic Kidney) cells were purchased from the American Type Culture Collection, USA. P19 murine embryonal carcinoma cells were kindly provided by A/Prof Motomi Osato (Cancer Science Institute, Singapore). HFE-145, an immortalized human normal gastric epithelial cell

line, was generously gifted by A/Prof Richie Soong (Cancer Science Institute, Singapore).

2.1.7 Drugs

2.1.7.1 Artemisinin

Artemisinin derivatives (GC001, GC003, GC006, GC008, GC009, GC010, and GC011) were synthesized and generously provided by our collaborator, Professor Richard K. Haynes (Hong Kong Science and Technology University, Hong Kong). The derivatives used in this study were prepared according to the literature methods [103,179]. The derivatives were reconstituted in dimethyl sulfoxide (DMSO) to a stock concentration of 25 mM and kept in aliquots at 4°C.

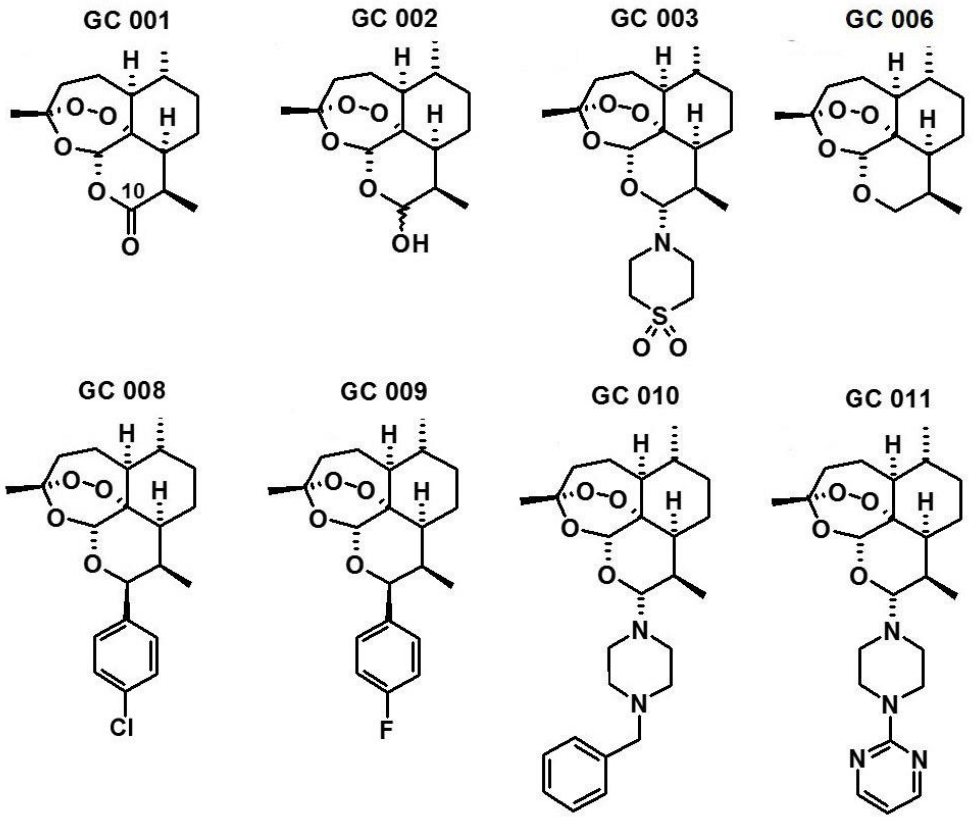

Figure 2.1. Chemical structures of artemisinin derivatives used

2.1.7.2 Bortezomib

Bortezomib (LC Laboratories, Woburn, MA), a specific and reversible proteasome inhibitor, was reconstituted in DMSO to a stock concentration of 10 mM and kept in aliquots at -20°C.

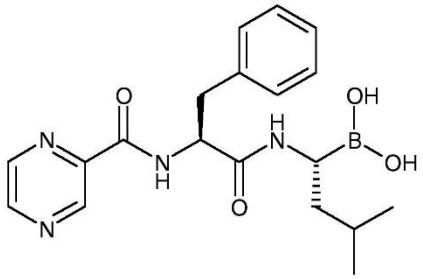

Figure 2.2 Chemical structure of Bortezomib

2.1.7.3 LY2157299

LY2157299 (Selleck Chemicals, US) is a selective small molecule transforming growth factor beta receptor kinase inhibitor with IC50 of 86 nM and 2 nM for TβRI and TβRII respectively. LY2157299 was reconstituted in DMSO to a stock concentration of 20 mM, and subsequently kept at -20°C.

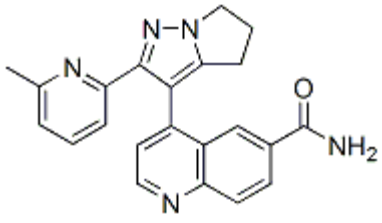

Figure 2.3 Chemical structure of LY2157299

2.1.7.4 Recombinant human TGFβ1

Recombinant Human TGF-β1 (R&D Systems, Abingdon, UK) was reconstituted in sterile 4 mM HCl containing 1 mg/mL bovine serum albumin to a stock concentration of 20 µg/mL, and subsequently kept at -20°C.

2.2 Methods

2.2.1 Cell Culture Treatment

2.2.1.1 Maintenance of Cell Lines

All gastric cancer cell lines and HFE-145 cell line were maintained in RPMI 1640 enriched with 10% heat-inactivated fetal bovine serum (FBS), in a humidified atmosphere of 5% CO2 at 37°C. 293T and P19 cells were cultured in DMEM supplemented with 10% heat-inactivated FBS in a humidified atmosphere of 5% CO2 at 37°C. For subculturing, cells were either directly split into new flasks containing fresh media at an appropriate split ratio, or if adherent, trypsinized with 0.05% trypsin-EDTA first, and then resuspended with culture media and split into new flasks containing fresh media. Cells were typically passaged every 2-3 days, before reaching confluency.

2.2.1.2 Cryopreservation of Cell Lines

For cryopreservation of cells, suspension cells were centrifuged at 200 g for 5 minutes, while adherent cells were trypsinized with 0.05% trypsin-EDTA prior to centrifugation, and cell pellets were resuspended in sterile-filtered freezing medium [90% (v/v) of heat-inactivated FBS, 10% (v/v) DMSO] at a cell density not exceeding 1 X 10^6 cells/mL. 1 mL cell suspensions were then aliquoted into sterile cryovials and placed into cryofreezing containers. The cells were then gradually frozen at a rate of 1°C/min in a -80°C freezer overnight. Cryovials were then transferred into liquid nitrogen for long term storage.

2.2.1.3 Thawing of Cells

Cryovials containing the cells were removed from liquid nitrogen storage and immediately transferred to a 37°C water bath to be thawed rapidly. An appropriate volume of pre-warmed culture media were added to the cell suspensions and centrifuged at 200 g for 5 min to remove traces of DMSO. The cells were then resuspended in fresh culture media and transferred to new flasks and subsequently incubated in a humidified atmosphere of 5% CO2 at 37°C.

2.2.1.4 Treatment of cells with drugs

Cells were seeded at a density of 2-4 X 10^5 cells/mL on sterile tissue culture plates, depending on the treatment and doubling time of the cells. The drugs (GC011, Bortezomib, TGF-β or LY2157299) and control vehicles were then diluted in complete growth medium to the required concentrations and added to the cells at the appropriate time-points. For adherent cell lines, cells were allowed to grow and attach overnight in a humidified atmosphere of 5% CO2 at 37°C prior to treatment.

2.2.1.5 Transfection of Cells

2.2.1.5.1 Transfection of 293T cells using Fugene 6

Transfection of 293T cells using Fugene 6® tranfection reagent was carried out according to the manufacturer's protocol. Cells were seeded at a density of 2 X 10^5 cells/mL on a 10-cm tissue culture plate and incubated overnight at 37°C and 5% CO_2. Approximately 18-22 hours after seeding, transfection was carried out. Briefly, 18 µl of Fugene 6 was diluted in 582 µL of serum-free

media and incubated for 5 minutes at room temperature. 6 µg of total DNA was then added to the diluted Fugene 6 and allowed to incubate for 15 minutes at room temperature. The DNA-Fugene 6 complex was then added dropwise to each plate of cells. Cells were assayed for analysis 48 hours post-transfection.

2.2.1.5.2 Transfection of P19 cells and SNU16 cells using Lipofectamine 2000

Cells were seeded at a density of 1 X 10^5 cells/mL (for P19) or 2 X 10^5 cells/mL (for SNU16) in serum-free DMEM in a 6-well plate. For each well of cells, 100 pmol of target and mock siRNA (refer to Table 8), or 2 µg of total DNA was diluted in OptiMEM® medium I to a total volume of 250 µl. 5 µl of Lipofectamine 2000 was diluted in 250 µl of OptiMEM® I medium and incubated for 5 minutes at room temperature. The diluted siRNAs and Lipofectamine 2000 was then combined and incubated at room temperature for 20 minutes to allow siRNA-Lipofectamine 2000 complexes to form. The complexes were then added to the cells and incubated for 4 hours at 37°C and 5% CO2 before replacing the media with DMEM supplemented with 10 % FBS. Cells were then assayed 48 hours post-transfection.

2.2.2 Analysis of Proteins

2.2.2.1 Total Protein Extraction from cells

Two lysis buffers were used to prepare cell lysates. Cells were firstly trypsinized (for adherent cells only) and cell pellets were then collected by centrifuging at 200g for 5mins at 4°C. The resulting pellets were rinsed twice with ice-cold 1X PBS (137 mM NaCl, 2.7 mM KCl, 4.3 mM NaH_2PO_4, 1.4 mM KH_2PO_4, pH7.4). The cells were then lysed using either 1 X SDS sample

buffer [250mM Tris-HCl (pH6.8), 40% glycerol, 9.2% SDS, 0.01% bromophenol blue, 20% β-mercaptoethanol] or CelLytic™ M reagent (supplemented with protease inhibitor cocktail tablet, 1 mM AEBSF, 1% (v/v) Phosphatase Inhibitor Cocktail 1 & 2). For cells lysed with 1 X SDS sample buffer, cells were lysed with 5 X pellet volume of the buffer. Cells were then sonicated twice at 5W for 10 seconds on ice (Branson Sonifier 150). The cell lysates were then heat inactivated at 50°C for 10 mins and subsequently stored at -80°C until further use. For cells lysed with the CelLytic M Reagent, appropriate volumes of the reagent were added to each pellet and cell lysates were sonicated at 5W on ice for 10 seconds twice. Lysates were then centrifuged at maximum speed for 20 minutes at 4°C to remove cellular debris, and supernatants were collected. Protein concentration was determined using BCA protein assay and 4 X SDS sample buffer was added to the lysates to a final 1 X SDS concentration. Lysates were then heat inactivated at 50°C for 10 minutes and subsequently stored at -80°C until further use.

2.2.2.2 Nuclear and Cytoplasmic Extraction of Protein from cells

Nuclear and cytoplasmic extracts of cells were prepared using Active Motif Nuclear Extract kit, according to the recommended protocol. Growth medium was first removed from cells and cells washed with PBS/phosphatase inhibitors. Cells were then gently scraped in PBS/phosphatase inhibitors and centrifuged at 500 rpm for 5 minutes. The cell pellets were then resuspended in 1 X Hypotonic Buffer and incubated on ice for 5 minutes. Detergent was added and suspension was vortexed to mix. Centrifugation was then performed at 14 000 x g for 30 seconds at 4°C and upernatants (cytoplasmic fraction) collected. Nuclear pellets were then resuspended in Complete Lysis

Buffer and vortexed for 10 seconds at the highest setting, followed by incubation on ice for 30 minutes on a rocking platform set at 150 rpm. Suspensions were then vortexed for 30 seconds at the highest setting, centrifuged for 10 minutes at 14 000 x g at 4°C and supernatants (nuclear fraction) collected. All supernatants were then sonicated twice at 5W for 10 seconds on ice and protein concentration was determined. 4 X SDS sample buffer was added to a final 1 X SDS concentration. Lysates were then heat inactivated at 50°C for 10 minutes and subsequently stored at -80°C until further use.

2.2.2.3 Protein Solubility Assay

Cells were pelleted at 300 g for 5 min and then resuspended in cell lysis buffer [50 mM Tris-HCl (pH 8.8), 100 mM NaCl, 5 mM $MgCl_2$, 0.5% NP-40, 1 μg/ml pepstatin, 1 μg/ml aprotinin, 200 μM AEBSF] before rotation at 4°C for 45 min. The soluble fraction (supernatant) was then separated from the insoluble fraction (pellet) by centrifugation at 20000 g for 10 minutes. The pellet was then resuspended in pellet buffer [20 mM Tris-HCl (pH 8.0), 15 mM $MgCl_2$, 1 μg/ml pepstatin, 1 μg/ml aprotinin, 200 μM AEBSF] and treated with DNase I for 30 min at 37°C. 4 X SDS sample buffer was then added to the fractions to a final 1 X concentration and subsequently heat-inactivated at 50°C for 10 minutes. Proteins were resolved with SDS-PAGE and transferred to PVDF membranes for western blotting. Coomassie blue staining was used to check for cross contamination between insoluble and soluble fractions.

2.2.2.4 Immunoprecipitation

Cells were collected by centrifugation at 200 g for 5 minutes, and washed in cold 1 X PBS. Cells were then lysed in IP buffer (20mM Tris pH7.4, 300mM NaCl, 0.5% NP-40, 1mM EDTA, 200µM AEBSF, 1 tablet/50ml cOmplete protease inhibitor cocktail, 1mM NaF, 20mM β-Glycerolphosphate, 10ul/ml Phosphatase Inhibitor Cocktail I, 10µl/ml Phosphatase Inhibitor Cocktail 2) at an appropriate volume (500 µl for every 10-cm plate). Lysates were sonicated twice at 5W for 10 seconds on ice and then centrifuged at 850 g for 5 minutes at 4°C. 100 µl of the lysate was heat inactivated at 50°C for 10 minutes and subsequently stored at -80°C to be analysed for loading input. Immunoprecipation was then carried out on the remaining supernatants with 10 µg of anti-Flag, anti-N-CoR antibody or normal goat IgG by rotation for 2.5 hours at 4°C. Protein G sepharose beads which were prepared by washing in IP buffer and resuspending in IP buffer were then added to each sample and lysates were rotated for another 1.5 hours. The bound protein-Protein G were then collected by centrifugation at 850 g for 5 minutes and washed 4 times with IP buffer. The bound protein was then released by the addition of 2 X SDS sample buffer to a final concentration of 1 X SDS. The samples were again centrifuged at 850 g for 5 minutes to remove protein G beads. The remaining supernatants were then heat inactivated at 50°C for 10 minutes and stored at -80°C until further analysis.

2.2.2.5 Protein Quantification

Protein quantification was carried out using Pierce® BCA Protein Assay kit, according to manufacturer's instructions. 200µl of the working reagent was

added to 5 µl of BSA standards or unknown samples in a 96-well plate and incubated at 37°C for 30 minutes. Absorbance was then measured at 562 nm on a plate reader and concentration was calculated against the BSA standard curve.

2.2.2.6 SDS PAGE

Cell lysates were resolved using the SDS-PAGE Bio-Rad Mini-Protean II system. Denaturing polyacrylamide gels were cast using a mini-Protean gel caster. Resolving gels (refer to Table 10) were prepared and allowed to set for 30 minutes. Stacking gels (refer to Table 10) were then prepared and allowed to set for another 30 minutes before being assembled into the electrophoresis chamber. The inner and outer chambers of the unit were then filled with ice-cold 1 X SDS-PAGE running buffer (25mM Tris-Base, 192 mM glycine, 0.1% SDS w/v). Protein samples were then loaded into the wells and electrophoresis was carried out at 4°C at a constant current of 10 mA through each stacking gel and increased to 20 mA through each resolving gel. After electrophoresis, the gels were either subjected to Western Blotting or stained with Coomassie Blue for 30 minutes at room temperature for visualization of total protein.

	Resolving Gel					**Stacking Gel**
Component	**6%**	**8%**	**10%**	**12%**	**15%**	**5%**
Water	5.3	4.6	4.0	3.3	2.3	6.8
30% Acrylamide/Bis (ml)	2.0	2.7	3.3	4.0	5.0	1.71
1.5 M Tris-HCl, pH 8.8 (ml)	2.5	2.5	2.5	2.5	2.5	-
0.5 M Tris-HCl, pH 6.8 (ml)	-	-	-	-	-	1.25
10% Sodium dodecyl sulphate (SDS) [ml]	0.1	0.1	0.1	0.1	0.1	0.1
10%	0.1	0.1	0.1	0.1	0.1	0.1

Ammomium persulfate (APS) [ml]						
TEMED (µl)	8	6	4	4	4	10
Total volume (ml)	**10**	**10**	**10**	**10**	**10**	**10**

Table 2.9. Preparation of SDS-PAGE denaturing gels

2.2.2.7 Western Blotting

After electrophoresis, resolved proteins were transferred onto pre-wet PVDF membranes using the wet transelectroblotting system (Bio-Rad, US) in ice-cold 1 X transfer buffer (48 mM Tris-base, 37 mM Glycine, 0.037% SDS w/v, 10% MeOH v/v) at a constant current of 75 mA for 2 hours at 4°C. The membrane was then blocked with 5% skimmed milk powder in PBS-T (1 X PBS, 0.01% Tween-20) at room temperature for 1 hour. The membrane was then incubated with the primary antibody at the appropriate dilutions in 5% milk/PBS-T (refer to Table 2) overnight at 4°C. Membranes were then washed 4 X 5 minutes in PBS-T before incubation with secondary antibodies in 2.5% milk/PBS-T for 1 hour at room temperature (refer to Table 3). Membranes were again washed 6 X 5 minutes in PBS-T before detection with enhanced chemiluminescent reagents and exposure to Fuji X-Ray film. After immunodetection, membranes were stripped of the bound antibodies using stripping buffer (200 mM glycine, 1% SDS, pH 2.5) for 30 minutes at room temperature, blocked in 5% mik/PBS-T and reprobed with other antibodies if needed.

2.2.3 Cell Based Assays

2.2.3.1 Cell Proliferation Assay

2.2.3.1.1 Cell Proliferation kit I [3-(4,5-dimetylthiazol-2-yl)-2,5-diphenyltetrazolium bromide (MTT)]

The cell proliferation assay was carried out according to the manufacturer's protocol. Cells were seeded into 96-well plates at 8 X 10^3 cells per well in 100µl culture medium containing different concentrations of the drug tested. Cells were then incubated at 37°C and 5% CO_2 for the durations stated. MTT substrate was then added to the cells and incubated at 37°C for 4 hours, followed by the addition of the lysis reagent for 18 hours at 37°C. The spectrophotometric absorbance was measured using a microplate reader (Ultramark, Bio-Rad, Hercules, CA) using a wavelength of 595 nm with a reference wavelength of 655 nm.

2.2.3.1.2 CellTiter 96® AQueous One Solution Cell Proliferation Assay (MTS)

The cell proliferation assay was carried out according to the manufacturer's protocol. Cells were seeded into 96-well plates at 8 X 10^3 cells per well in 100µl culture medium containing different concentrations of the drug tested. Cells were then incubated at 37°C and 5% CO_2 for the durations stated. 10 µl of the MTS reagent was added to each well and incubated at 37°C for 3 hours. Absorbance was subsequently recorded at 490 nm on a microplate reader (Ultramark, Bio-Rad, Hercules, CA).

2.2.3.2 Immunofluorescent Staining

For suspension cells, 100-200 µl of cells were cytospun onto Shandon cytoslides® at 1000 rpm for 5 minutes in a cytospin centrifuge. For attached cells, cells were seeded onto cover slips placed in a 6-well tissue culture plate and allowed to attach overnight at 37°C and 5% CO_2. Cells were then fixed

with 4% paraformaldehyde at 37°C, washed with 1 X PBS, and permeabilized with 0.2% Triton X-100 in 1 X PBS for 5 minutes on ice. After washing a further three times in 1 X PBS, cells were blocked with 5% BSA/PBS for 30 minutes. Cells were then stained with primary antibody (refer to Table 4) at 1:100 dilution in 5% BSA/PBS for 2 hours, washed with 1 X PBS, and incubated in the dark with fluorescence-labelled secondary antibodies (refer to Table 5) at 1:200 dilution in 2.5% BSA/PBS for 1 hour. After washing three times in 1 X PBS, the cell nuclei were then counterstained with 150 nM 4',6-diamidino-2-phenylindole (DAPI) in 5% BSA/PBS for 5 minutes. Cells were then mounted with SlowFade® Gold antifade reagent and coverslips were sealed. Images were subsequently visualized and captured using AxioPlan 2 imaging fluorescence microscope (Carl Zeiss).

2.2.3.3 Immunohistochemistry staining

Immunohistochemical staining of tissue microarray was done using the goat ImmunoCruz™ Staining System, according to manufacturer's protocol. The tissue microarray slides were firstly baked at 60°C for 10 min to melt the wax and improve adhesion before staining. Heat treatment was then applied for antigen retrieval by soaking slides in 10 mM sodium citrate buffer, pH 6.0 at 95°C for 10 minutes. Slides were then allowed to cool in buffer for 20 minutes, before washing in deionized H_2O three times for 2 minutes each. Excess liquid was then removed carefully from the sides of the slides between each wash. Endogenous peroxidise activity was quenched with 1-3 drops of peroxidase block, followed by rinsing in PBS for 2 minutes. The slides were then incubated in serum block for 20 minutes, followed by incubation with 5 µg goat anti-N-CoR antibody for 2 hours at room temperature. The slides were

then rinsed twice in PBS for 2 minutes each. Next, the slides were incubated for 30 minutes in 1-3 drops of biotinylated secondary antibody, and again rinsed in PBS twice for 2 minutes each. The slides were then incubated in 1-3 drops of HRP-streptavidin complex for 30 minutes and rinsed twice in PBS for 2 minutes each. The slides were then further incubated with HRP Substrate chromogen solution for 5 minutes and rinsed in deionized H_2O for 2 minutes. Slides were counterstained with Mayer's hematoxylin for 10 seconds and immediately washed several times with deionized H_2O. Slides were then finally mounted with SlowFade® Gold antifade reagent and covered with coverslips. Images were subsequently visualized and captured using AxioPlan 2 imaging fluorescence microscope (Carl Zeiss).

2.2.3.4 Detection of Apoptosis by Flow Cytometry

Detection of phosphatidylserine (PS) on the outer leaflet of apoptotic cells was performed using Annexin V-FITC Apoptosis Detection Kit according to the manufacturer's recommendations. Briefly, cells were collected and pellets were washed once with ice-cold 1 X PBS. Cell pellets were then resuspended in 1 X Annexin V binding buffer at a concentration of 1 X 10^6 cells/ml. 5 µl of FITC conjugated anti-Annexin V antibody and Propidium Iodide were added to 100 µl of the cell suspension. Mixture was then vortexed gently and incubated for 15 minutes in the dark at room temperature. 400 µl of 1 X Binding Buffer was then added to each sample and cells were analysed by flow cytometry within an hour. Flow cytometry was performed using fluorescence-activated cell sorting (BD LSR II Flow Cytometer, NJ, USA).

2.2.3.5 In vivo ubiquitination assay

293T cells were transfected with 2 μg of pact-N-CoR-FLAG expression vector, 2 μg of pcDNA3-Myc-Ub expression vector and 2 μg of either pact-RUNX1, pact-RUNX3 or empty actin vector. Thirty hours after transfection, the cells were treated with 10 μM MG132 for another 12 hours. Immunoprecipitation was then carried out as per Section 2.2.2.3.

2.2.4 Gene Expression Analysis

2.2.4.1 RNA extraction

Purification of total RNA was carried out using RNeasy® Mini Kit protocol. Up to 1 x 10^7 cells, depending on the cell line, were disrupted in Buffer RLT, a highly denaturing guanidine-thiocyanate containing buffer which inactivates RNases (0.01% β-mercaptoethanol was added before use) by homogenizing with needle and syringe. 1 volume of 70% ethanol was then added to the homogenized lysates before being applied to the RNeasy Mini spin columns for binding of RNA to the resin. The RNA-resin was then washed with DNase I containing buffer RW1 to remove DNA and protein contaminants. Purified RNA was finally eluted in 30 μl of DEPC treated water and its concentration determined using Nanodrop Spectrophotometer ND-1000 (Thermo Fisher Scientific, Lafayette, CO, USA). All binding, washing, and elution steps were performed by centrifugation at 10,000 rpm at room temperature.

2.2.4.2 Reverse transcription

3 μg of purified RNA was used for cDNA synthesis using RT-PCR System kit. To each sample, 3 pmoles of oligo-dT (18-mer) and DEPC-treated water

was added to a final volume of 21 µl and incubated at 65°C for 15 minutes before immediately quenching on ice. 10 µl of 5 X RT buffer, 1 µl of 25 mM dNTPs, 0.5 µl of RNasin Inhibitor, 1 µl of murine reverse transcriptase and sterile water were then added to each sample. Samples were further incubated at 42°C for 1 hour to generate cDNA. cDNA synthesis was completed after inactivation of transcriptase by incubation at 95°C for 5 minutes. cDNAs were then stored at –20°C until subjected to semi-quantitative PCR or real-time PCR analysis.

2.2.4.3 Semi-quantitative Polymerase Chain Reaction (PCR)

A PCR mastermix (1.5 mM of $MgCl_2$, 1 X Green GoTaq® Reaction Buffer, 0.2 mM of each dNTP, 1 µM of each downstream and upstream primer, 1.25 units of GoTaq® DNA Polymerase and nuclease-free water topped up to 49 µl per reaction) was prepared and added to 1µl of cDNA template diluted 1:10 in nuclease-free water for a total reaction volume of 50 µl per sample. PCR amplification was carried out under conditions as stated in Table 2.10 using Thermal Cycler GeneAmp®PCR System 9600 (Applied Biosystems, CA, USA). Depending on the primers, the annealing temperature and number of cycles were optimized accordingly (Refer to Table 2.6).

Steps	Temperature (°C)		Time
1. Initializing	94		5 mins
2. Denaturation	94	30 cycles	30s
3. Annealing	*		30s
4. Extension/Elongation	72		30s
5. Final Elongation	72		7 mins
6. Final Hold	4		∞

Table 2.10. PCR amplification steps.
*** Refer to Table 2.6 for annealing temperatures for each primer**

2.2.4.4 DNA agarose gel electrophoresis

Agarose gel electrophoresis was carried out to analyse PCR products. 1-2 % w/v agarose gel (1-2 g of electrophoretic grade agarose powder in 100 ml 1 X TAE buffer [40 mM Tris-acetate (pH 7.8), 1 mM EDTA]) stained with GelRed™ Nucleic Acid gel stain (Biotium) at a 1:10000 dilution were prepared. PCR products were then resolved by electrophoresis in 1 X TAE buffer at 100V for 25 minutes. Gene expression levels were then visualized under trans UV on the Gel Doc System (Bio-Rad, CA,USA).

2.2.4.5 Real-time PCR

Real time PCR analysis was carried out using the Taqman® Gene Expression Assay System (Applied Biosystems, CA,USA) and Ct values were recorded using the ABI Prism 7300 Real Time PCR system (Applied Biosystems, CA, USA). The PCR reaction and PCR conditions used are as listed in Table 2.11 and 2.12 respectively.

Component	**Volume used per reaction (µl)**
2 X Taqman Universal PCR master mix	12.5
20 X Primer Mix	1.25
Nuclease-Free Water	10.25
cDNA (diluted 1:3 in nuclease-free water)	1
Total Volume	25

Table 2.11. Real Time PCR Reaction using the Taqman® Gene Expression Assay System.

Step	**Temperature (0C)**	**Time**	**Number of Cycles**
Initial denaturation	95	10 min	1
Denaturing	94	15 s	40
Annealing	60	1 min	
Elongation	60	10 min	1

Table 2.12. PCR conditions using the ABI Prism 7300 system.

Data was analysed using the ddcT study protocol, in which the comparative Ct method was employed ($\Delta\Delta Ct = \Delta Ct_{,sample} - \Delta Ct_{,reference}$). Untreated samples were used as reference samples and Ct values of both reference and target samples were normalized to that of the endogenous housekeeping gene HPRT. Expression levels in the reference sample for all genes were set to 0.

2.2.5 Proteosome Activity Assay

Measurement of proteosomal activity in MKN74 cells treated with Bortezomib was carried out using Proteosome Glo™ Assay system, which measures three proteolytic activities associated with the proteasome - chymotrypsin-like, trypsin-like, and caspase-like. components. The luminogenic substrates provided for the chymotrypsin-like, trypsin-like, and caspase-like activities are Suc-LLVY- aminoluciferin, Z-LRR-aminoluciferin, and Z-nLPnLD-aminoluciferin, respectively. Substrate cleavage generates a "glow-type" luminescent signal produced by the luciferase reaction. Briefly, cells were trypsinized, washed 2 X with complete medium, and resuspended in complete medium adjusted to the desired density. 2000 cells were seeded into each well in 25 µl of complete medium and returned to the incubator until measurement was to be carried out. The Proteosome-Glo™ Cell-Based reagents and plate containing cells were then allowed to equilibrate to room temperature. 25 µl of each of the Proteosome-Glo™ Cell-Based reagent was added to well. Samples were then shaken at 700 rpm for 2 minutes and incubated at room temperature for 10 minutes. Luminescence was then measured using a microplate reader (Ultramark, Bio-Rad, Hercules, CA).

2.2.6 Luciferase Reporter Assay

P19 cells were transfected with the Ig Cα promoter reporter construct and target DNA using Lipofectamine 2000 (Invitrogen, Lidinggo, Sweden), according to the protocol provided by the manufacturer (refer to 2.2.3.2). The cells were harvested 48 hours post-transfection, and Firefly and *Renilla* luciferase activities were assayed with the Dual-Luciferase Reporter Assay System (Promega, Madison, WI, USA), according to manufacturer's instructions. In brief, growth medium was removed from cells and cells were then washed briefly with 1 X PBS. 500 µL of 1 X PLB was added to each well and plates were then placed on a rocking platform for 15 minutes at room temperature. Lysates were then transferred into microcentrifuge tubes and cleared of cellular debris by centrifugation at high speed for 30 seconds at 4°C. 20 µl of each of the PLB lysates were then transferred into the luminometer tubes containing 100 µl of LAR II and mixed by pipetting up and down 2-3 times. The firefly luciferase activity was then recorded. 100 µl of Stop & Glo® Reagent was then added to each tube, and vortexed briefly to mix. The *Renilla* luciferase activity was then recorded. Firefly luciferase activity was normalized with respect to the *Renilla* luciferase activity.

CHAPTER 3

Results

3.1 GC011, an artemisinin derivative, selectively attenuates growth of TGF-β-sensitive gastric cancer cells by inhibiting N-CoR-induced repression of TGF-β apoptotic signaling pathway.

3.1.1 Artemisinin derivatives demonstrate differential cytotoxicity on human gastric cancer cell lines SNU5 and SNU16.

It has been reported that artemisinin and its derivatives demonstrate differential anti-malarial activities.[103,179] In recent years, artemisinin derivatives have also emerged as a novel class of anti-cancer agent with pleiotropic anti-cancer responses in many types of cancer cells. Despite the mounting evidence of its antineoplastic properties, only one study had tested the artemisinin compounds on gastric cancer cells.[180] Furthermore, while artemisinins have been shown to affect various cellular molecular pathways involved in several hallmarks of malignancy, none has yet been reported in gastric cancer cells. Due to this lack of evidence, this present study aims to investigate the anti-tumor effects of artemisinins in gastric cancer cells and elucidate the molecular cellular pathway involved.

Firstly, to investigate if artemisinin derivatives differ in their anti-tumor activities against gastric cancer cells, we performed a small-scale screening of a panel of seven 10-aminoartemisinin compounds (Fig. 2.1 & 3.1) against human gastric cancer cell lines SNU16 and SNU5, the prototypic TGF-β sensitive and resistant gastric cancer cell lines respectively, using a wide range of drug concentrations and incubation periods. MTT assay was performed to compare the effects of these derivatives on the cell viability of these cell lines. The TGF-β sensitive cell line SNU16 displayed differential cytotoxic profiles

when treated with each artemisinin derivative. Out of the seven derivatives tested, GC003, GC008, GC010 and GC011 inhibited the growth of SNU16 cells in both dose- and time-dependent manner (Fig. 3.2A). These four derivatives demonstrated significant growth inhibitory effects, with IC_{50} values of 3.8 μM, 3.8 μM, 3.9 μM and 2.1 μM at 96 hours respectively (Fig. 3.2B). In particular, GC011 was capable of inhibiting approximately 30% cell growth even with a low dose of 1 μM at 48 hours. In contrast, all the derivatives displayed little or no growth inhibitory effects on the TGF-β resistant cell line SNU5, even at 10 μM concentrations and treatment periods of up to 96 hours (Fig. 3.3). Artemisinin derivative GC011 (Fig. 3.1) is therefore identified as the most potent suppressor of growth of TGF-β sensitive gastric cancer cells SNU-16 among this panel of derivatives.

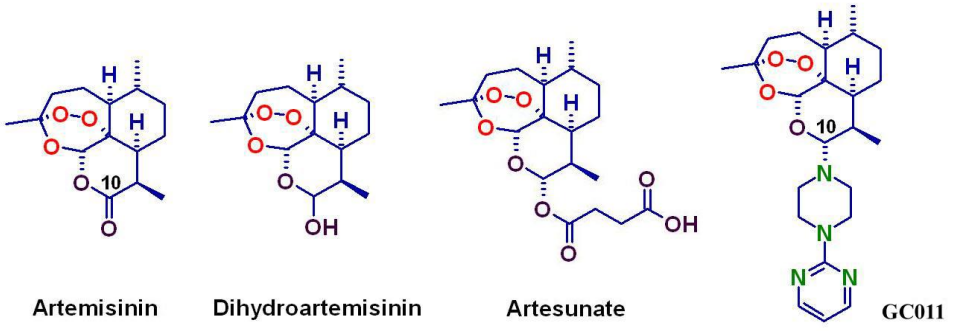

Figure 3.1. Artemisinin and its derivatives dihydroartemisinin and artesunate. The active pharmacophore is the peroxide bridge that bestows antimalarial activity, and the derivatives are now widely used for treatment of malaria. GC011 is a newer derivative prepared from dihydroartemisinin that possesses potent antimalarial activity in *in vitro* screens. The pyrimidinylpiperazinyl unit attached to C10 in GC011 confers enhanced lipophilicity as compared to artemisinin and the derivatives dihydroartemisinin and artesunate.

A

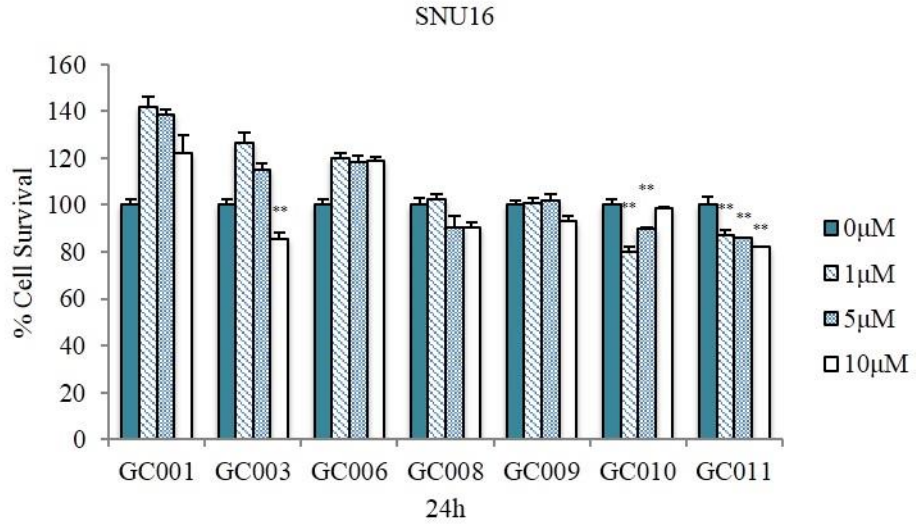
SNU16
% Cell Survival
160
140
120
100
80
60
40
20
0
GC001 GC003 GC006 GC008 GC009 GC010 GC011
24h
0μM
1μM
5μM
10μM

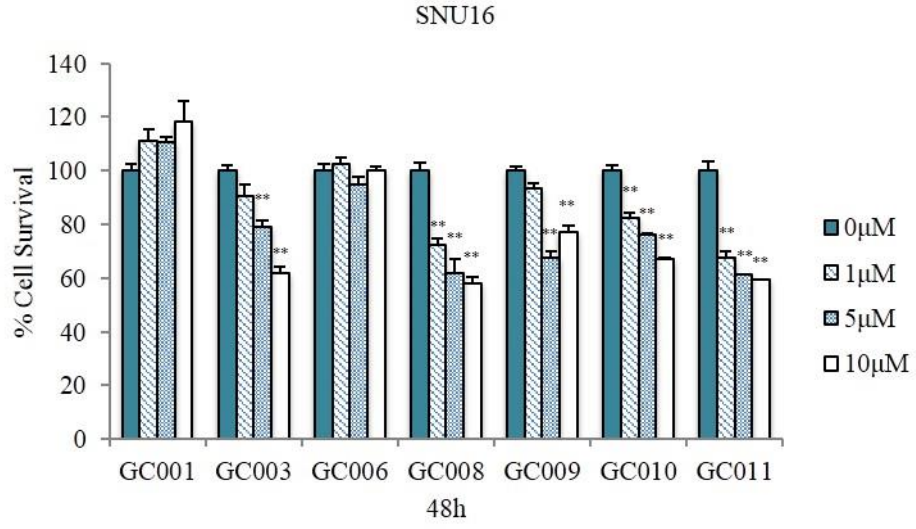
SNU16
% Cell Survival
140
120
100
80
60
40
20
0
GC001 GC003 GC006 GC008 GC009 GC010 GC011
48h
0μM
1μM
5μM
10μM

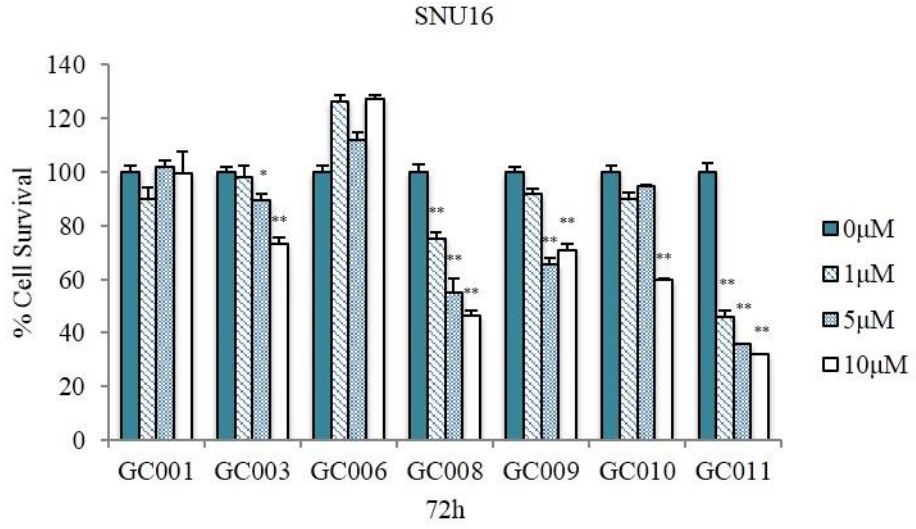
SNU16
% Cell Survival
140
120
100
80
60
40
20
0
GC001 GC003 GC006 GC008 GC009 GC010 GC011
72h
0μM
1μM
5μM
10μM

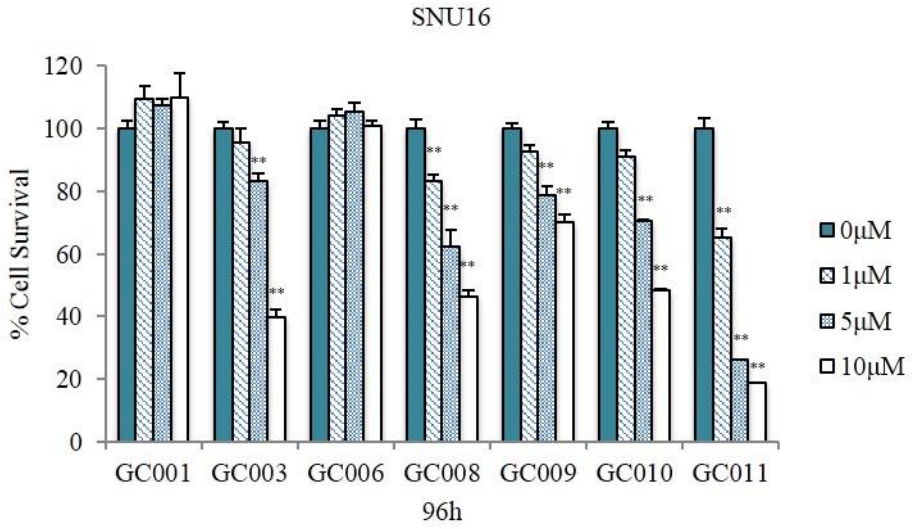

B

Compound	IC_{50} Value (μM) at			
	24 h	48 h	72 h	96 h
GC003	20.4	6.5	9.5	3.8
GC008	16.5	5.4	4.0	3.8
GC010	28.8	7.8	7.1	3.9
GC011	10.9	5.7	2.3	2.1

Figure 3.2. Differential effects of artemisinin derivatives on growth of TGF-β sensitive gastric cancer cell line, SNU16. (A) Growth of SNU16 cells treated with artemisinin derivatives (GC001, GC003, GC006, GC008, GC009, GC010 and GC011) in a dose-dependent manner for a total duration of 24h, 48h, 72h or 96h was determined by MTT assay. The values plotted in bar graph are average of three independent experiments. *$p < 0.05$ and **$p < 0.01$, compared with untreated controls. (B) IC_{50} values at 24, 48, 72 and 96 hours were obtained for all four compounds. All cell lines were cultivated and maintained under the same culture conditions.

A

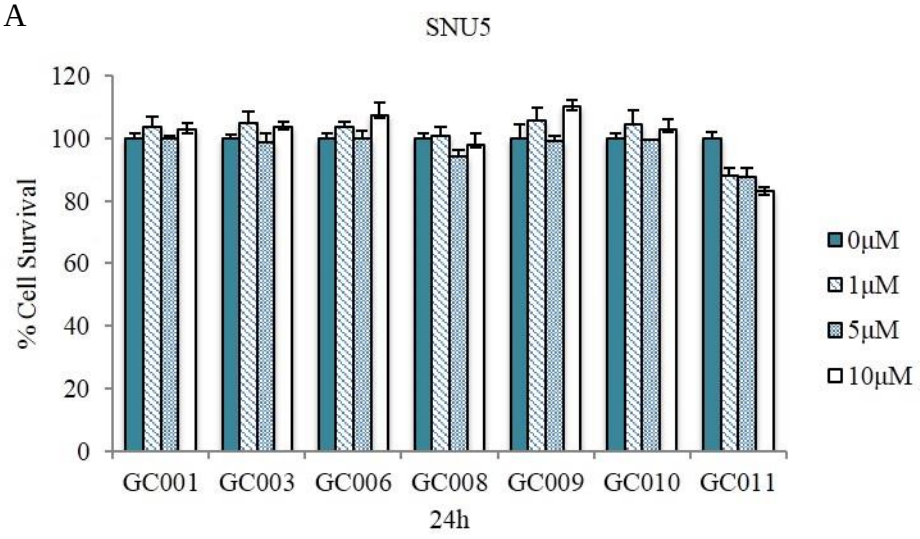
SNU5
120
100
80
60
40
20
0
% Cell Survival
0μM
1μM
5μM
10μM
GC001
GC003
GC006
GC008
GC009
GC010
GC011
24h

B

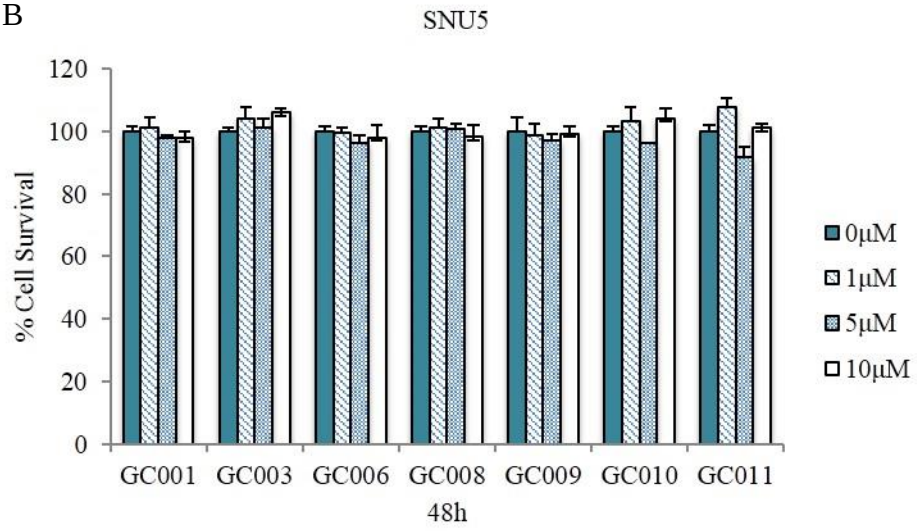
SNU5
120
100
80
60
40
20
0
% Cell Survival
0μM
1μM
5μM
10μM
GC001
GC003
GC006
GC008
GC009
GC010
GC011
48h

C

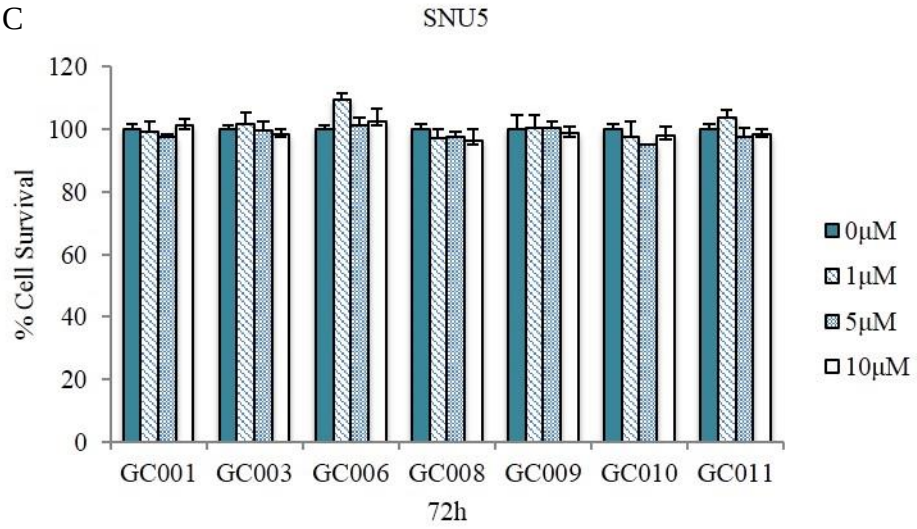
SNU5
120
100
80
60
40
20
0
% Cell Survival
0μM
1μM
5μM
10μM
GC001
GC003
GC006
GC008
GC009
GC010
GC011
72h

D

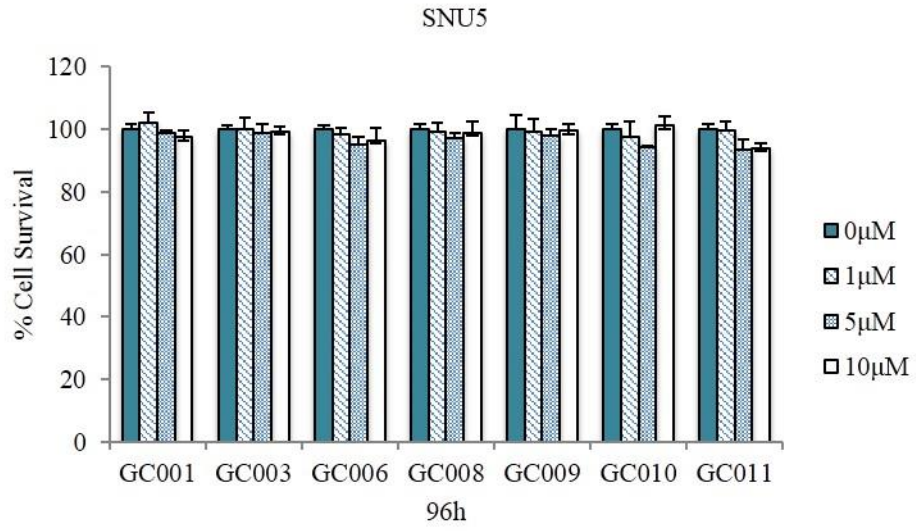

Figure 3.3. Artemisinin derivatives do not promote growth arrest in TGF-β resistant gastric cancer cell line, SNU5. Growth of SNU5 cells treated with artemisinin derivatives (GC001, GC003, GC006, GC008, GC009, GC010 and GC011) in a dose-dependent manner for a total duration of 24h, 48h, 72h or 96h was determined by MTT assay. The values plotted in bar graph are average of three independent experiments.

3.1.2 GC011 inhibits growth of TGF-β-sensitive gastric cancer cells but not in TGF-β-resistant gastric cancer cells or normal gastric cells.

As GC011 displayed a high level of selective cytotoxicity for the TGF-β sensitive gastric cancer cell line SNU16 as compared to TGF-β resistant SNU5 cells, this compound was selected for further testing and its activity screened on a panel of gastric cancer cell lines with differential sensitivity to TGF-β. As demonstrated in Figure 3.4, GC011 promoted a dose-dependent growth inhibition in both SNU16 and another TGF-β sensitive gastric cancer cell line, SNU620,[181-183] whereas gastric cancer cells that are resistant to TGF-β-induced growth inhibition were not sensitive to GC011, suggesting that GC011 may act as a TGF-β agonist. Additionally, both TGF-β and GC011 had no growth inhibitory effects on a normal gastric epithelial cell line, HFE-145, at the doses indicated (Fig. 3.4A & B). In SNU16 cells, the growth inhibition mediated by 1 μM GC011 was close to 35% after 96 hours of treatment, while at 5 uM concentration it was around 73% (Figure 3.4A). At comparable doses and time-points, most TGF-β resistant gastric cancer cells were still resistant to GC011-induced growth inhibition (Figure 3.4A & B). As observed in the initial screening, the proliferation of TGF-β sensitive SNU16 cells was inhibited in a dose-dependent manner with different concentrations of GC011 (0, 1, 5 and 10 μM) at 48, 72 and 96 hours. Treatment with 5 μM and 10 μM of GC011 at different times (24, 48, 72 and 96 hours) demonstrated that cell growth was also inhibited in a time-dependent manner (Figure 3.5A). In contrast, growth of TGF-β resistant SNU5 cells was hardly affected by GC011 (Figure 3.5B).

A

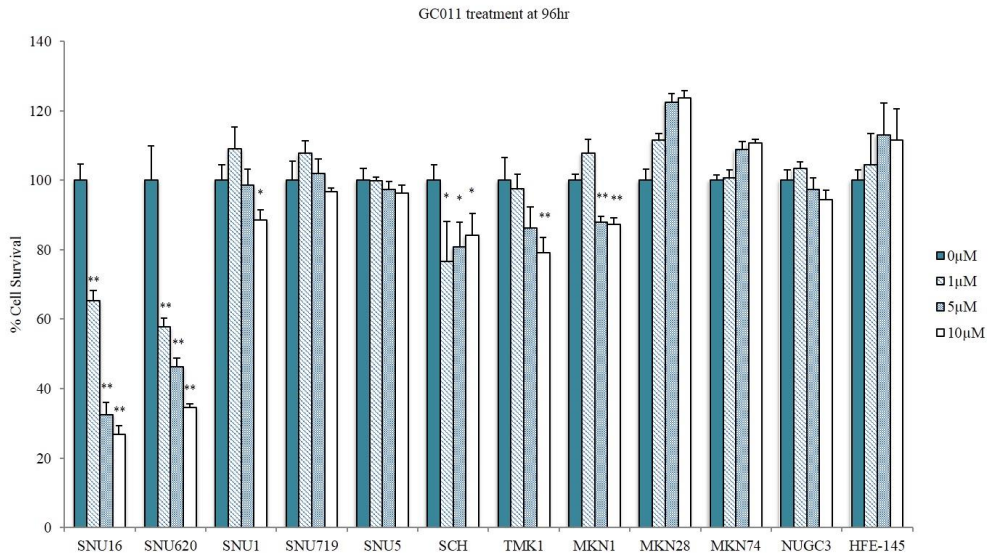

B

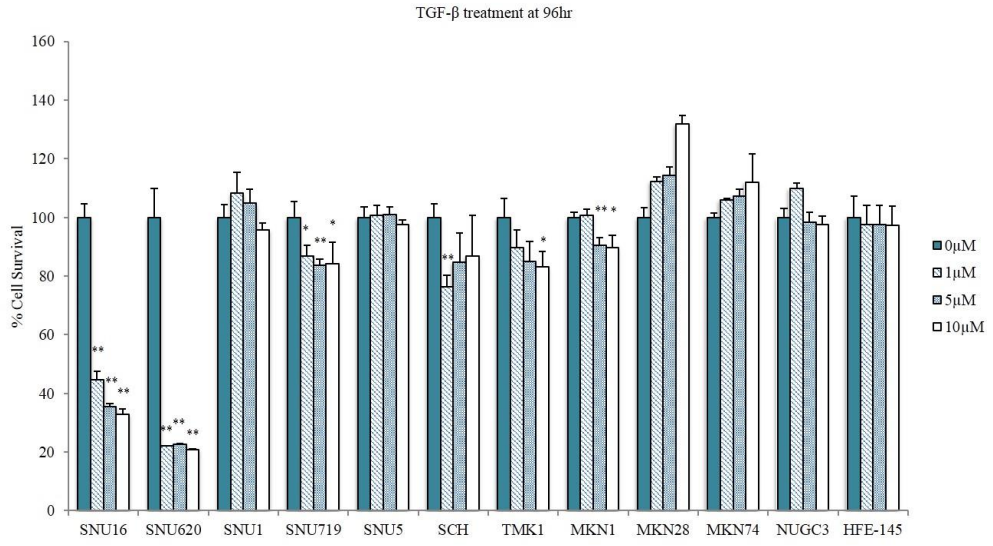

Figure 3.4. GC011 promotes selective growth inhibition in TGF-β sensitive gastric cancer cells but not in TGF-β resistant gastric cancer cells and normal gastric cells. Growth of various gastric cancer cells treated with GC011 (A) or TGF-β (B) in a dose-dependent manner for 96 hours was determined by MTS assay. The values plotted in bar graph are average of three independent experiments. All cell lines were cultivated and maintained under same culture conditions. *$p < 0.05$ and **$p < 0.01$, compared with untreated controls.

A

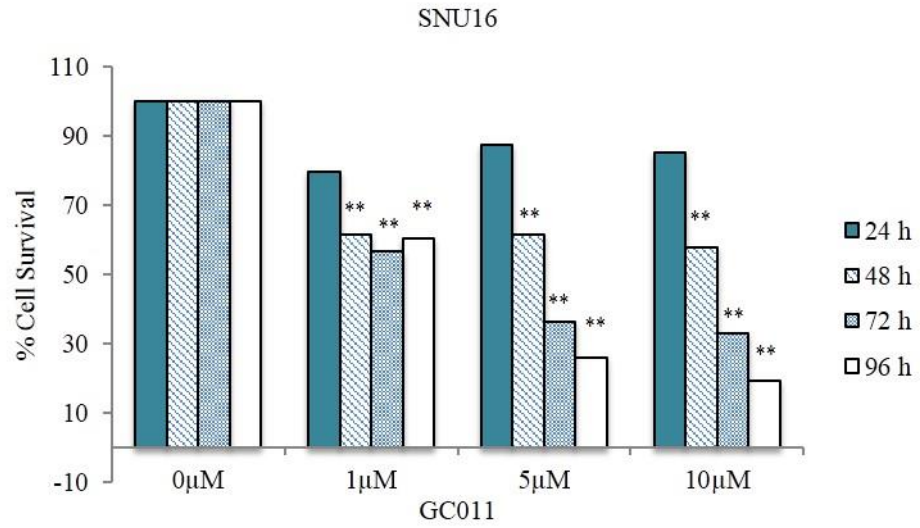

B

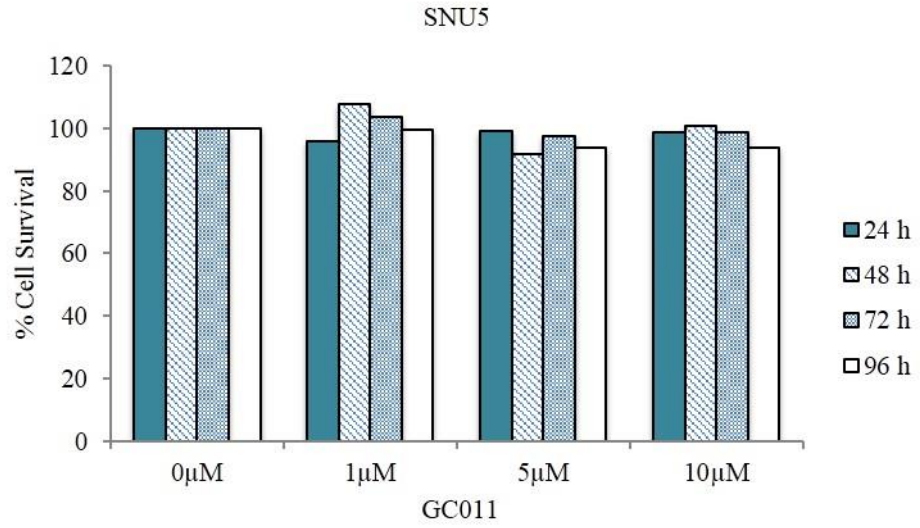

Figure 3.5. GC011 promotes selective growth arrest in TGF-β sensitive gastric cancer cells in a dose- and time-dependent manner. (A) SNU5 and (B) SNU16 cells were treated with various concentrations of GC011 as stated for 24h, 48h, 72h, or 96h and growth was determined by MTS assay. The values plotted in bar graph are average of three independent experiments. All cell lines were cultivated and maintained under same culture conditions.

3.1.3 GC011 induces apoptosis in TGF-β sensitive SNU-16 cells.

Apoptosis is a widely studied mechanism in antitumor therapy as its manipulation is an effective strategy for cancer control. As TGF-β signalling is known to contribute to growth arrest in cells by regulating apoptosis, we next investigated whether GC011-induced growth inhibition in TGF-β sensitive cells was mediated through apoptosis. The signaling mediated by TGF-β contributes to growth arrest by inducing apoptosis characterized by the activation of PARP and caspase-3 through proteolytic processing.[45] To this aim, we first determined the effect of GC011 on the viability of TGF-β sensitive SNU16 and SNU620 cells, as well as TGF-β resistant SNU5 cells, using a FACS based Annexin V assay. SNU5, SNU16 and SNU620 cells were treated with GC011 in a dose-dependent manner for a total duration of 96 hours and stained with propidium iodide (PI) and fluorescence labelled Annexin V antibody, and relative percentage of apoptotic cells was then determined by flow cytometry. GC011 selectively induced apoptosis in TGF-β sensitive cells. This was demonstrated by an observed dose-dependent increase in FITC-Annexin–positive/PI-negative cells (early apoptotic) and FITC-Annexin/PI double-positive cells (late apoptotic) in TGF-β sensitive SNU16 and SNU620 cells. As expected, GC011 had no observable effect on SNU5 cells (Figure 3.6). Additionally, western blots revealed similar activation of caspase-3 and cleavage of PARP in both GC011 and TGF-β treated SNU16 cells (Figure 3.7A), but not in SNU5 cells (Figure 3.7B).

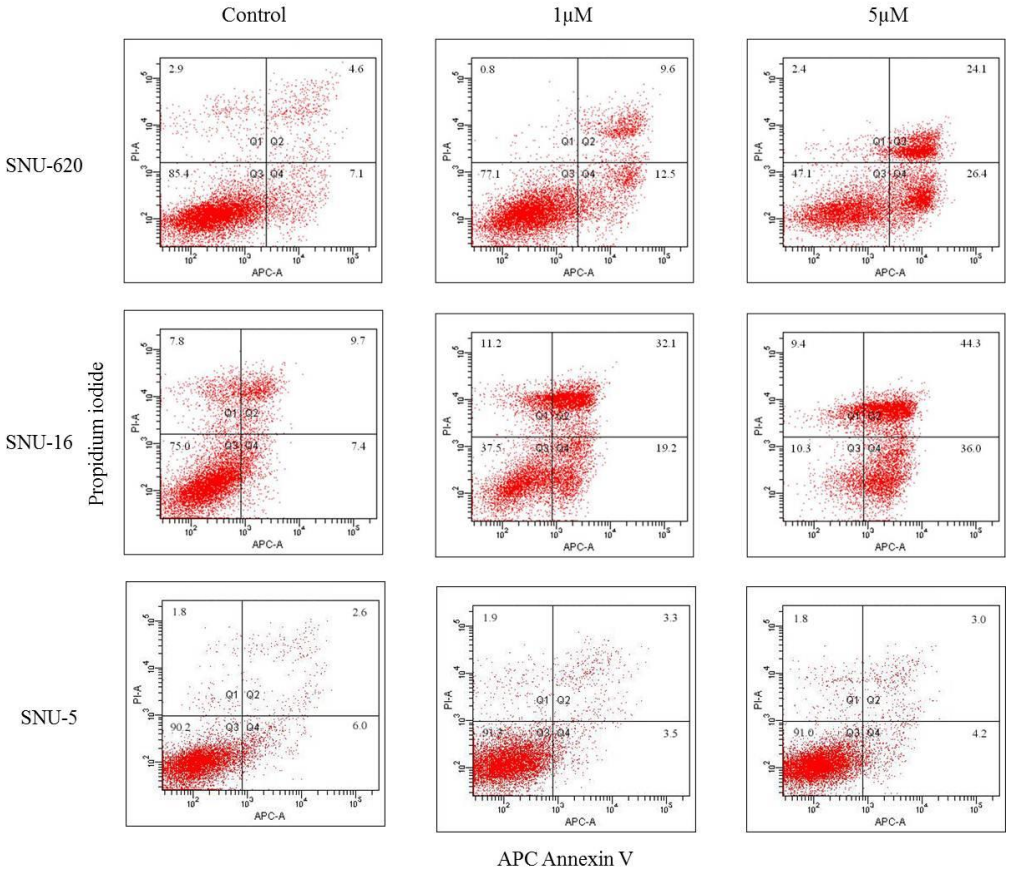

Figure 3.6. GC011 promotes apoptosis of TGF-β sensitive gastric cancer cells. Relative level of phosphatidylserine exposure, which is indicative of the extent of apoptosis in mammalian cells, in SNU5, SNU16 and SNU620 cells treated with GC011 in a dose-dependent manner for 96 hours was determined by FACS after staining the cells with FITC-Annexin V and nuclear staining dye PI.

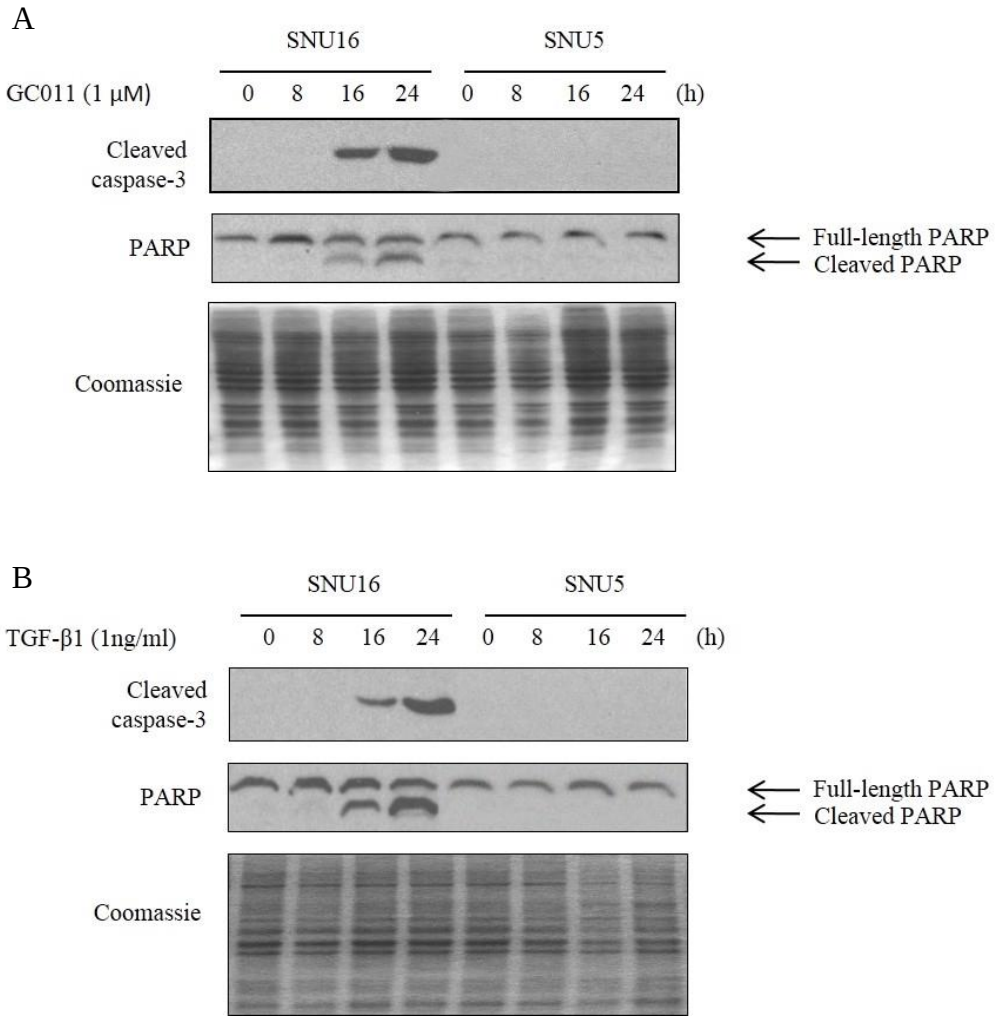

Figure 3.7. GC011 activates caspase-3 and PARP in TGF-β sensitive SNU16. Activation of PARP and caspase-3 in SNU16 and SNU5 cells treated with GC011 or TGF-β1 in a time-dependent manner was determined in western blotting assay performed with anti-PARP or anti-caspase-3 antibodies. As an indication of loading control, level of total protein in each sample was determined by coomassie blue staining.

3.1.4 GC011 activates Smad signaling and up-regulates the expression of TGF-β target genes in TGF-β sensitive cell line, SNU16.

Given that only TGF-β-sensitive cells appear to be sensitive to GC011, we postulate that GC011 may act as a TGF-β agonist. In order to validate the hypothesis, the activation of the TGF-β signaling pathway in these cells was also investigated. The signal initiated by TGF-β ligand is primarily transmitted across the cell through the phosphorylation and nuclear translocation of Smad2/3 proteins, which then co-operate with other Smad proteins to induce the expression of TGF-β target genes such as *PAI-1* and *p21*.[184] To test whether GC011 could also induce the phosphorylation of Smad2/3 proteins as observed with TGF-β stimulation, relative levels of Smad2 and Smad3 proteins in SNU5 and SNU16 cells treated with 1 μM GC011 in a time-dependent manner was determined by western blotting assay. In SNU16 cells treated with 1 μM GC011, the level of phosphorylated Smad3 protein was significantly enhanced within 8 hours of treatment and the level was maintained throughout the duration up to 24 hours (Fig. 3.8A). Level of phosphorylated Smad2 protein was also elevated within 24 hours in GC011-treated cells relative to untreated cells (Fig. 3.8A). This GC011-induced increase in Smad2 and Smad3 phosphorylation was comparable to the increase in Smad2 and Smad3 phosphorylation induced by TGF-β (Fig. 3.8B). In contrast, no significant upregulation of Smad2/3 phosphorylation was observed in SNU5 cells (Fig. 3.8A & B). Attenuation of Smad levels in TGF-β treated cells was also observed, whereas in GC011 treated cells, the Smad levels were maintained. In TGF-β treated cells, the observed attenuation may be explained by the induction of the negative feedback mechanism that

normally controls the intensity and duration of TGF-β signaling response, through the activation of I-Smads and Smurfs. Although GC011 may activate the Smad signaling pathway, it is possible that it acts independently of the negative feedback loop.

In addition to the phosphorylation of Smad2 and Smad3, real-time PCR analysis revealed a significant increase in the transcript levels of TGF-β target genes *PAI-1* and *p21* in SNU16 cells treated with GC011 (Fig. 3.9A). Protein expression of these two target genes are also up-regulated by GC011 treatment, similar to that observed in TGF-β–treated SNU16 cells, but were unchanged in SNU5 cells (Fig. 3.9B).

Next, a luciferase assay was performed on TGF-β responsive P19 embryonal carcinoma cells transfected with a reporter plasmid driven by mouse germ line IgCα promoter that contains a TGF-β-responsive element (TβRE) (Fig. 3.10A) [10]. Consistent with previous findings [11], TGF-β displayed a dose-dependent increase in IgCα promoter activity in P19 cells, with the maximum increase achieved at 1.5 μM concentration (Figure 3.10B). Interestingly, GC011 also induced a nearly identical dose-dependent increase in IgCα promoter activity in P19 cells, suggesting that GC011 may exert a TGF-β like regulatory effect on the TGF-β-responsive promoter element (Figure 3.10C). Taken together, these findings collectively suggested that GC011-induced apoptosis of SNU16 cells could be an outcome of activation of the TGF-β-dependent growth inhibitory pathway.

A

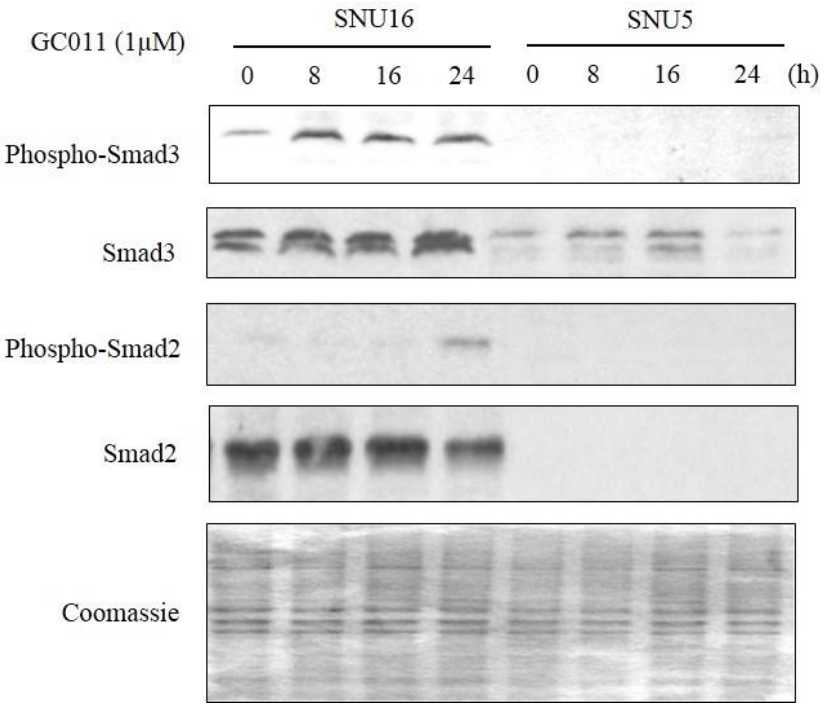
GC011 (1μM)
SNU16
SNU5
0 8 16 24 0 8 16 24 (h)
Phospho-Smad3
Smad3
Phospho-Smad2
Smad2
Coomassie

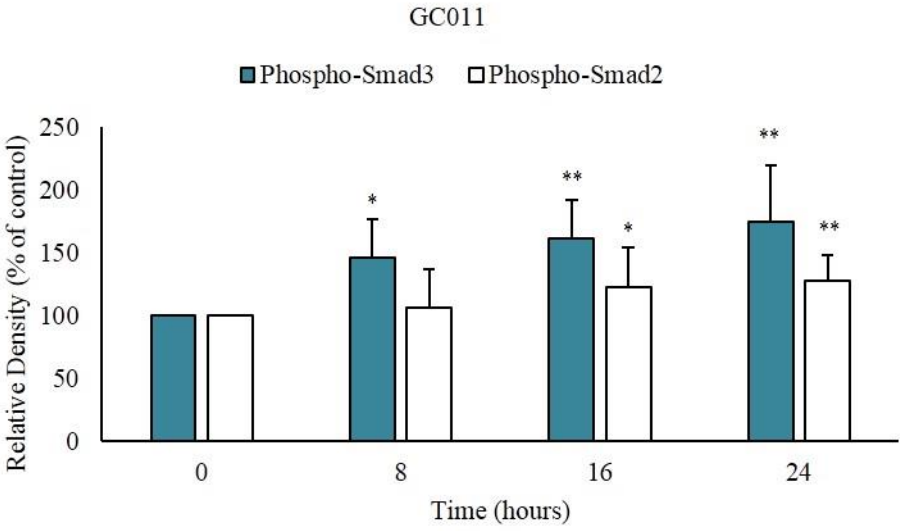
GC011
Phospho-Smad3
Phospho-Smad2
Relative Density (% of control)
250
200
150
100
50
0
0
8
16
24
Time (hours)
*
**
*
**
**

B

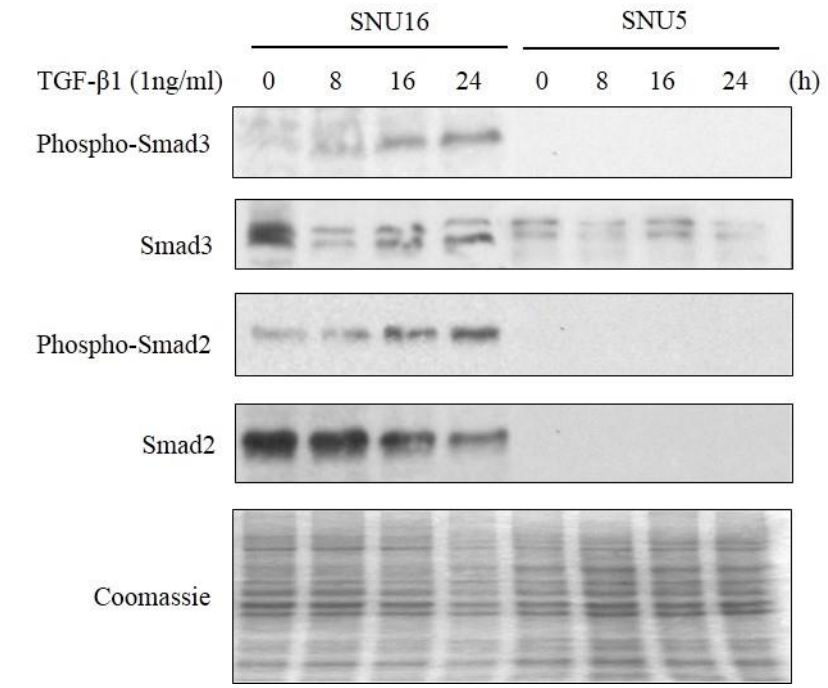

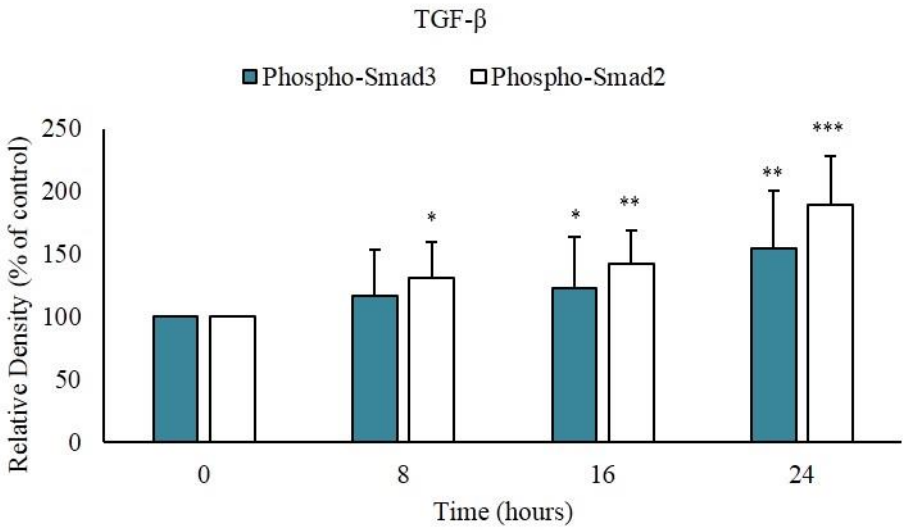

Figure 3.8. GC011 induces the phosphorylation of Smad2 and Smad3 in TGF-β sensitive cell line SNU16. Level of phosphorylated Smad2 and Smad3 in SNU16 and SNU5 cells treated with 1μM GC011 (A,C) or 1 ng/mL TGF-β (B,D) was determined by western blotting assay performed with (A,B) and quantitative densitometry analysis (C,D) of protein expression. For western blotting, level of Smad2 and Smad3 proteins in each sample was determined with anti-Smad2, anti-Smad3, phospho-specific Smad2 or Smad3 antibodies. As an indication of loading control, level of total protein in each sample was determined by Coomassie Blue staining. For quantitative densitometry analysis, the values plotted in bar graph are average of three independent experiments. *$p<0.05$, **$p<0.01$ and ***$p<0.001$, compared with respective untreated controls.

A

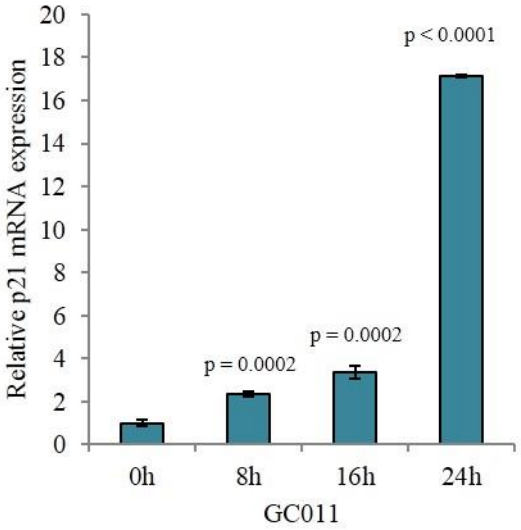
Relative p21 mRNA expression
20
18
16
14
12
10
8
6
4
2
0
p < 0.0001
p = 0.0002
p = 0.0002
0h
8h
16h
24h
GC011

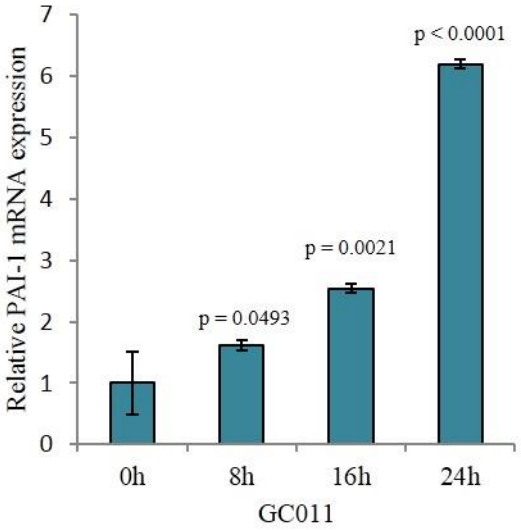
Relative PAI-1 mRNA expression
7
6
5
4
3
2
1
0
p < 0.0001
p = 0.0021
p = 0.0493
0h
8h
16h
24h
GC011

B

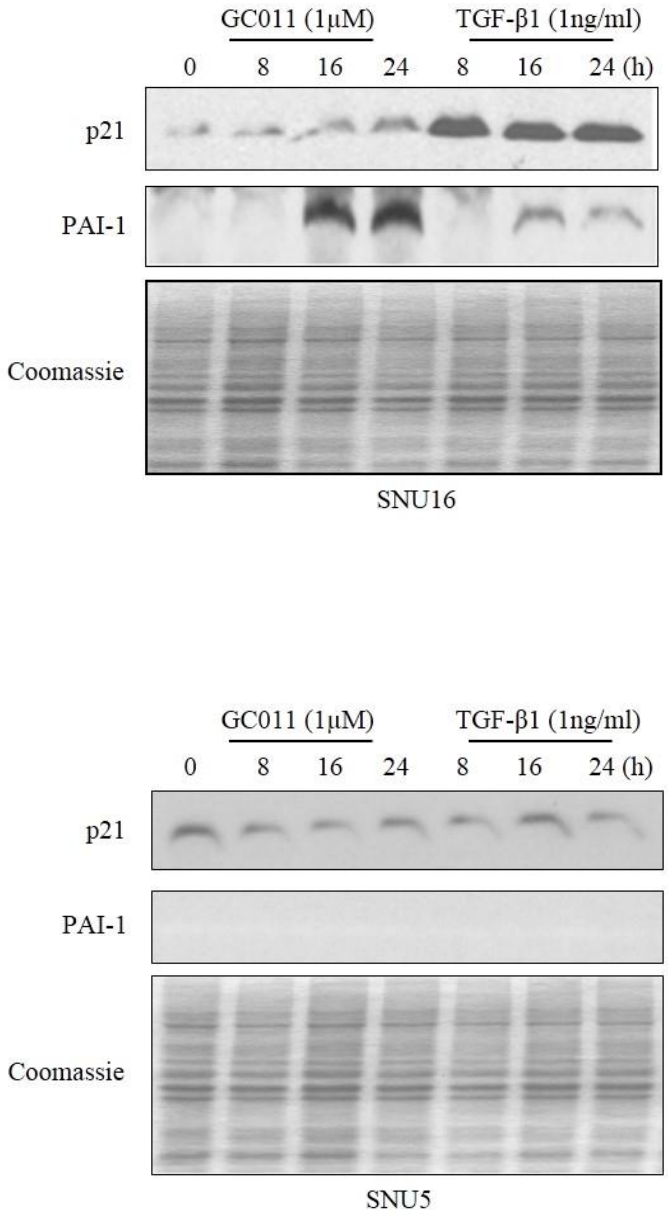

Figure 3.9. GC011 up-regulates the expression of TGF-β target genes in TGF-β sensitive SNU16. Levels of *p21* and *PAI-1* mRNA and protein in SNU16 and SNU5 cells treated with GC011 or TGF-β was respectively determined by real-time PCR analysis (A) and western blot using anti-p21 or anti-PAI-1 antibodies (B). As an indication of loading control, level of total protein in each sample was determined by Coomassie Blue staining. The values plotted in the bar graphs are average of three independent experiments.

A

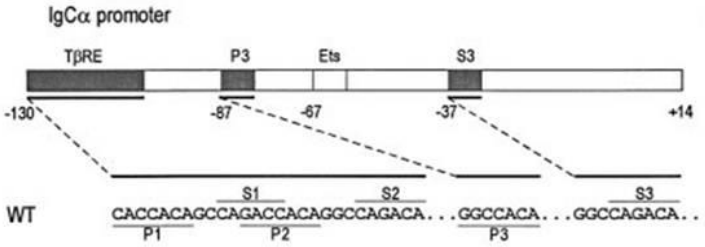
IgCα promoter
TβRE
P3
Ets
S3
-130
-87
-67
-37
+14
S1
S2
S3
WT
CACCACAGCCAGACCACAGGCCAGACA...GGCCACA...GGCCAGACA..
P1
P2
P3

B

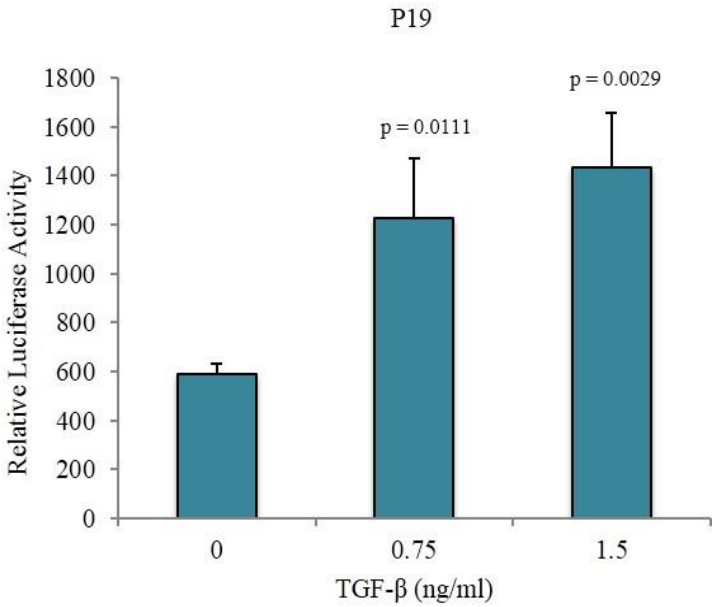
P19
Relative Luciferase Activity
1800
1600
1400
1200
1000
800
600
400
200
0
p = 0.0111
p = 0.0029
0
0.75
1.5
TGF-β (ng/ml)

C

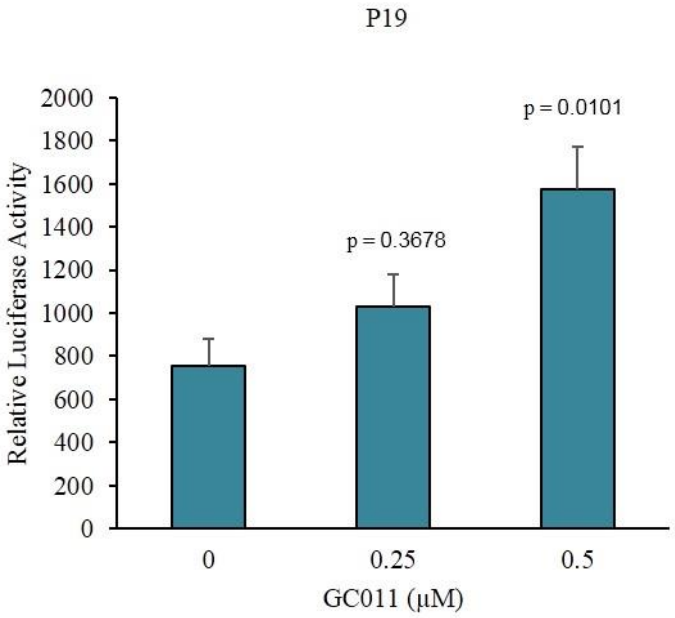

Figure 3.10. GC011 activates the promoter of TGF-β responsive gene in TGF-β responsive P19 cells. (A) Smad binding motifs (indicated as S1, S2, and S3) in TGF-β response element (TβRE) of mouse germ line IgCα gene are highlighted. (B & C) Effect of TGF-β1 or GC011 on the activity of a reporter plasmid driven by IgCα promoter that contains a TβRE was determined in P19 embryonal carcinoma cells. P19 cells were treated with TGF-β1 (B) or with GC011 (C) in a dose-dependent manner for a total duration of 24 hours. The values plotted in bar graph are average of three independent experiments. *p* values as compared with untreated controls.

3.1.5 Growth inhibition induced by GC011 is dependent on the TGF-β signaling pathway.

Using semi-quantitative PCR analysis, we first determined transcript levels of TGF-β1, TGF-β2, TGF-β3, TGF-β type I receptor (TβRI) and TGF-β type II receptor (TβRII) in our panel of gastric cancer cell lines and compared them with the TGF-β responsiveness as reported earlier in Section 3.16. Expression of TGF-β2 ligand was not detected in both TGF-β sensitive cell lines SNU16 and SNU620 suggesting that there is no direct correlation with the responsiveness to growth inhibition by GC011 and the expression of TGF-β2. In concordance with previous reports,[63,185] both SNU1 and SNU5 had no

detectable expression of TGF-βRII, which explains its loss of responsiveness to TGF-β-induced growth inhibition. There was no detectable TGF-β1 expression in MKN7 and TMK1 cells. The remaining cell lines retained expression of all three TGF-β ligands and both TGF-β receptors, but are still resistant to TGF-β signaling (Fig. 3.11A).

PCR analysis of cDNAs obtained from SNU16 cells treated with 1 μM of GC011 in a time-dependent manner revealed that only TGF-β1 mRNA expression was upregulated, further suggesting that the other two isoforms of TGF-β are not involved in GC011-induced growth inhibition (Fig. 3.11B). TGF-β1 protein levels examined with western blotting also showed a marked increase with GC011 treatment (Fig.3.11C). Additionally, GC011 treatment did not significantly affect the mRNA expression of both TGF-βI and TGF-βII receptors (Fig. 3.11B).

To further determine the involvement of the TGF-βR-Smad signaling pathway in GC011-induced growth inhibition in SNU16 cells, we introduced siRNAs to suppress either TβRI, TβRII, Smad2 or Smad3 respectively to inactivate the TGF-β signaling pathway. As indicated in Figure 3.12A, silencing Smad2 almost completely reversed growth inhibition induced by GC011, whereas Smad3 silencing reversed it to a lesser extent, despite the higher efficacy of Smad3 siRNA in downregulating Smad3 protein as compared to Smad2 siRNA. This observation suggests that GC011 target genes may have a higher dependency on Smad2, as subtle alterations in Smad2 expression levels already cause a significant effect on GC011-mediated growth inhibition. Similarly, knockdown of TβRI and TβRII completely abolished the growth inhibition induced by GC011 in SNU16 cells (Fig. 3.12B). Treatment with

LY2157299, a potent and selective TGF-β receptor type I and type II inhibitor with IC_{50} of 86nM and 2nM respectively, also abrograted the growth inhibitory effects of GC011 in SNU-16 cells (Fig. 3.12C).

Taken together, these findings suggest that activation of TGF-βR-Smad signaling is required for GC011-induced growth inhibition in SNU16 cells and that GC011 may also operate via directly upregulating TGF-β1 expression and therefore stimulating the TGF-βR-Smad signaling pathway to induce growth inhibition in TGF-β-sensitive cells.

A

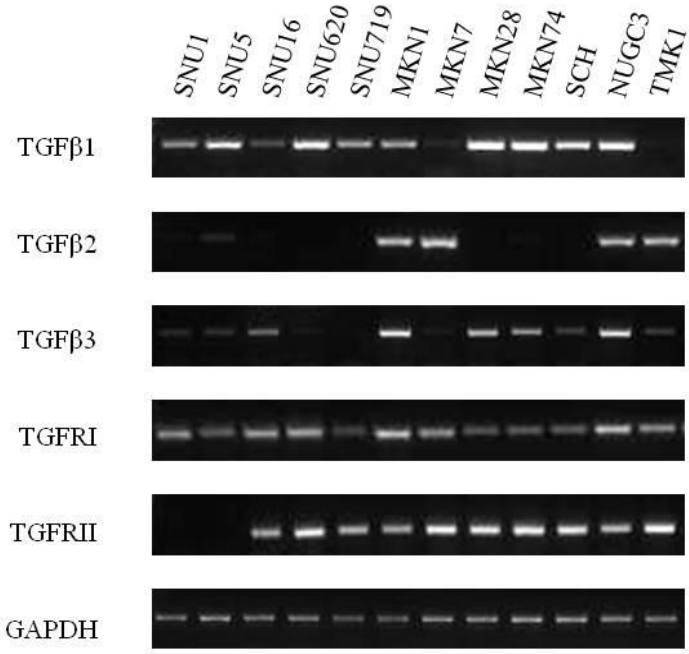

B

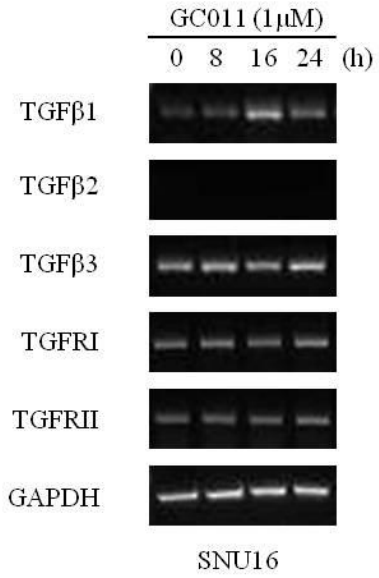

C

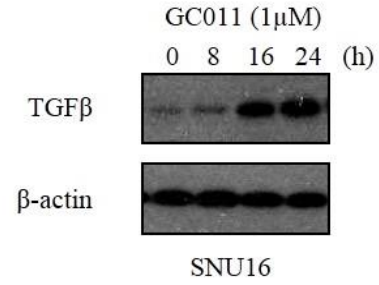

Figure 3.11. Semi-quantitative PCR analysis of TGFβ genes in a panel of gastric cancer cell lines. (A) cDNAs were obtained from total RNA extracted from gastric cancer cell lines as indicated and TGF-β1, TGF-β2, TGF-β3, TβRI, and TβRII transcript levels were analysed by semiquantitative RT-PCR. (B) cDNAs obtained from total RNA extracts of GC011-treated SNU16 cells were subjected to semiquantitative RT-PCR. (C) Level of TGF-β1 protein in SNU16 cells treated with 1 μM GC011 for indicated time points was measured using western blotting with anti-TGF-β1 antibody.

A

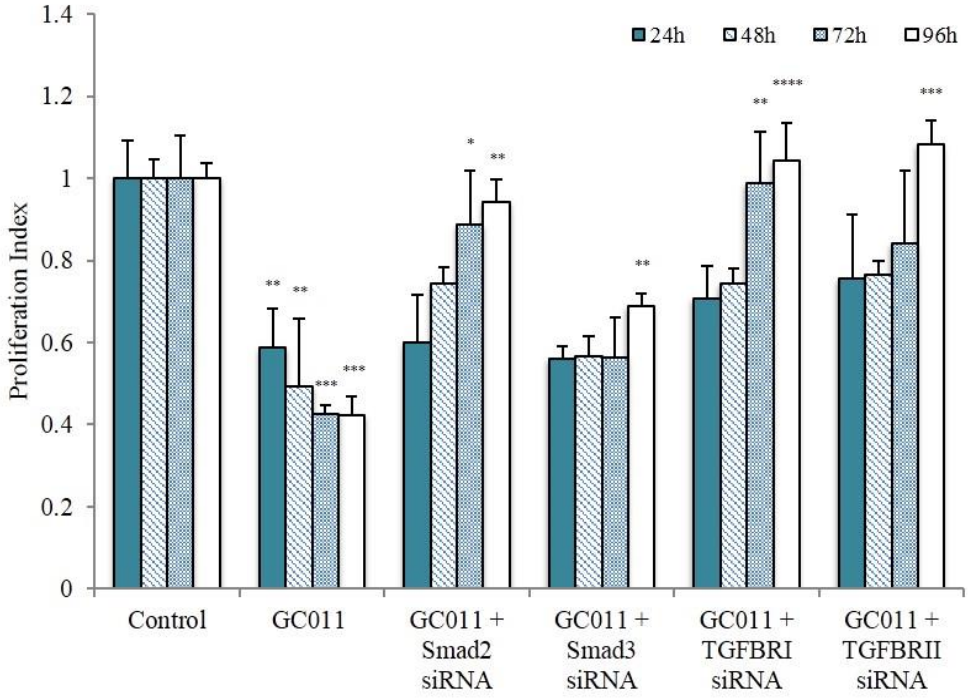
24h
48h
72h
96h
Proliferation Index
1.4
1.2
1
0.8
0.6
0.4
0.2
0
Control
GC011
GC011 + Smad2 siRNA
GC011 + Smad3 siRNA
GC011 + TGFBRI siRNA
GC011 + TGFBRII siRNA

B

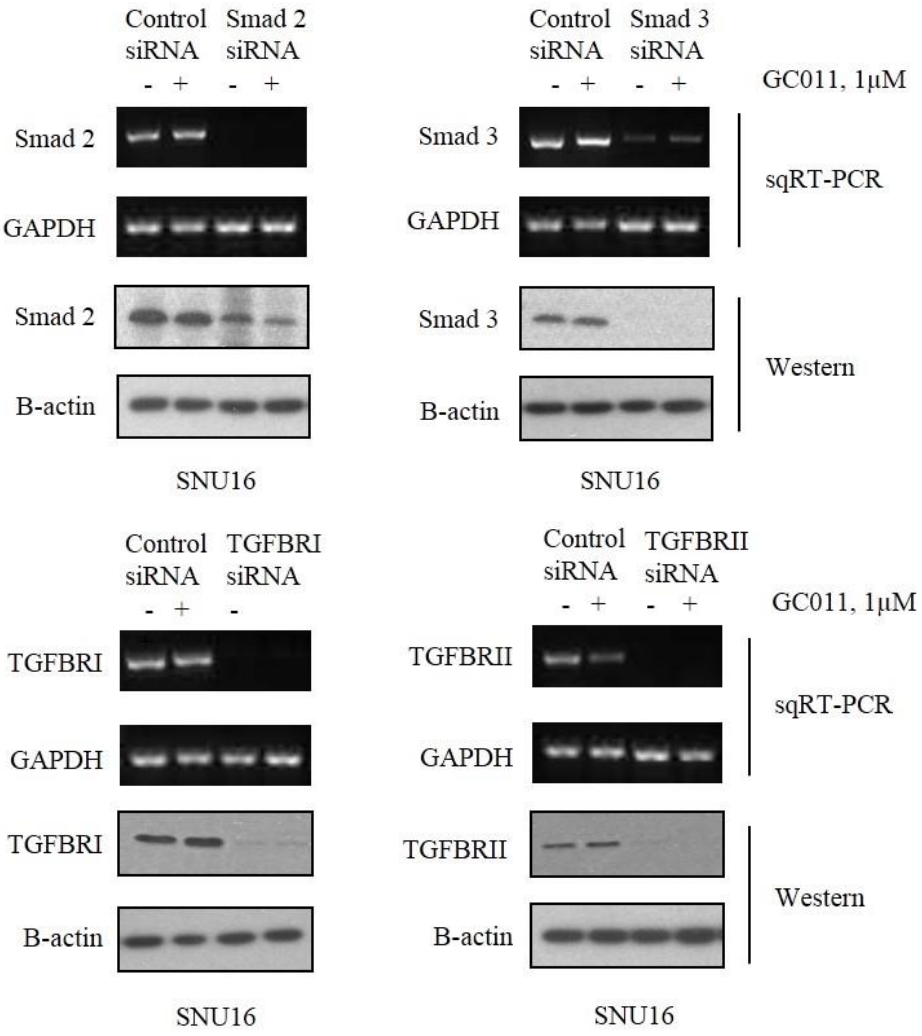
Control siRNA
Smad 2 siRNA
- + - +
Smad 2
GAPDH
Smad 2
B-actin
SNU16
Control siRNA
Smad 3 siRNA
- + - +
GC011, 1μM
Smad 3
GAPDH
sqRT-PCR
Smad 3
B-actin
Western
SNU16
Control siRNA
TGFBRI siRNA
- + -
TGFBRI
GAPDH
TGFBRI
B-actin
SNU16
Control siRNA
TGFBRII siRNA
- + - +
GC011, 1μM
TGFBRII
GAPDH
sqRT-PCR
TGFBRII
B-actin
Western
SNU16

C

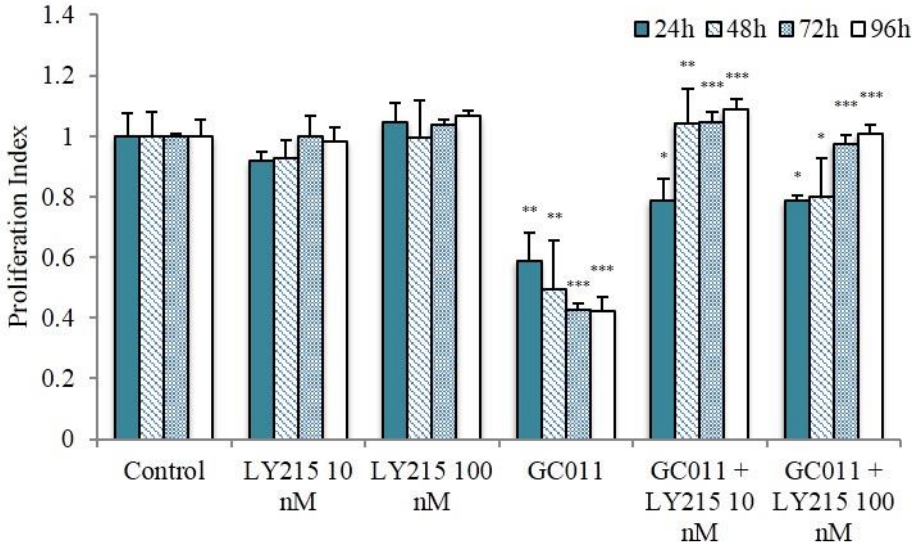

Figure 3.12. GC011-induced growth arrest is mediated by the TGF-β signaling pathway. (A) Effect of TGF-β gene knockdown on the proliferation of GC011-treated SNU16 cells transfected with non-silencing control, Smad2, Smad3, TβRI, or TβRII siRNA was determined using MTS assay. The values presented in each bar represent the average of three independent experiments. *$p < 0.05$, **$p < 0.01$, ***$p < 0.001$, ****$p < 0.0001$, untreated vs GC011, and GC011 vs siRNA transfected cells. (B) Knockdown efficiency in experiments performed was determined by semi-quantitative RT-PCR and its protein expression examined by western blotting. (C) SNU16 cells were treated with GC011 (1μM) in the presence and absence of LY2157299, a potent TGF-β receptor I (TβRI) inhibitor, and its effect on growth proliferation was determined by MTS assay. The values presented in each bar represent the average of three independent experiments. *$p < 0.05$, **$p < 0.01$, ***$p < 0.001$, ****$p < 0.0001$, untreated vs GC011, and GC011 vs LY2157299.

3.1.6 GC011 induces down-regulation of N-CoR/HDAC1 in TGF-β responsive cells.

Next, we aimed to understand the molecular mechanism underlying the difference in responsiveness towards TGF-β. In the nucleus, Smad heterodimers bind to various transcriptional factors and transcriptional activators and corepressors, leading to transcriptional regulation of target genes. N-CoR has been postulated to be part of the repressor complex targeted

to TGF-β target genes.[184] As such, we investigated the status of N-CoR in the prototypical TGF-β sensitive and resistant cell lines, SNU16 and SNU5.

Transcriptional control imparted by N-CoR is primarily mediated in the nucleus. Aberrant cytosolic distribution of N-CoR protein would imply dysregulation in N-CoR-mediated transcriptional control of target genes. To investigate a link between N-CoR status and TGF-β responsiveness of gastric cancer cells, subcellular distribution of N-CoR protein in SNU16 and SNU5 cells was determined using immunofluorescence assay. In TGF-β sensitive SNU16 cells, relative level of nuclear N-CoR protein was significantly higher when compared to its level in TGF-β resistant SNU5 cells, where its expression was mainly in the cytoplasm (Figure 3.13). As N-CoR is a corepressor, this data suggests that it is mislocalised in the cytoplasm and is thus non-functional in SNU5 cells.

The notion that N-CoR function might have been compromised in TGF-β resistant cells was further confirmed by the significantly lower level of N-CoR protein in SNU5 cells when compared to its level in SNU16 cells using western blotting assay (Figure 3.14).

The ultimate outcome of TGF-β signaling on cell fate determination is achieved through the sequential activation of downstream TGF-β target genes which usually remain suppressed in the absence of TGF-β stimulation. As observed in retinoic acid (RA) signalling, it is likely that an N-CoR containing chromatin remodeling complex also keeps a tab on TGF-β target genes in the absence of TGF-β stimulation. Although there is no evidence yet, activation of TGF-β target genes would likely require abrogation of N-CoR/HDAC-

mediated transcriptional repression followed by the recruitment of transcriptional activator complex containing DNA binding Smad proteins.[186] Therefore, to test whether TGF-β or GC011 can antagonize any N-CoR-mediated transcriptional repression through inducing N-CoR degradation or displacement as observed with retinoic acid, level of N-CoR protein in whole cell extracts of SNU5 and SNU16 cells treated with TGF-β or GC011 in a dose-dependent manner was determined using western blotting assay. Both TGF-β and GC011 promoted a selective dose- and time-dependent down-regulation of N-CoR protein in SNU16 cells, while in TGF- β resistant SNU5 cells, no N-CoR down-regulation by either GC011 or TGF-β was observed (Figures 3.15A & B). GC011 also promoted a TGF-β–like down-regulation of HDAC1 protein in TGF-β sensitive SNU16 cells but not in TGF-β resistant SNU-5 cells (Figure 3.16). Additionally, siRNA-induced ablation of N-CoR led to a significant up-regulation of IgCα promoter activity in P19 cells (Figure 3.17A & 3.17B). These findings suggest that the artemisinin derivative GC011 can function as a potent TGF-β agonist and sensitize TGF-β sensitive SNU16 cells to apoptosis by overriding the N-CoR-induced transcriptional repression of pro-apoptotic TGF-β target genes.

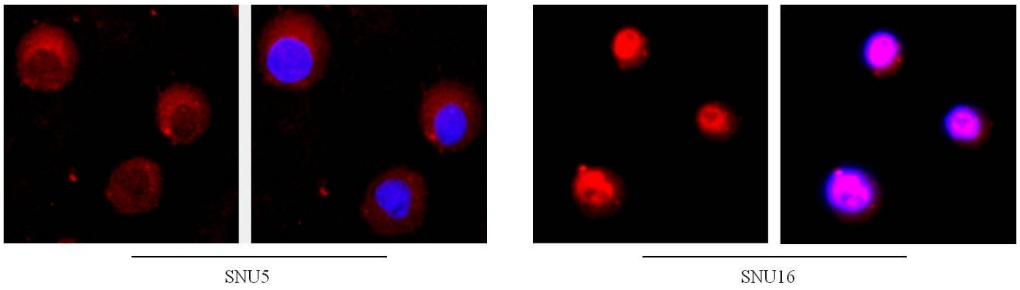

Figure 3.13. N-CoR localization is mainly cytosolic in TGF-β resistant SNU5 cells but nuclear in TGF-β sensitive SNU16. Subcellular distribution of N-CoR (red) in TGF-β resistant cell line, SNU5, and TGF-β sensitive cell line, SNU16, was determined by staining the cells with anti-N-CoR antibody and fluorescence-labelled secondary antibody. Nucleus was stained with DAPI (blue). Cells were visualised using confocal microscopy.

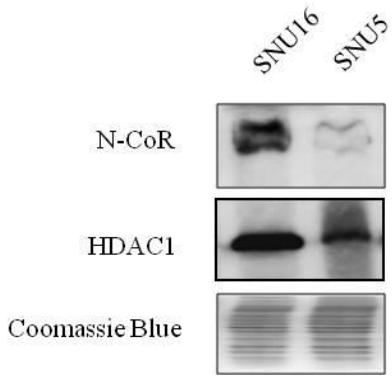

Figure 3.14. Level of N-CoR in TGF-β-resistant SNU5 cells is down-regulated as compared to that in TGF-β sensitive SNU-16 cells. Level of N-CoR protein in whole cell extracts of TGF-β sensitive SNU16 cells and TGF-β resistant SNU5 cells was determined in western blotting assay with N-CoR antibody. As an indication of loading control, level of total protein in each sample was determined by coomassie blue staining.

A

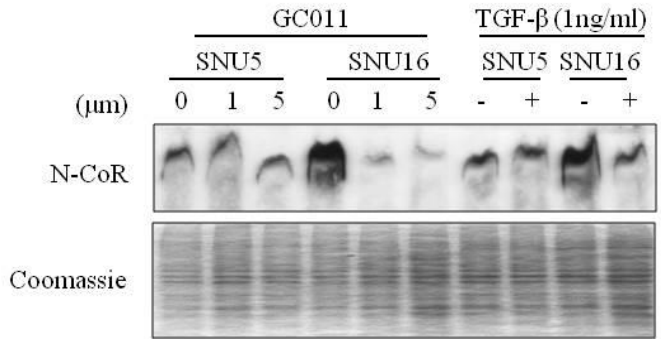

B

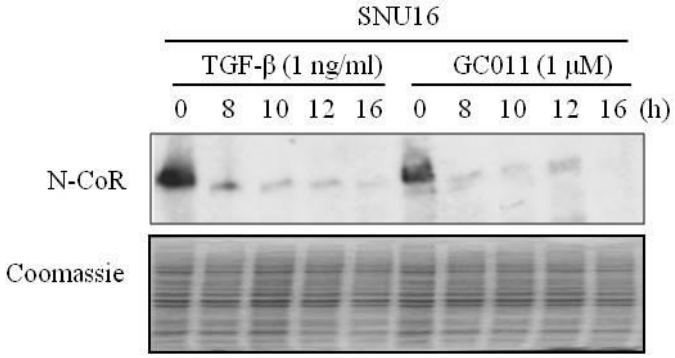

Figure 3.15. GC011 induces down-regulation of N-CoR in TGF-β responsive cells. Level of N-CoR protein in whole cell extracts of SNU16 and SNU5 cells treated with GC011 or TGF-β was determined in western blotting assay with anti-N-CoR antibody (A). Level of N-CoR protein in whole cell extracts of SNU16 cells treated with GC011 or TGF-β in a time-dependent manner was determined in western blotting assay with N-CoR antibody (B). As an indication of loading control, level of total protein in each sample was determined by Coomassie Blue staining.

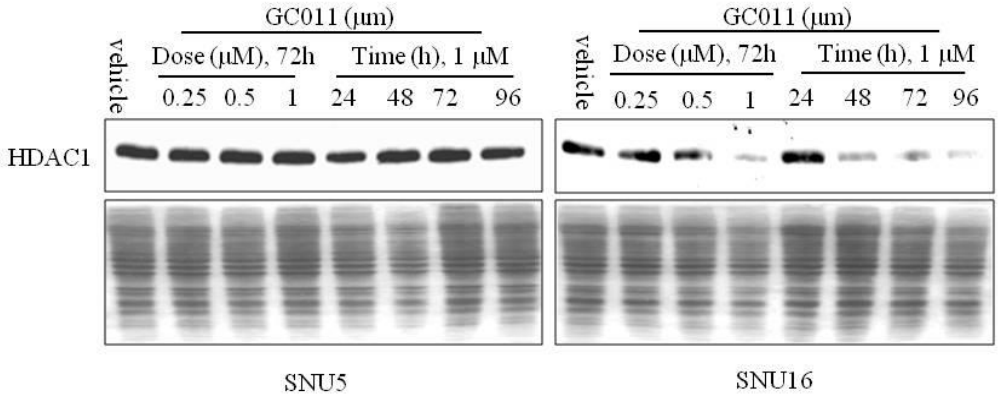

Figure 3.16. GC011 induces down-regulation of HDAC1 in TGF-β responsive cells. Level of HDAC1 protein in whole cell extracts of SNU16 and SNU5 cells treated with vehicle or GC011 in a dose and time-dependent manner was determined in western blotting assay with HDAC1 antibody. As an indication of loading control, level of total protein in each sample was determined by Coomassie Blue staining.

A

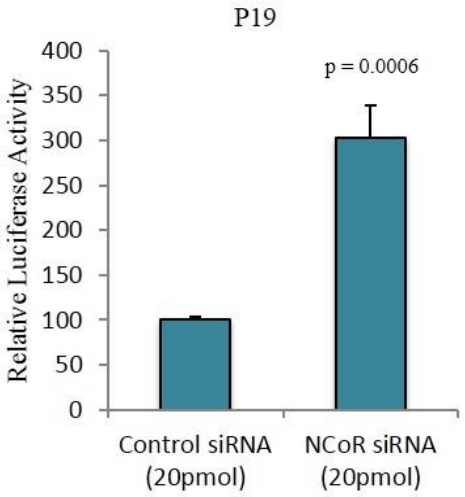

B

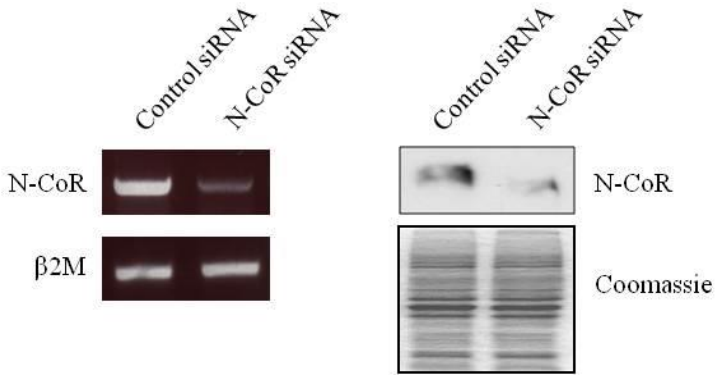

Figure 3.17. N-CoR silencing activates the promoter of TGF-β responsive gene. Effect of N-CoR ablation (A) on the activity of the IgCα promoter was determined by relative luciferase assay performed in P19 cells transfected with control or anti-N-CoR siRNA (B). The values plotted in the bar graph are average of three independent experiments. *p* values as compared with untreated controls.

3.2 RUNX3 induces degradation of N-CoR via the ubiquitin-proteosome pathway and possibly regulates N-CoR-mediated repression of TGF-β target genes.

3.2.1 Loss of RUNX3 protein expression in gastric cancer cells

Almost all gastric cancer cell lines have an impaired TGF-β signaling pathway, and are resistant to TGFβ (Fig. 3.4). RUNX3, a known tumor suppressor in gastric cancer, has been shown to form complexes with receptor-regulated Smads (R-Smads) that regulate target gene expression, making it is a downstream target of the TGF-β signaling pathway. Its role in TGF-β-induced apoptosis has also been well-documented. Another member of Runt-related transcription factor family, RUNX1, has also been linked to carcinogenesis, although its involvement has been better studied in leukemia. As GC011 also appeared to be inducing TGF-β-mediated growth inhibition and apoptosis in SNU16 cells, we postulate that RUNX may also be a downstream target of GC011. We therefore first examined RUNX1 and RUNX3 protein expression in gastric cancer cell lines. Consistent with previous reports, RUNX3 protein was lost in most of the gastric cancer cell lines (11 out of 13),[62] but was highly expressed in TGF-β responsive SNU16 cells. Amongst the TGF-β resistant cell lines, only SNU1 expressed RUNX3, while the expression level was very low in SNU5 cells. Expression of RUNX1 was detectable in most of the gastric cancer cell lines however (9 out of 13) (Fig. 3.18).

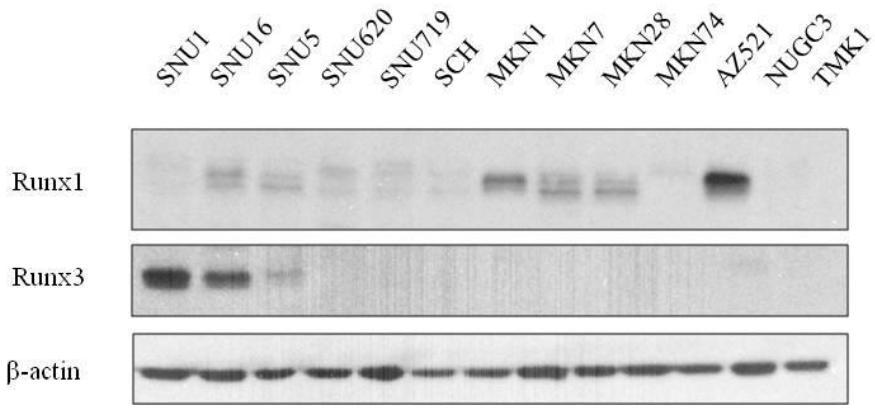

Figure 3.18. Expression of RUNX1 and RUNX3 protein in gastric cancer cell lines. Whole cell extracts were prepared from a panel of human gastric cancer cell lines and 10 μg of crude lysates were resolved by SDS-PAGE. RUNX1 and RUNX3 protein expression were determined via western blotting with anti-Runx1 or anti-RUNX3 antibody. β-actin expression was used as loading control.

3.22 RUNX1 and RUNX3 promote N-CoR degradation.

Previous reports have shown that TGF-β stimulation induces nuclear translocation of RUNX3 in SNU16 cells, where it performs its function as a transcription factor. We have also shown that N-CoR is primarily localised in the nucleus of TGF-β sensitive cells. As TGF-β1 selectively promotes down-regulation of N-CoR and HDAC1 proteins in TGF-β sensitive cells (Fig. 3.12 & 3.13), we hypothesize that RUNX3 may play a role in TGFβ-induced N-CoR/HDAC1 loss. To demonstrate this, we ectopically expressed flag-tagged N-CoR in 293T cells along with *RUNX1*, *RUNX2* and *RUNX3*, and determined the level of exogenous N-CoR protein via western blotting. Cells transfected with *RUNX1* and *RUNX3* exhibited a marked loss in the expression of flag-tagged N-CoR, whereas transfection with *RUNX2* did not result in any significant downregulation (Fig. 3.19). This finding suggests a putative role of Runx1 and Runx3 in N-CoR degradation, but not Runx2.

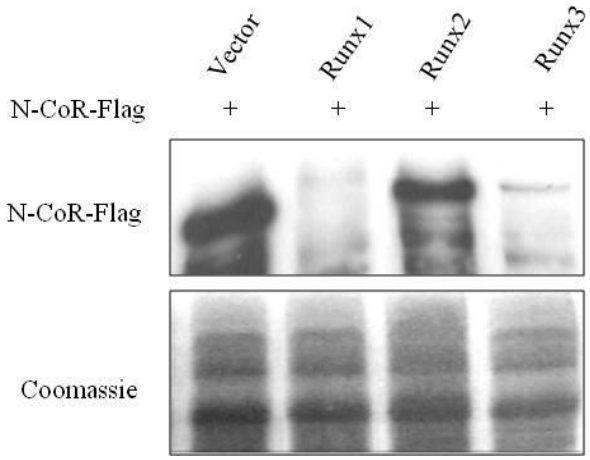

Figure 3.19. *RUNX1* and *RUNX3* promote the degradation of N-CoR protein. 293T cells were transfected with N-CoR-FLAG expression plasmid and plasmids expressing *RUNX1*, *RUNX2* or *RUNX3*. The N-CoR levels were examined by Western blotting and determined using anti-FLAG antibody. As an indication of loading control, level of total protein in each sample was determined by Coomassie Blue staining. (*Contributed by Pang Sze Li)

3.23 RUNX1 and RUNX3 induce translocation of nuclear N-CoR into cytoplasm.

To examine whether Runx1/3-induced degradation of N-CoR was associated with any deregulated subcellular distribution, we next assessed the subcellular localization of ectopically expressed flag-tagged N-CoR protein in 293T cells co-transfected with *RUNX1*, *RUNX2* or *RUNX3* using immunofluorescence staining analysis. Ectopic N-CoR was predominantly confined to the nucleus in cells transfected with empty vector, but when cells were co-transfected with *RUNX1* and *RUNX3*, expression of ectopic N-CoR was observed to be mainly cytosolic. As expected, N-CoR signal was also significantly weaker in cells co-transfected with *RUNX1* and *RUNX3*, probably as a result of Runx1- or Runx3-induced degradation of N-CoR. As expected, transfection of *RUNX2* did not result in any translocation of N-CoR. As such, it is likely that Runx1

and Runx3 are involved in the export of N-CoR from the nucleus to the cytosol where it is then targeted for degradation.

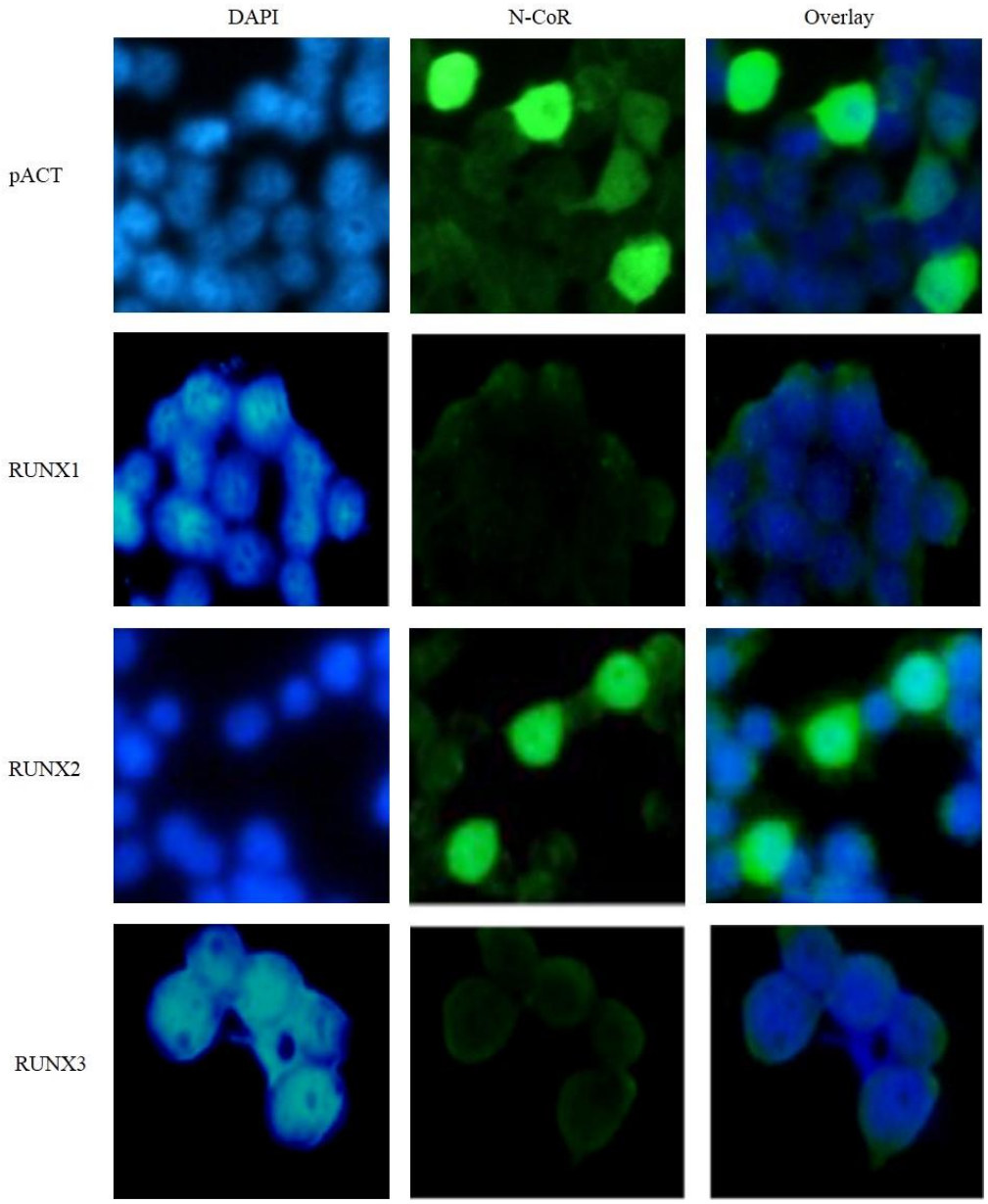

Figure 3.20. *RUNX1* and *RUNX3* induce the translocation of nuclear N-CoR to cytosol. 293T cells were transfected with the N-CoR-FLAG expression plasmids and with either empty pACT vector or expression vectors encoding *RUNX1*, *RUNX2* or *RUNX3*. The exogenous N-CoR signals were detected by anti-FLAG antibody (green) and nuclear DNA was stained with DAPI (blue). In the panels indicated as overlay, both signals are superimposed. (*Contributed by Pang Sze Li)

3.24 RUNX1 and RUNX3 induce the ubiquitination of N-CoR

Next, to determine if Runx1/Runx3-induced proteolytic degradation of N-CoR was via a proteosomal pathway, we first tested the effect of a known proteasome inhibitor, MG132, on Runx1 and Ru~~u~~nx3 mediated degradation of N-CoR. 293T cells co-transfected with flag-tagged N-CoR expression plasmids and *RUNX1, RUNX3* or empty vector, were subsequently treated with MG132 and N-CoR expression was determined by western blotting. It was observed that MG132 significantly inhibited both Runx1 and Runx3-induced degradation of N-CoR protein, suggesting that N-CoR undergoes proteosomal degradation in the presence of Runx1 and Runx3 (Fig. 3.21).

As majority of intracellular proteins are degraded by the ubiquitin-proteosome pathway (UPP), an *in vivo* ubiquitination assay was subsequently performed on 293T cells by co-expressing Flag-tagged N-CoR and Myc-ubiquitin along with empty vector or vector expressing *RUNX1* or *RUNX3*. Flag-tagged N-CoR was immunoprecipitated with anti-Flag antibody and level of ubiquitin-conjugated N-CoR was then determined by western blotting with anti-myc antibody. As shown in Fig. 3.22, both Runx1 and Runx3 augmented the conjugation of ubiquitin to N-CoR. Taken together, these results suggest that ubiquitin-mediated proteosomal proteolysis may be the major mechanism of Runx1/3-mediated degradation of N-CoR.

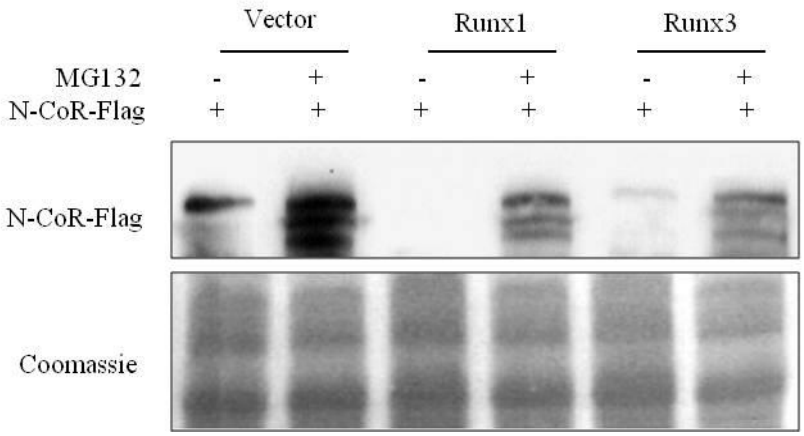

Figure 3.21. MG132 significantly reverses Runx1- and Runx3-induced degradation of N-CoR protein. 293T cells transfected with the N-CoR-FLAG expression plasmid and plasmids expressing *RUNX1, RUNX2* or *RUNX3* were treated with MG132. N-CoR-FLAG was immunoprecipitated and its expression was detected by western blotting with anti-FLAG antibody. As an indication of loading control, level of total protein in each sample was determined by Coomassie Blue staining. (*Contributed by Pang Sze Li)

A

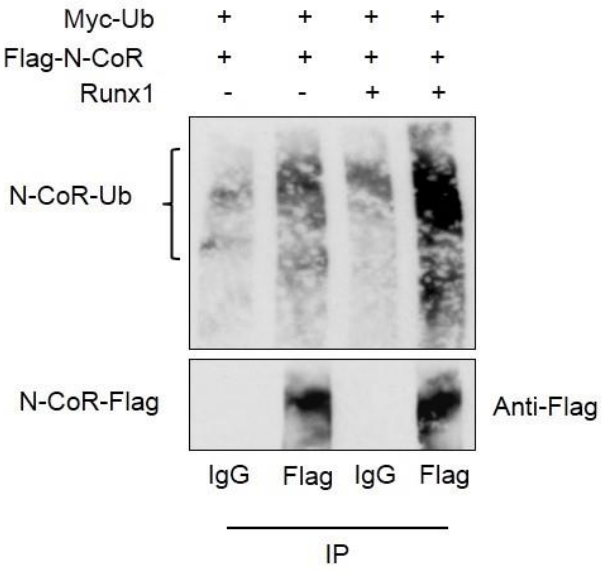

B

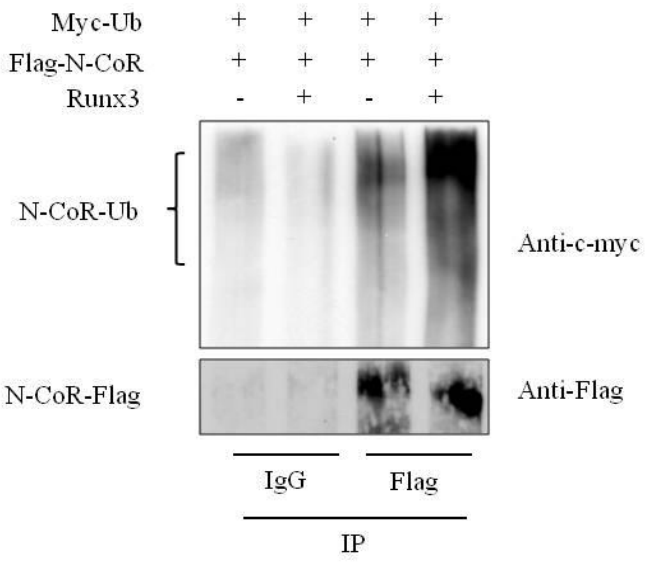

C

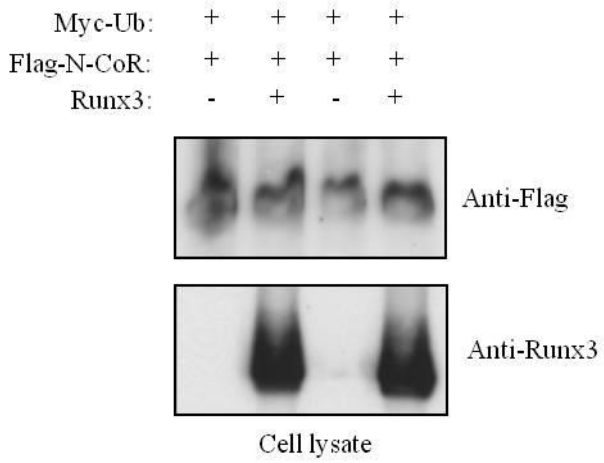

Figure 3.22. N-CoR degradation by Runx3 is mediated by the ubiquitin-proteosome pathway (UPP). 293T cells were transfected with the N-CoR-FLAG expression plasmid, myc-ubiquitin plasmid, and plasmids expressing *RUNX1* (A) or *RUNX3* (B), and subsequently treated with MG132. N-CoR-Flag was immunoprecipitated with anti-FLAG antibody, and level of ubiquitinated complexes were detected by western blotting using anti-c-myc antibodies. (C) The levels of N-CoR-FLAG and RUNX3 in each sample was examined by Western blotting and detected with anti-FLAG and anti-RUNX3 antibody.

3.25 Deletion analysis of RUNX1 and RUNX3 reveals intrinsic domains linked to N-CoR degradation

To investigate which domains of *RUNX1* and *RUNX3* are involved in N-CoR degradation, we assessed the effect of five deletion mutants on Runx1/3-mediated N-CoR degradation. The N-terminal sequence and part of the DNA-binding Runt homology domain was deleted in RUNX1.1 whereas the entire N-terminus and Runt domain was abolished in RUNX1.2. RUNX3.1 contained only the N-terminal sequence and the Runt domain, whereas RUNX3.2 contained only the transcription activation domain, transcription inhibitory domain, and a conserved VWRPY sequence at the C-terminal. Only the N-terminus was deleted in RUNX3.3 (Fig. 3.23). 293T cells were transfected with flag-tagged N-CoR and the deletion mutants and the effect of each deletion construct on the level of exogenous N-CoR was analysed by western blotting.

Both RUNX1 constructs containing deletions in the N-terminal sequence and the conserved Runt domain significantly inhibited N-CoR degradation, although RUNX1.1, which only lacked part of the Runt domain, abrogated N-CoR degradation to a lesser extent. While this suggests a role of the N-terminus and Runt domain in N-CoR degradation, the deletion of N-terminus in the RUNX3.3 mutant however did not abolish N-CoR degradation, implying that the N-terminal sequence is not required for N-CoR degradation. Additionally, construct RUNX3.2, which also lacked the Runt domain, only weakly inhibited N-CoR degradation. This suggests the involvement of other domains other than the Runt domain in N-CoR degradation. This might also explain why RUNX2 does not play a role in N-CoR degradation, despite

sharing the same conserved Runt domain with RUNX1 and RUNX3 (Fig. 3.24).

Consistent with this notion, we found that deletion construct RUNX3.1, which only contained the N-terminus and Runt domain, could not completely inhibit the degradation of N-CoR (Fig. 3.24). The data thus far suggests that both the Runt domain and the distal C-terminal sequence exert effects that are required, but not individually sufficient, for N-CoR degradation.

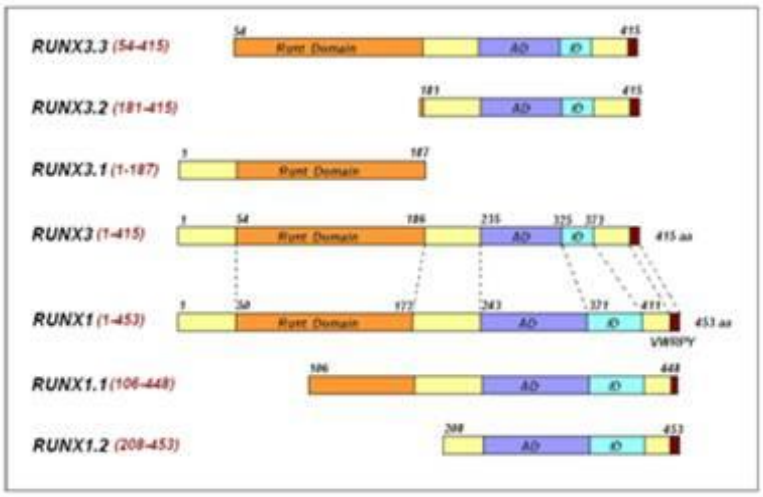

Figure 3.23. A schematic representation of RUNX1, RUNX3 and their deletion derivatives. The numbers indicate the positions of the amino acids that flank each of the protein domains shown above. AD: activation domain; ID: Inhibition domain; VWRPY: Binding motif for members of the Groucho protein family.

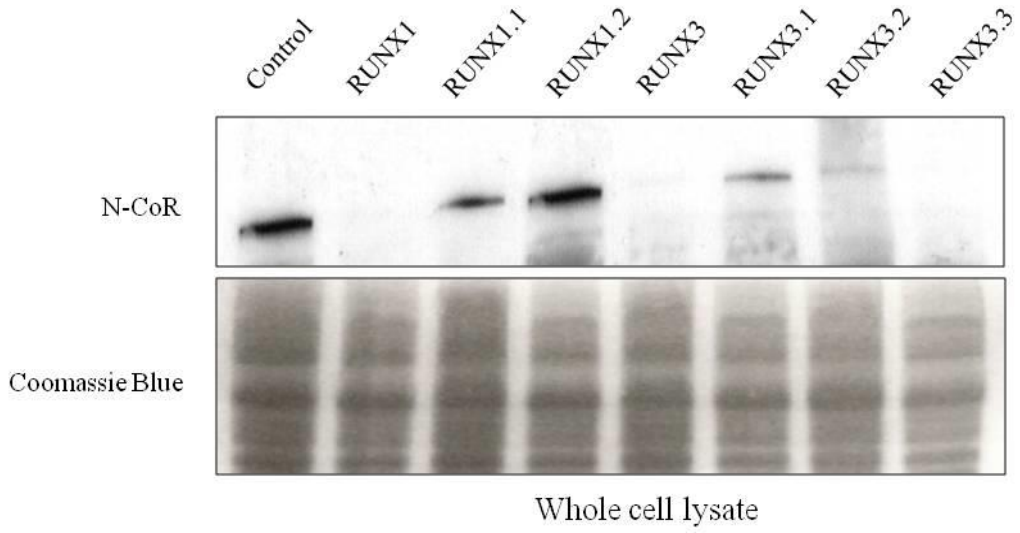

Figure 3.24. Mapping of intrinsic domains of RUNX1 & RUNX3 involved in N-CoR degradation. 293T cells were co-transfected with N-CoR-FLAG expression plasmid and plasmids expressing deletion mutants of RUNX1 and RUNX3 as indicated in Figure 3.23. The N-CoR protein levels were determined using anti-FLAG antibody. As an indication of loading control, level of protein in each sample was determined by Coomassie Blue staining. (*Contributed by Pang Sze Li)

3.26 N-CoR overexpression abrogrates Runx3-induced activation of TGF-β responsive promoter, Ig Cα.

We have shown that ablation of N-CoR significantly enhanced the transcriptional activation of the IgCα promoter, suggesting that N-CoR may play a part in the repression of TGF-β target genes. As Runx3 is a downstream target of the TGF-β signaling pathway, and also induces the cytoplasmic translocation and degradation of N-CoR, we hypothesize that N-CoR-mediated repression of TGF-β target genes may be mediated by Runx3.

As previously reported,[69] the IgCα germline promoter contained both TGF-β responsive element and RUNX binding sites. P19 cells were again transfected with IgCα reporter plasmids and increasing amounts of Runx3 plasmids at the indicated amounts, and luciferase activity was monitored. As expected, transcriptional activity of the promoter was significantly enhanced by Runx3, in a dose-dependent manner (Fig. 3.25). Next, we assessed the effect of N-CoR overexpression on the RUNX3-induced activation of the promoter. The transcriptional activation of the promoter induced by Runx3 was significantly decreased only when 1 μg of N-CoR-Flag was introduced into the cells, suggesting that overexpression of N-CoR abrogates Runx3-induced activation of the IgCα promoter (Fig. 3.26A). When 0.5 μg of N-CoR plasmids was transfected into the cells, N-CoR protein expression was almost undetectable, probably because Runx3 could still sufficiently promote N-CoR degradation (Fig.3.26B). Accordingly, transcriptional activity of the promoter promoted by Runx3 was not inhibited at this amount (Fig.3.26A). The data collectively suggests that interaction between N-CoR and Runx3 may play a role in repression and activation of TGF-β target genes.

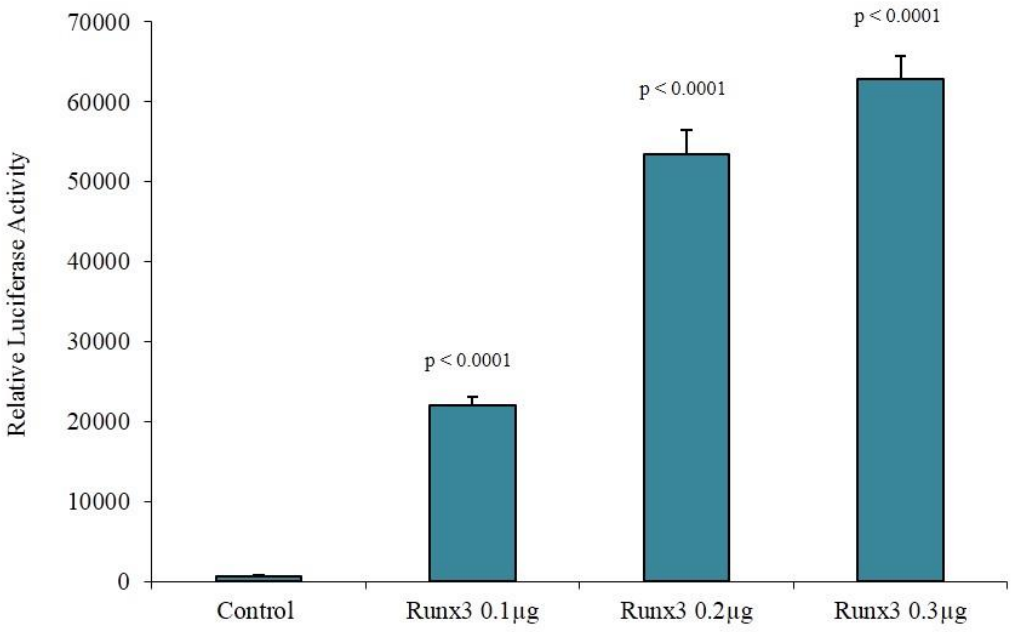

Figure 3.25. Runx3 significantly enhances the transcriptional activity of the TGF-β responsive IgCα promoter. P19 cells were transfected with 0.15 µg of reporter plasmids and expression plasmids containing either empty vector or Runx3 at the indicated amounts, and the luciferase activity was determined. The values plotted in the bar graph are average of three independent experiments. *p* values as compared with untreated controls.

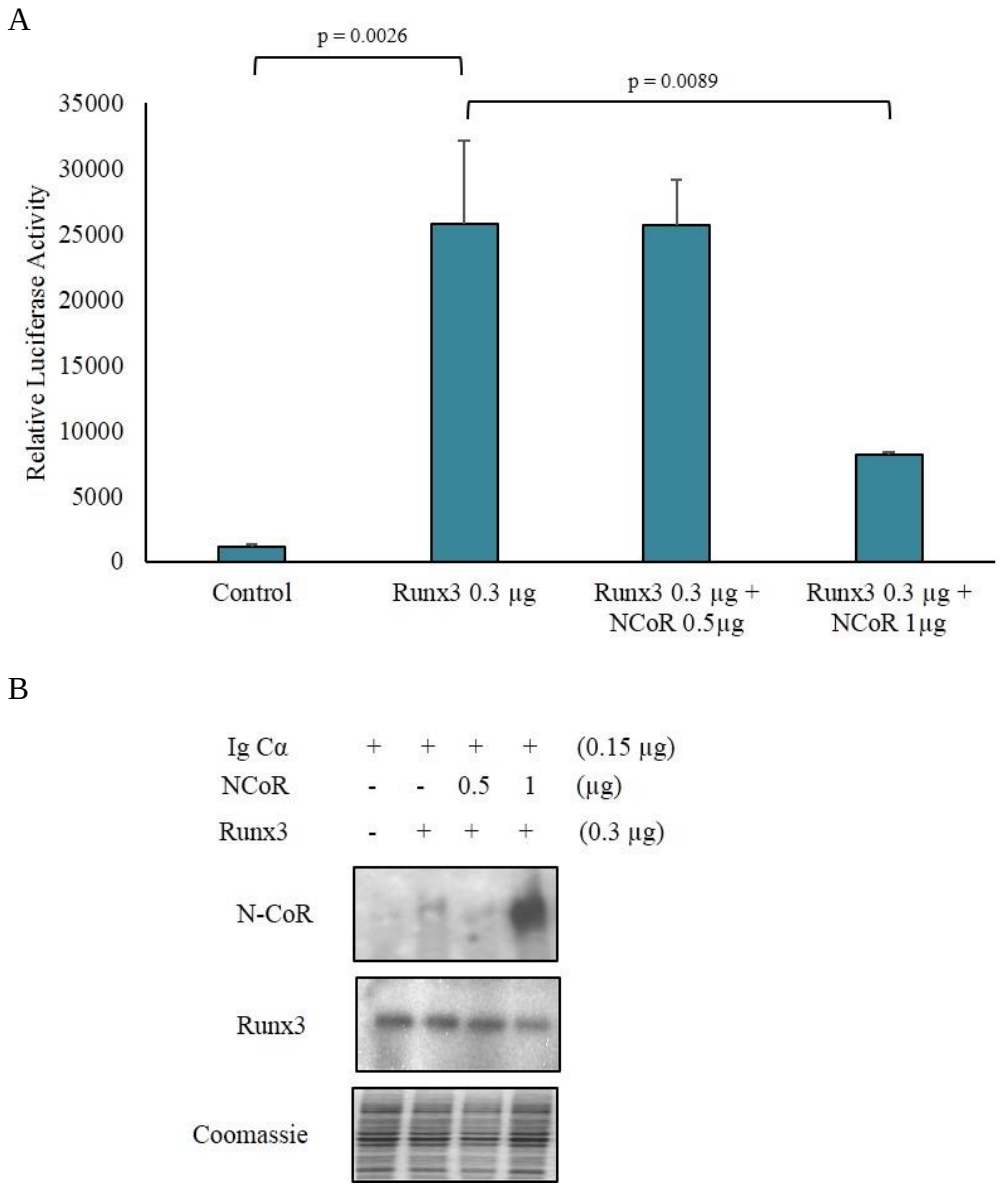

Figure 3.26. Overexpression of N-CoR abrogates Runx3-induced activation of the IgCα promoter. (A) P19 cells were transfected with 0.15 µg of reporter plasmid, 0.3 µg of Runx3 plasmid, and expression plasmids encoding flag-tagged N-CoR in the indicated combinations, and the luciferase activity was determined. The values plotted in the bar graph are average of three independent experiments. (B) Level of N-CoR and RUNX3 was determined by western blotting using anti-flag antibody and anti-RUNX3 antibodies respectively. As an indication of loading control, level of protein in each sample was determined by Coomassie Blue staining. *p* values, as compared with untreated controls, or with Runx3 controls.

3.3 N-CoR is misfolded in gastric cancer.

3.31 N-CoR loss in gastric cancer cells is a post-transriptional event.

The identification of GC011 as a potent inducer of TGF-β growth inhibitory pathway is potentially useful in clinical scenarios in which responsiveness to the tumor suppressive signals of the TGF-β pathway still remains, such as early stage cancers, or for a selected group of TGF-β sensitive tumor subtypes. However, gastric cancer cells which are no longer sensitive to the growth inhibitory effects of TGF-β would be resistant to GC011 treatment, indicating a need for an alternative therapeutic approach for such cases.

Previously, our laboratory has reported a role of misfolded conformation dependent loss (MCDL) of N-CoR in the pathogenesis of acute promyelocytic leukemia (APL)[187] and subsequently identified inhibition of N-CoR misfolding as an attractive strategy for treatment. Since we have previously determined that N-CoR protein in TGF-β resistant cell line SNU5 was down-regulated (Fig. 3.11) and aberrantly localized in the cytosol (Fig. 3.10), we postulate that an APL-like loss of N-CoR may be involved in gastric cancer as well. To determine this, we proceeded to investigate the status of N-CoR in a panel of commercially available gastric cancer cell lines. Western blot analysis of whole crude extracts of the cell lines revealed N-CoR protein to be differentially expressed. In concordance with our previous findings, TGF-β sensitive cell lines SNU16 and SNU620 expressed N-CoR at the protein level. Compared to these two cell lines, N-CoR protein expression was significantly downregulated in most of the remaining cell lines (Fig. 3.27). This observed downregulation of N-CoR in gastric cancer cells was not seen at the

transcriptional level, as both semi-quantitative PCR and real-time PCR analysis revealed no significant downregulation of transcript levels as compared to SNU16 cells (Fig. 3.28). This data suggests that the observed N-CoR loss in the remaining cell lines is likely a post-transcriptional event.

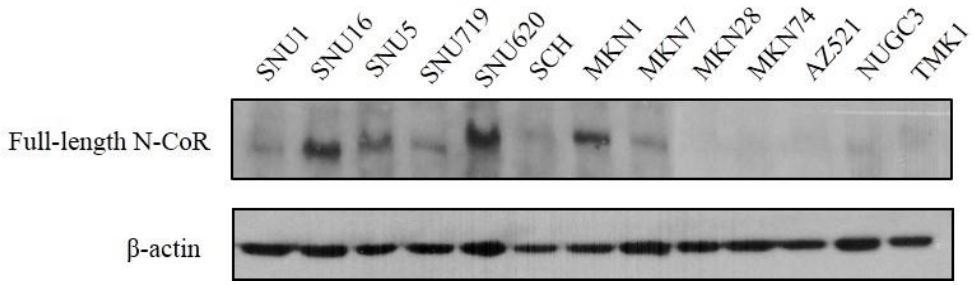

Figure 3.27. Differential N-CoR protein expression in gastric cancer cell lines. Whole cell extracts were prepared from a panel of human gastric cancer cell lines and 100 μg of each sample were resolved in SDS-PAGE. N-CoR protein expression was determined via western blotting with anti-N-CoR antibody. β-actin expression was used as loading control.

A

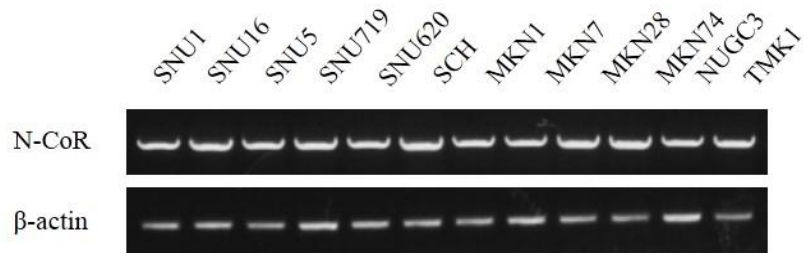

B

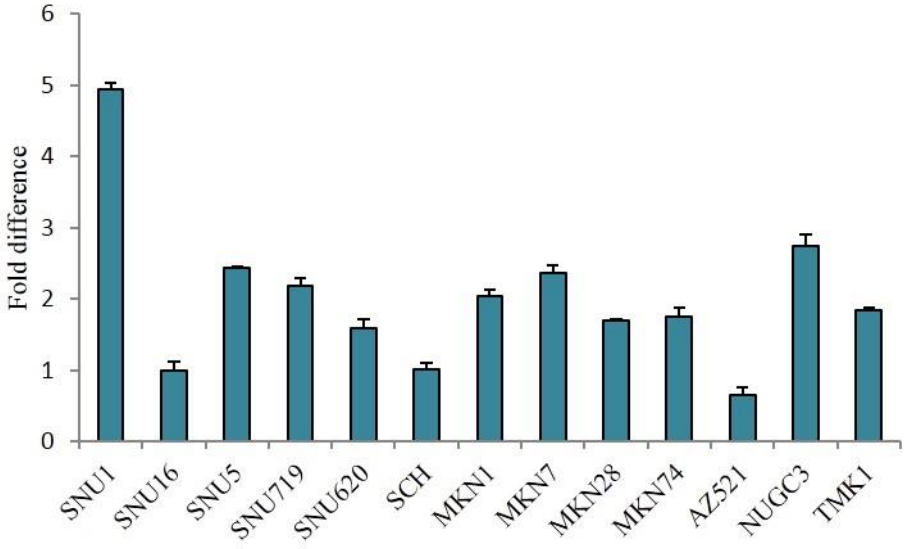

Figure 3.28. Loss of N-CoR protein expression is a post-transcriptional event. Low levels or loss of N-CoR protein expression in gastric cancer cell lines do not correlate with N-CoR transcript expression as determined by semi-quantitative PCR (A) and real-time PCR (B) analysis. Relative expression of N-CoR gene gastric cancer cell lines were determined by real time PCR analysis. Data was analyzed using the comparative Ct method using the expression level N-CoR gene in SNU-16 cells as the reference value, and the level of expression of the HPRT gene was used as control. Raw Ct values which registered as undetermined were set to 40. (Results presented are the average of 3 independent experiments.)

3.32 N-CoR is predominantly mislocalized in the cytosol of most gastric cancer cell lines and is linked to ER stress.

In its normal state, N-CoR is a ubiquitously expressed corepressor which mediates repression associated with nuclear receptors and a myriad of other transcription factors in the nucleus. Previous studies in our laboratory have determined that N-CoR in its native conformation is soluble in buffers containing organic detergent and is largely confined to the nucleus, whereas misfolded N-CoR is detergent-insoluble, largely localized in the endoplasmic reticulum, and is associated with ER stress amplification. As N-CoR protein in majority of the gastric cancer cells was shown to be significantly downregulated, we hypothesized that this N-CoR loss may be triggered by its misfolding. To test this possibility, we first analysed the subcellular distribution of N-CoR in gastric cancer cell lines by immunofluorescent staining. The results demonstrated that a significant amount of N-CoR was detected in the cytoplasm of most of the gastric cancer cell lines. In contrast, N-CoR was mainly localized in the nucleus of TGF-β-sensitive cell lines, SNU16 and SNU620 (Fig. 3.29A). Consistent with this data, western blot analysis of nuclear and cytoplasmic extracts of SNU16, SNU620, SNU5 and MKN74 cells respectively indicated that while majority of N-CoR was found in the nuclear fractions of TGF-β responsive SNU16 and SNU620 cells, N-CoR was largely cytoplasmic in SNU5 and MKN74 cells (Fig. 3.29B).

Next, we assessed the solubility of N-CoR protein in three cell lines, SNU5, SCH and SNU16 cells in organic detergent NP-40. Consistent with our hypothesis that N-CoR is misfolded in most gastric cancer cells, it was found

that a significant portion of N-CoR detected in SNU5 and SCH was insoluble in NP-40 detergent. In contrast, N-CoR in SNU-16 cells was largely detected in the soluble fraction, further indicating that the N-CoR in SNU16 cells is not compromised in its conformation (Fig. 3.30).

To investigate if misfolded N-CoR in gastric cancer cells contributes to ER stress amplification, expression levels of ER resident proteins GRP78 and PDI protein in gastric cancer cells was determined. The data revealed that both GRP78 and PDI levels was significantly higher across all gastic cancer cell lines as compared to that observed in SNU16 cells, which expressed N-CoR mainly in the nucleus, suggesting that the presence of misfolded N-CoR in the other cell lines was responsible for the increased ER stress levels observed (Fig. 3.31). These findings collectively indicated a role of misfolded N-CoR in the amplification of ER stress in gastric cancer cells.

A

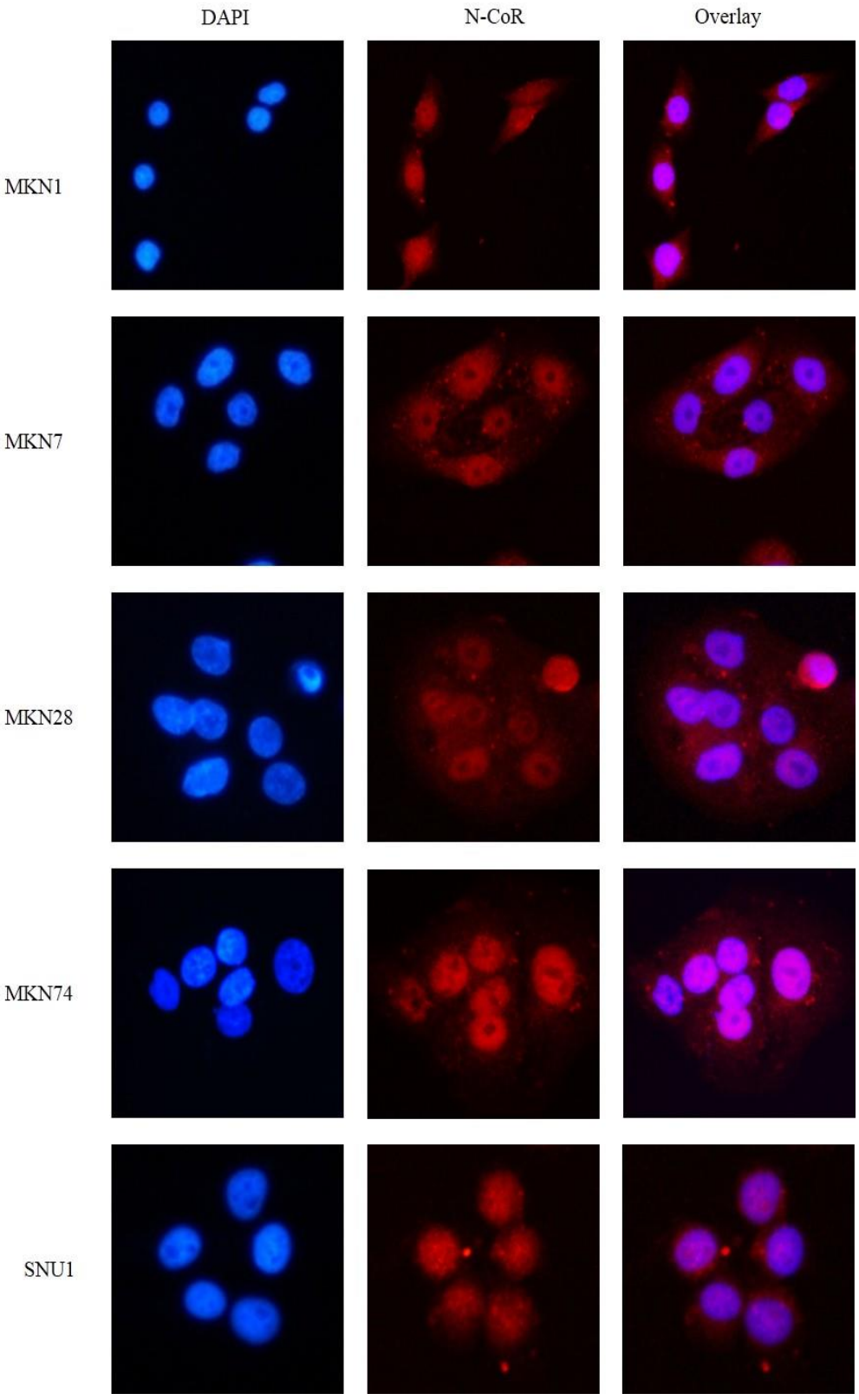

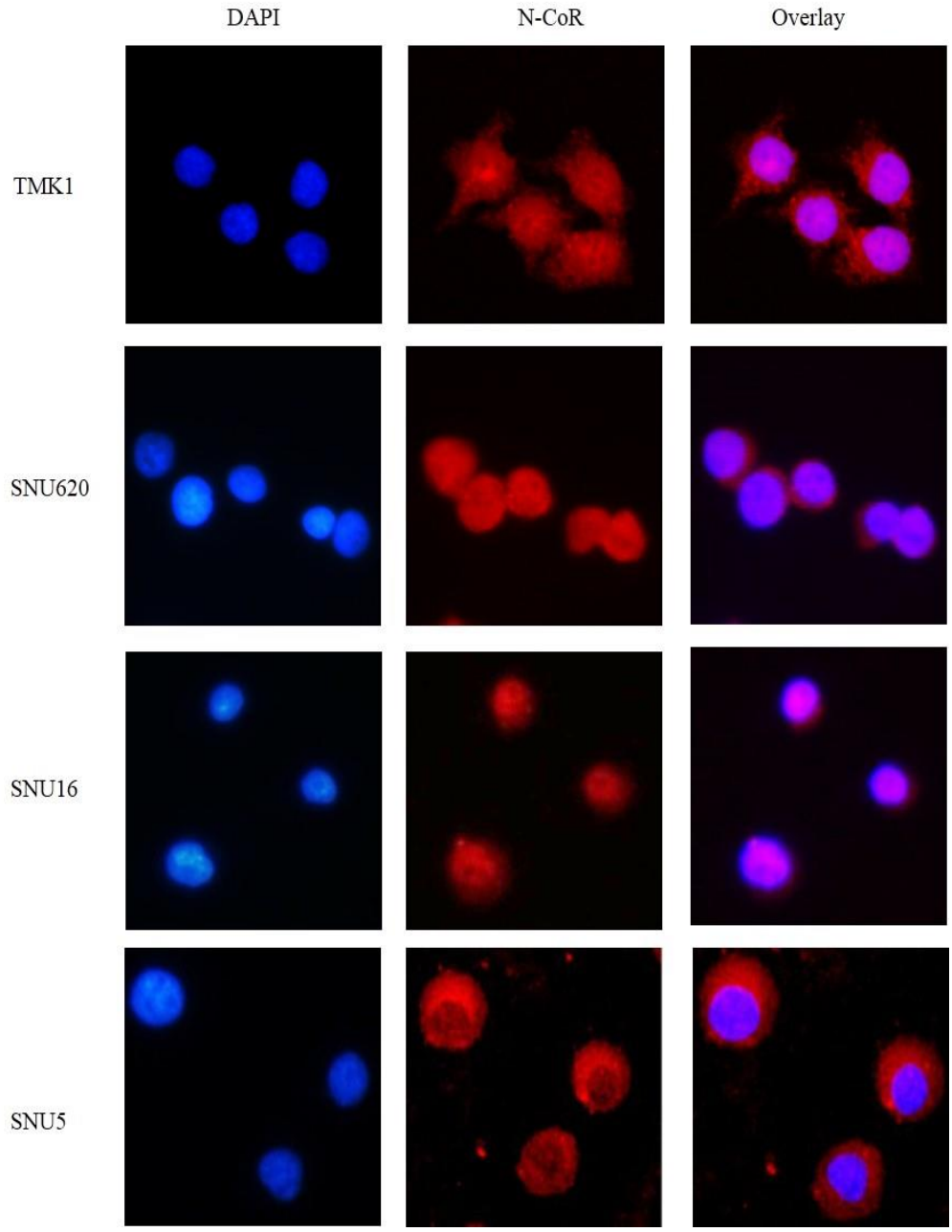
DAPI
N-CoR
Overlay
TMK1
SNU620
SNU16
SNU5

B

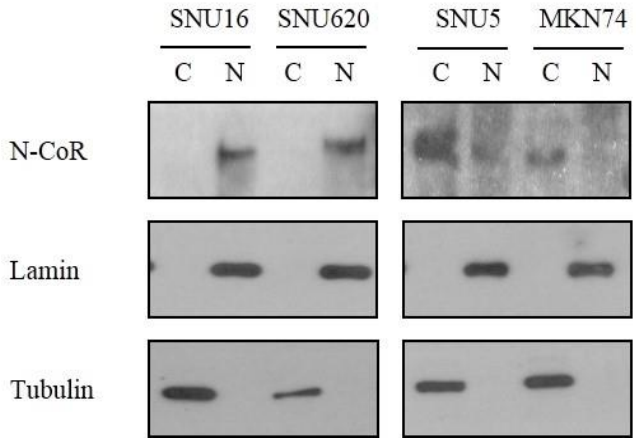
SNU16
SNU620
SNU5
MKN74
C N C N C N C N
N-CoR
Lamin
Tubulin

Figure 3.29. Aberrant cytoplasmic N-CoR is present in all gastric cancer cell lines, with the exception of TGF-β sensitive SNU16 and SNU620 cells. Subcellular distribution of N-CoR was determined in various gastric cancer cells by immunofluorescence staining and fractionation assay. (A) Cells were stained with an anti-N-CoR antibody (red) and counterstained with DAPI for nuclear detection (blue) and cells were visualised using confocal microscopy. (B) 100 μg (SNU16 & SNU620) or 200 μg (SNU5 & MKN74) of nuclear and cytoplasmic extracts were loaded for western blotting for detection of N-CoR with anti-N-CoR antibody. Level of lamin (nuclear marker) and tubulin (cytoplasmic marker) was determined to check for cross contamination of nuclear and cytoplasmic extracts and also as loading controls.

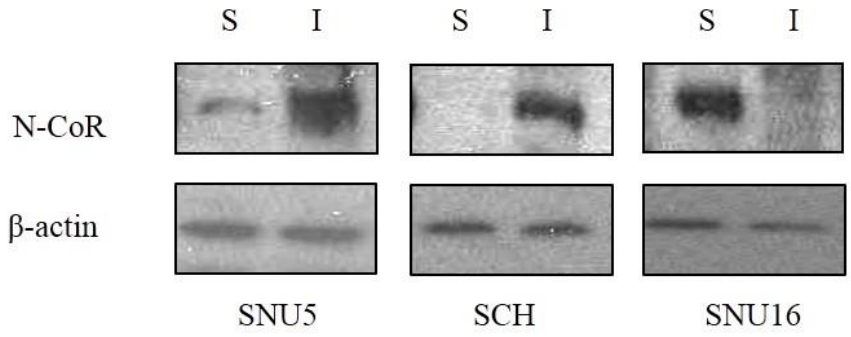

Fig. 3.30. A significant portion of N-CoR protein in SNU5 and SCH cell lines is detergent-insoluble, whereas N-CoR in SNU16 cells is largely soluble. Protein solubility assay was performed on SNU5, SCH and SNU16 cell lines to determine the relative solubility of N-CoR protein in detergent. Soluble (S) and insoluble (I) fractions were obtained and N-CoR level in each fraction was determined by western blotting using anti-N-CoR antibody.

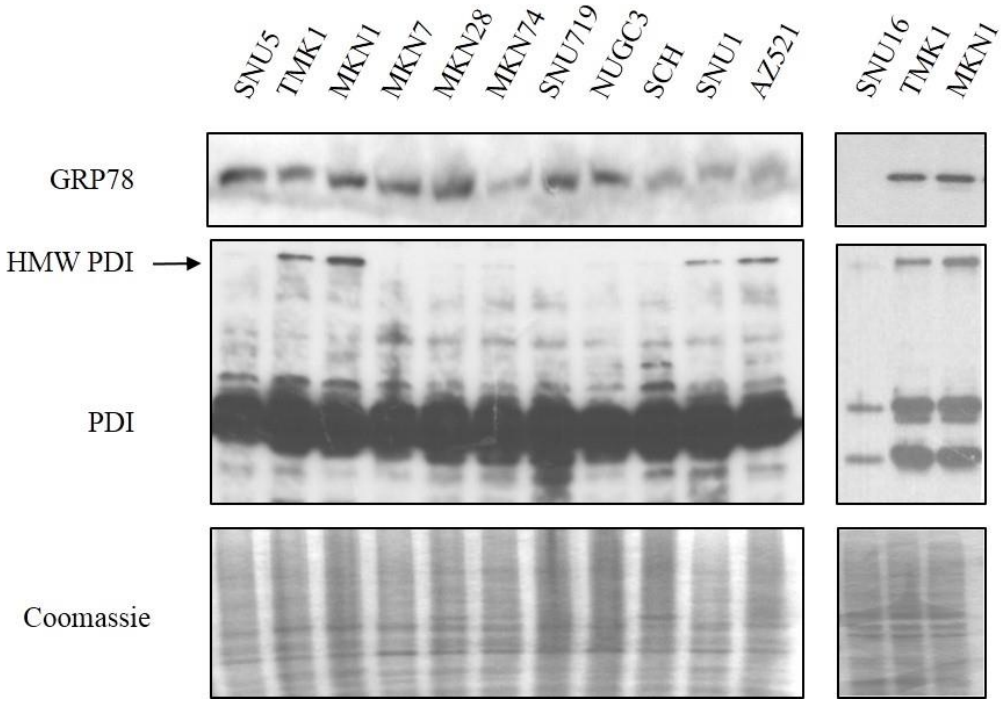

Fig. 3.31. Misfolded N-CoR in gastric cancer cells is linked to ER stress amplification. Relative level of ER stress in gsatric cancer cells was analysed by determining the levels of native and high molecular weight (HMW) PDI and GRP78 proteins via western blotting with anti-PDI and anti-GRP-78 antibodies. As an indication of loading control, level of protein in each sample was determined by Coomassie Blue staining.

3.33 N-CoR is mislocalized in the cytosol of human gastric tissue.

Next, we performed western blot analysis of crude protein extracts from human stomach tumor tissues, with extract from 293T cells as a positive control for N-CoR protein expression. Our results demonstrated that N-CoR expression at the protein level was also significantly reduced in clinical specimens (Fig. 3.32A). Additionally, immunohistochemical staining of a tissue array containing biopsy cores from human gastric tissue, both normal and tumor, showed that nuclear N-CoR was excluded from about 82% of the tumor cores (44 out of 54), 18.5% (10 out of 54) expressed N-CoR in both nucleus and cytoplasm, and all 54 tumor samples exhibited cytoplasmic distribution. In contrast, majority of the normal tissue samples displayed N-CoR in both nucleus and cytoplasm (88.9%, 8 out of 9) (Fig. 3.32B). Collectively, these findings suggested that the reduction of N-CoR protein expression and its aberrant cytoplasmic localization appear to be general traits of human gastric cancer cell lines and tumors, and that these traits may arise as a result of its misfolding.

A

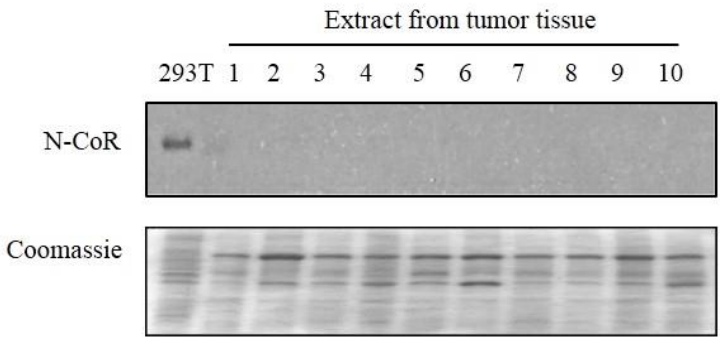

B

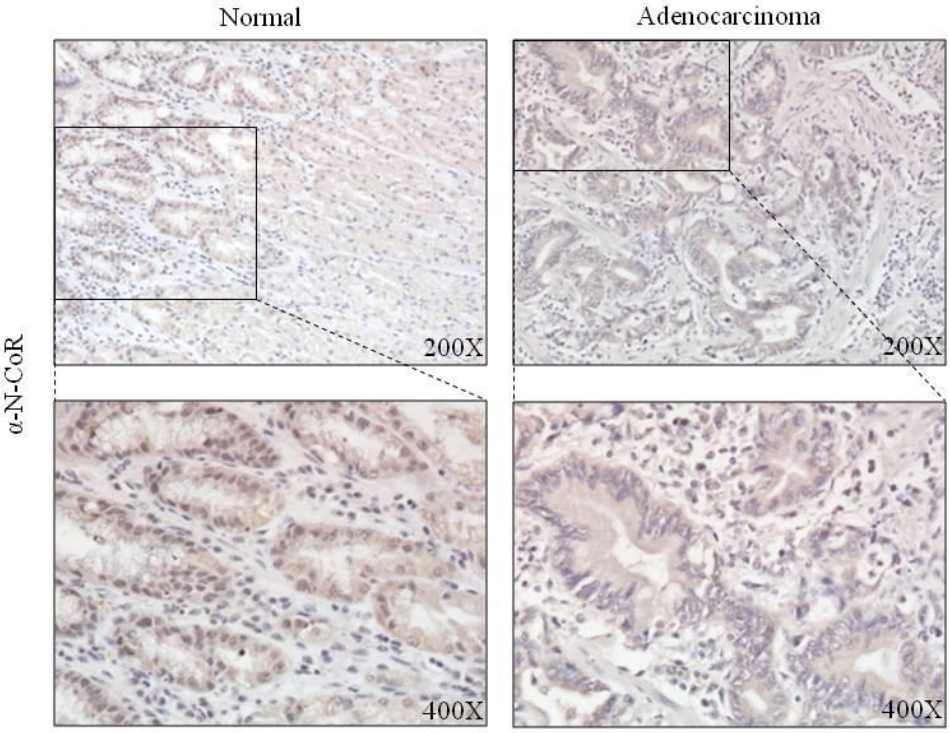

C

N-CoR localization	Normal (n=9)	Adenocarcinoma (n=54)
Nucleus + Cytoplasm -	1 (11.1%)	0
Nucleus – Cytoplasm +	0	44 (81.5%)
Nucleus + Cytoplasm +	8 (88.9%)	10 (18.5%)

Figure 3.32. N-CoR expression and localisation in human gastric tissue. (A) Crude extracts from patient tumor tissue are analysed via western blot for expression of N-CoR using anti-N-CoR antibody. (B) Immunohistochemistry staining of a tissue microarray of biopsy cores from human gastric tissue, both tumor and normal, using anti-N-CoR antibody. Counterstaining was done with hematoxylin. The boxed regions on the top panel were enlarged in the lower panel.

3.4 Bortezomib, a 26S proteasome inhibitor, therapeutically targets the UPR pathway in gastric cancer by inhibiting the degradation of misfolded N-CoR.

3.41 Bortezomib promotes growth arrest in gastric cancer cells.

Previous findings in our laboratory have associated endoplasmic reticulum-associated degradation (ERAD) and protease-mediated degradation of misfolded N-CoR with resistance to UPR-induced apoptosis in APL.[188] As N-CoR in gastric cancer cells appear to be misfolded, we postulated that inhibition of misfolded N-CoR degradation in these cells may sensitize them to UPR-induced apoptosis. Bortezomib, a dipeptidyl boronic acid compound that reversibly blocks the proteolytic activity of the proteasome, is an FDA-approved drug for the treatment of multiple myeloma (MM), and various studies have reported its antitumor activities on other cancer types, including gastric cancer.[166-170] It has been reported that treatment of MM cells with bortezomib causes the abnormal accumulation or misfolding of Ig proteins within ER by suppressing ERAD, thus inducing ER stress and UPR, which eventually leads to the induction of apoptosis.[153,189] Therefore, we decided to investigate the effects of bortezomib in gastric cancer cells and determine if a similar mechanism underlies its antitumor activity.

We firstly examined the effect of bortezomib on growth of 12 gastric cancer cell lines as well as immortalized normal human gastric epithelial cell line, HFE-145. Cells were treated with bortezomib at concentrations ranging from 50 nM to 1 μM, for 24, 48 or 72 hours, and cell viability was measured by MTS assay. Results showed that bortezomib inhibited cell growth in a time

and concentration-dependent manner. While the gastric cancer cell lines displayed differential sensitivity to bortezomib, most of the cell lines showed significant growth imhibition with the lowest concentration of 50 nM bortezomib by 48 hours (Fig. 3.33B). In MKN74 cells, growth inhibition by 50 nM bortezomib was about 25% at 24 hours (Fig. 3.33A), and increased to 81% at 72 hours (Fig. 3.33C). Growth of SCH cells were already significantly inhibited at 24 hours (Fig. 3.33A) with 53% growth inhibition which increased to 84% at 72 hours (Fig. 3.33C). It was noted that even after 72 hours at maximal concentration of 1 μM of bortezomib treatment, cell growth of HFE-145 cells were not inhibited (Fig. 3.33). These data suggests that bortezomib at low concentration significantly inhibits growth of gastric cancer cells, but not in normal gastric cells.

A

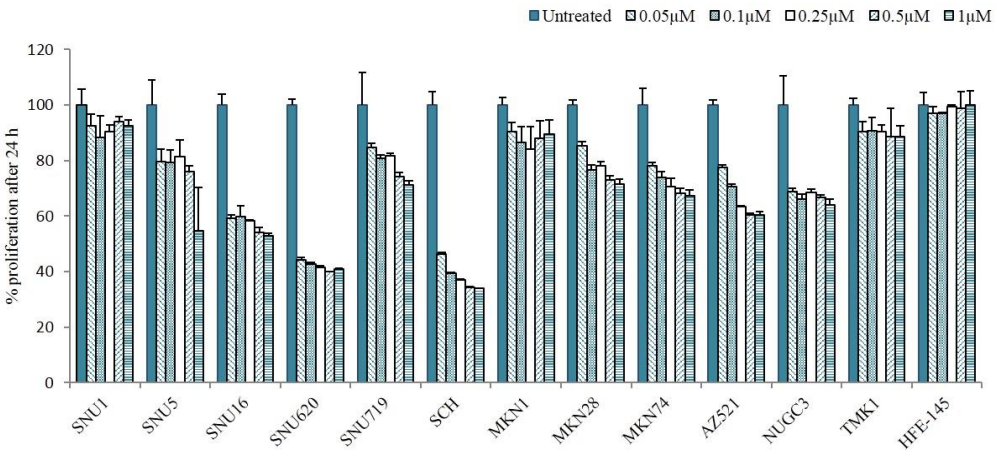

B

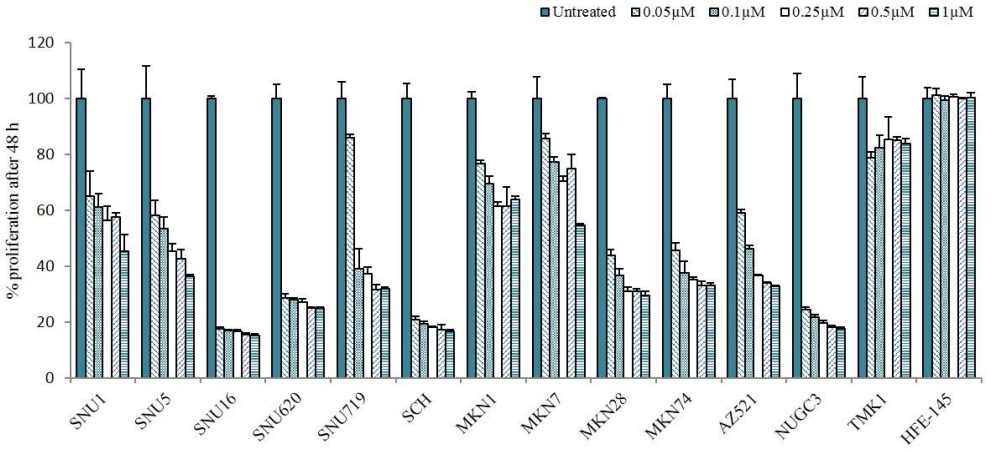

C

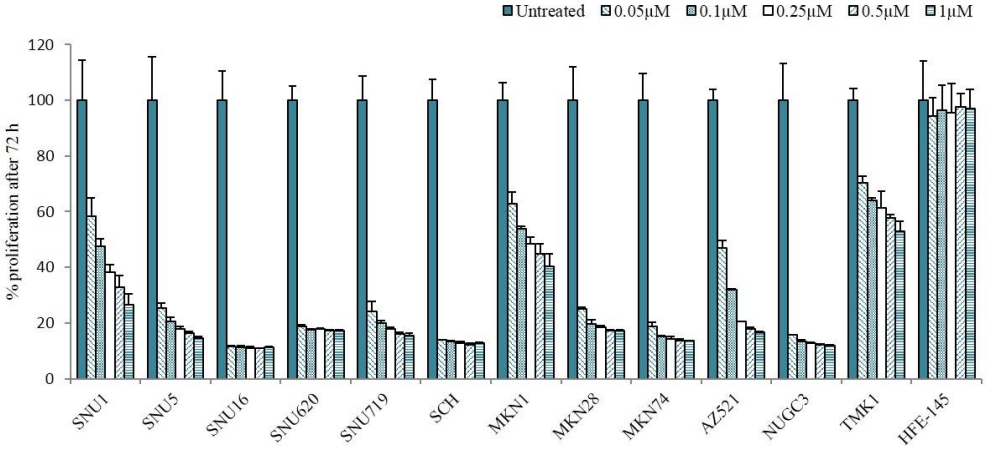

Figure 3.33. Bortezomib inhibits growth of gastric cancer cells in a time- and dose-dependent manner, but does not affect growth of normal HFE-145 cells. 12 gastric cancer cell lines and an immortalized human normal gastric epithelial cell line, HFE-145, were treated with various concentrations of bortezomib for the durations as indicated and the growth kinetics of the treated cells was measured by the MTS assay. A total of 3 wells were measured for each treatment at each time-point.

3.42 Bortezomib activates the apoptotic pathway in gastric cancer cells.

We then focused on MKN74 cells to further analyse the cellular response to bortezomib. To confirm whether the observed bortezomib-mediated growth inhibition was associated with apoptosis, we next performed fluorescence-activated cell sorting (FACS) on cells stained with AnnexinV-FITC/PI. In line with the growth inhibition data, bortezomib treatment potently induced apoptosis of MKN74 cells after 48 hours. This was shown by a dose-dependent increase in FITC-Annexin-positive/PI-negative early apoptotic cells and FITC-Annexin-positive/PI-double positive late apoptotic cells, from 32.7% cell death detected at 12.5 nM bortezomib, to 56.7% cell death at 50nM (Fig. 3.34).

We next assessed the effect of bortezomib treatment on protein levels of members of the apoptotic machinery; namely caspase-3, -9 and poly (ADP-ribose) polymerase (PARP). Again, MKN74 cells were treated with bortezomib ranging from 0 to 50 nM for 24 hours. As expected, bortezomib treatment resulted in a dose-dependent caspase-9 and caspase-3 activation, as well as PARP cleavage (Fig. 3.35). Taken together, the data therefore suggests that bortezomib induces apoptosis in gastric cancer cells.

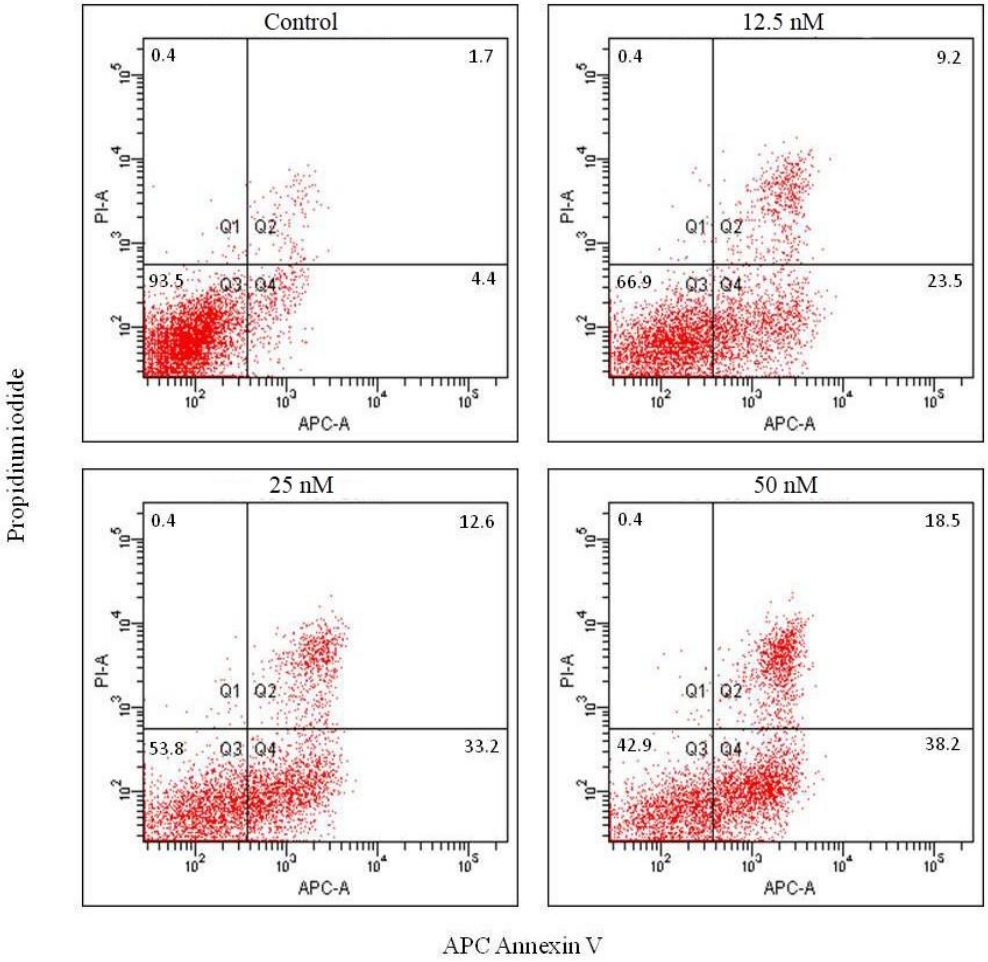

Figure 3.34. Bortezomib induces apoptosis in MKN74 cells. MKN74 cells were treated with increasing concentrations of bortezomib as stated for 48 hours. Fluorescence-activated cell sorting analysis was performed on the cells after reaction using AnnexinV-FITC and propidium iodide for detection of apoptotic cells.

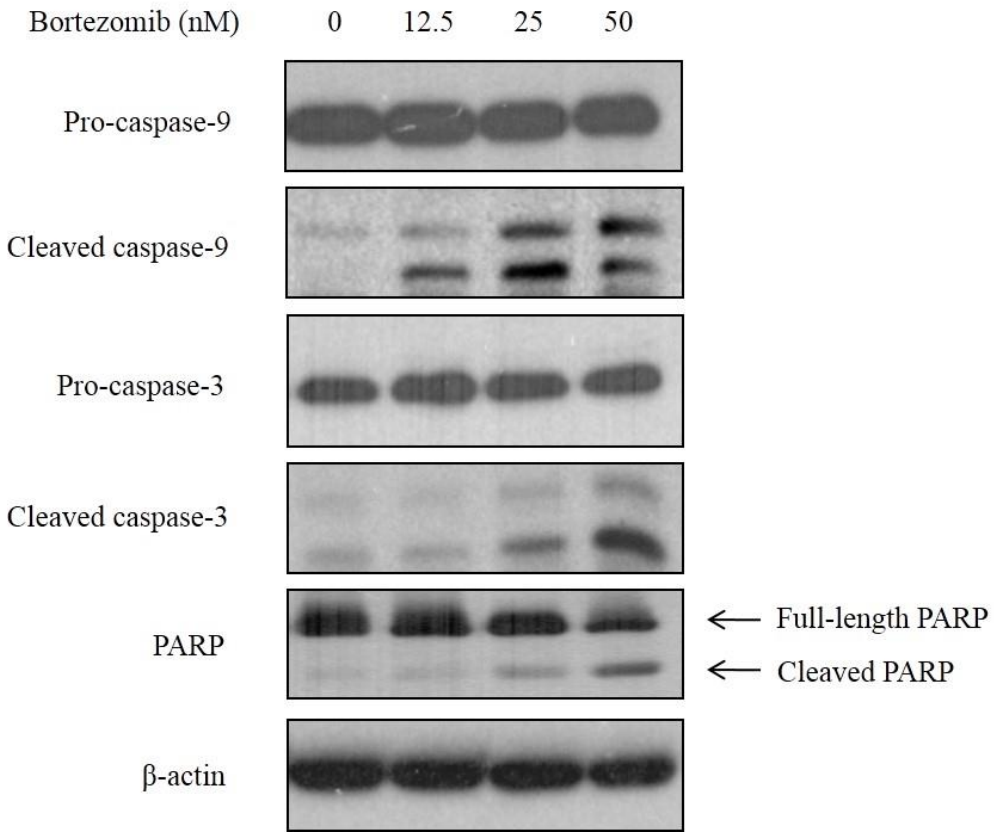

Figure 3.35. Bortezomib activates the apoptotic pathway in MKN74 cells. MKN74 cells were treated with bortezomib in a dose-dependent manner for 24 h. Western blot analysis of the crude lysates prepared in SDS lysis buffer were carried out using anti-caspase 9, anti-caspase 3, and anti-PARP antibodies. β-actin expression was used as loading control.

3.43 Bortezomib promotes the accumulation of misfolded N-CoR by blocking its degradation of N-CoR in gastric cancer cells.

The protein expression of N-CoR was previously screened in a panel of gastric cancer cell lines, and it was found that N-CoR expression was downregulated in most cell lines. To investigate if bortezomib has any effect on N-CoR expression, western blot analysis was carried out on MKN74 cells treated with increasing concentrations of bortezomib (0-50 nM) for 24 hours. The resulting data revealed that treatment of MKN74 cells with bortezomib led to a stabilization of N-CoR protein in a dose-dependent manner (Fig. 3.36A). Treatment of two other cell lines, SCH and SNU5, with 50 nM bortezomib at 24 hours likewise resulted in an upregulation of N-CoR protein expression (Fig. 3.36B).

It was postulated that bortezomib may cause accumulation of misfolded N-CoR, similar to the accumulation of misfolded Ig in multiple myeloma. To test this hypothesis, the subcellular distribution and solubility of N-CoR stabilized by bortezomib were assessed. Western blot analysis of the nuclear and cytoplasmic extracts of bortezomib-treated MKN74 cells revealed that bortezomib led to a significant accumulation of N-CoR in the cytoplasm of MKN74 cells in a dose-dependent manner (Fig. 3.37A). In contrast, the level of N-CoR in the nuclear extracts increased to a much smaller extent with bortezomib treatment. Solubility assessment of N-CoR in bortezomib-treated MKN74 cells also showed that detergent-insoluble N-CoR accumulated to a much greater extent as compared to detergent-soluble N-CoR (Fig. 3.37B).

Together, these data suggest that bortezomib promotes the accumulation of misfolded N-CoR in the cytoplasm.

Several studies have identified the involvement of several kinases in the regulation of co-repressor function. IKKα (inhibitor of nuclear factor kappa-B kinase subunit alpha kinase) and MEKK-1 (MEK-1 kinase), both serine-threonine protein kinases, have been shown to phosphorylate SMRT (silencing mediator for retinoid and thyroid hormone receptors), another major nuclear receptor co-repressor closely related to N-CoR, resulting in its nuclear export[190,191] N-CoR has likewise been shown to be phosphorylated by IKKα.[94] Other than altering the receptor interaction properties of corepressors, phosphorylation of corepressors has also been proposed to change its subcellular distribution from a nuclear to a cytoplasmic distribution, thereby relieving it of its repressive function on target gene expression. Previous studies in our laboratory also suggest that post-translational modification such as glycosylation, phosphorylation, and ubiquitination may significantly alter the conformation and function of N-CoR. To investigate if N-CoR misfolding in gastric cancer cells is also accompanied by a similar post-translational modification, level of serine-threonine phosphorylation in misfolded N-CoR stabilized by bortezomib was determined. N-CoR in bortezomib-treated MKN74 cell extracts was immunoprecipitated using anti-N-CoR antibody, resolved by SDS-PAGE, and western blot analysis was carried out for detection of serine/threonine phosphorylation using anti-pan-phospho serine/threonine antibody. The results showed that the N-CoR in MKN74 cells were phosphorylated at the serine/threonine residues, and stabilized N-CoR following bortezomib treatment also displayed serine/threonine

phosphorylation (Fig. 3.38). The concomitant increase of phosphorylation level and N-CoR protein stabilized by bortezomib treatment suggests that while phosphorylation of N-CoR in MKN74 may possibly play a role in its misfolding or aberrant localisation, bortezomib does not inhibit its aberrant phosphorylation to rescue its native conformation. This further suggests that bortezomib promotes the accumulation of misfolded N-CoR, possibly by inhibiting its degradation instead.

A

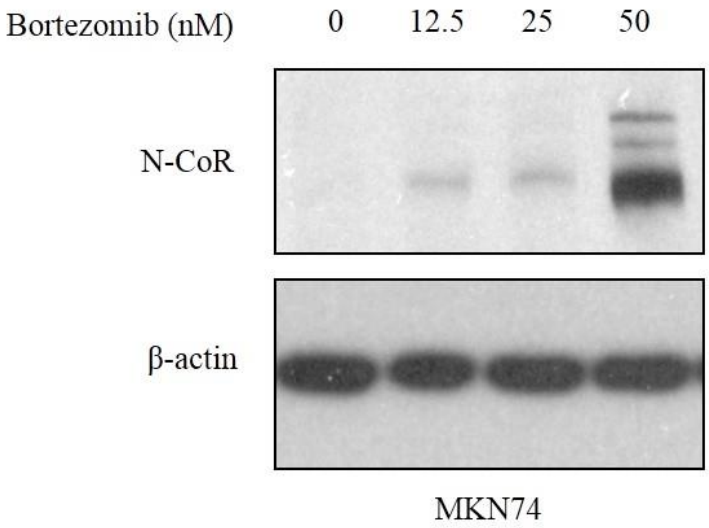

B

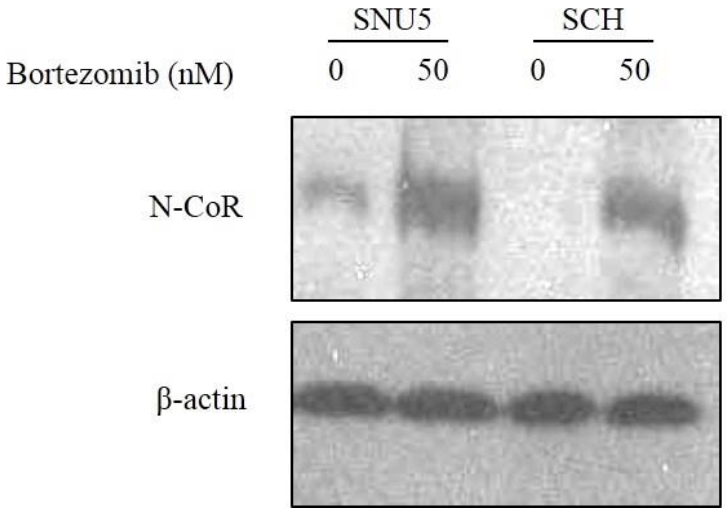

Figure 3.36. **Bortezomib stabilises N-CoR in gastric cancer cells.** (A) MKN74 cells were treated with increasing doses of bortezomib as stated for 24 h and protein extracts were prepared in SDS loading buffer. (B) SNU5 and SCH cells were treated with 50 nM of bortezomib for 24 hours and crude extracts were obtained. N-CoR was detected by western blotting using anti-N-CoR antibody and level of β-actin expression was determined as an indication of loading control.

A

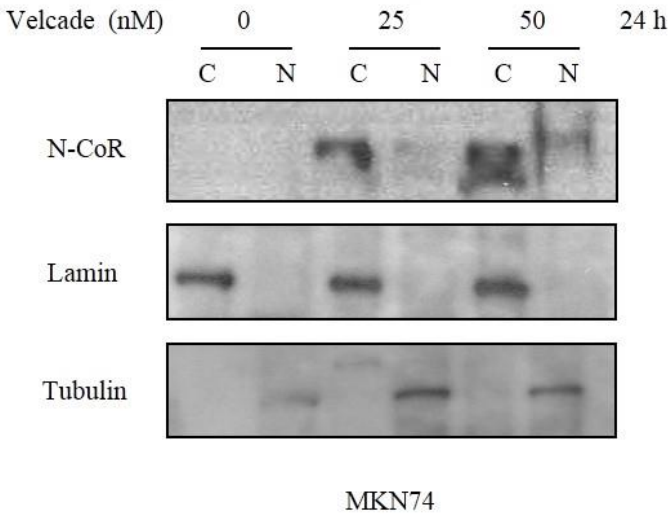

B

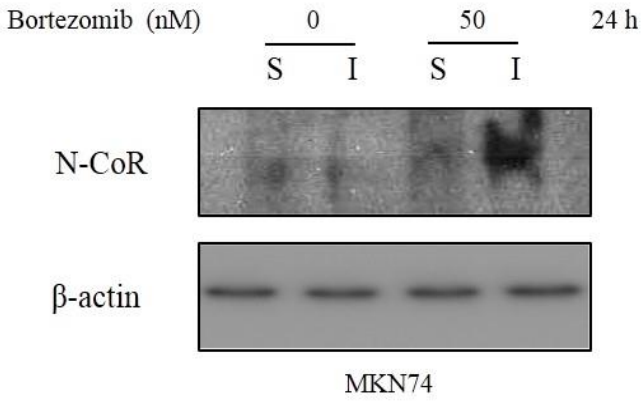

Figure 3.37. **Misfolded N-CoR accumulates in the cytoplasm of MKN74 cells with bortezomib treatment.** (A) MKN74 cells were treated with increasing doses of bortezomib as stated for 24 hours and nuclear and cytoplasmic extracts were obtained. N-CoR was detected by western blotting using anti-N-CoR antibody. Level of lamin (nuclear marker) and tubulin (cytoplasmic marker) was determined to check for cross contamination of nuclear and cytoplasmic extracts and also as loading controls. (B) Protein solubility assay was performed on MKN74 cells treated with 50 nM bortezomib for 24 hours to determine the relative solubility of N-CoR protein in detergent. Soluble (S) and insoluble (I) fractions were obtained and N-CoR level in each fraction was detected by western blotting using anti-N-CoR antibody. Level of β-actin expression was determined as an indication of loading control.

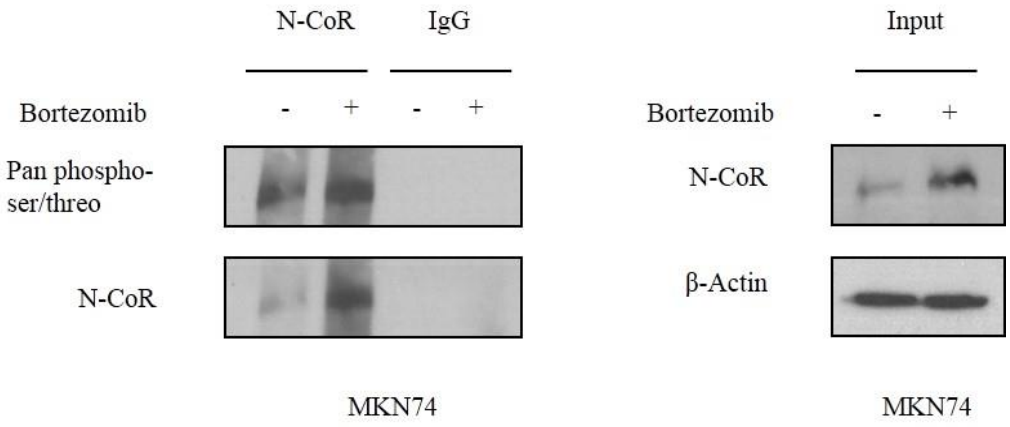

Figure 3.38. Misfolded N-CoR in MKN74 cells displays aberrant serine/threonine phosphorylation. Levels of serine/threonine phosphorylated N-CoR in MKN74 cells treated with bortezomib was determined by staining the immunoprecipitated N-CoR protein with a pan-phospho serine/threonine antibody. An aliquot of immunoprecipitated N-CoR was also stained with N-CoR antibody. Level of total N-CoR protein pulled down in each treated sample was determined by western blotting and β-actin expression was used as a loading control.

3.44 Bortezomib inhibits the trypsin-like, chymotrypsin-like and caspase-like activities of the proteasome in MKN74 cells.

Given its function as a proteasome inhibitor, it is very likely that accumulation of misfolded N-CoR by bortezomib is a result of its inhibition of the proteasome. To validate this hypothesis, a proteasome activity assay was performed to measure proteosomal activity in MKN74 cells treated with 0 - 50 nM bortezomib for 4 or 24 hours. Three proteolytic activities associated with the proteasome (chymotrypsin-like, trypsin-like, and caspase-like) were measured. The results showed that bortezomib treatment significantly inhibited all three proteolytic activities of the proteasome, in a dose- and time-dependent manner. Significant proteosomal inhibition was already detected at 4 hours post treatment with bortezomib (Fig. 3.39). This data suggests that accumulation of misfolded N-CoR mediated by bortezomib is most likely due to inhibition of its degradation due to proteosomal inhibition.

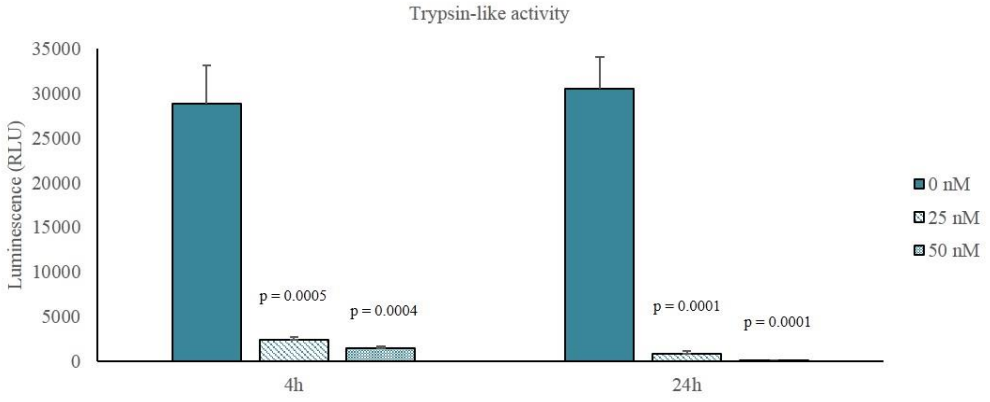

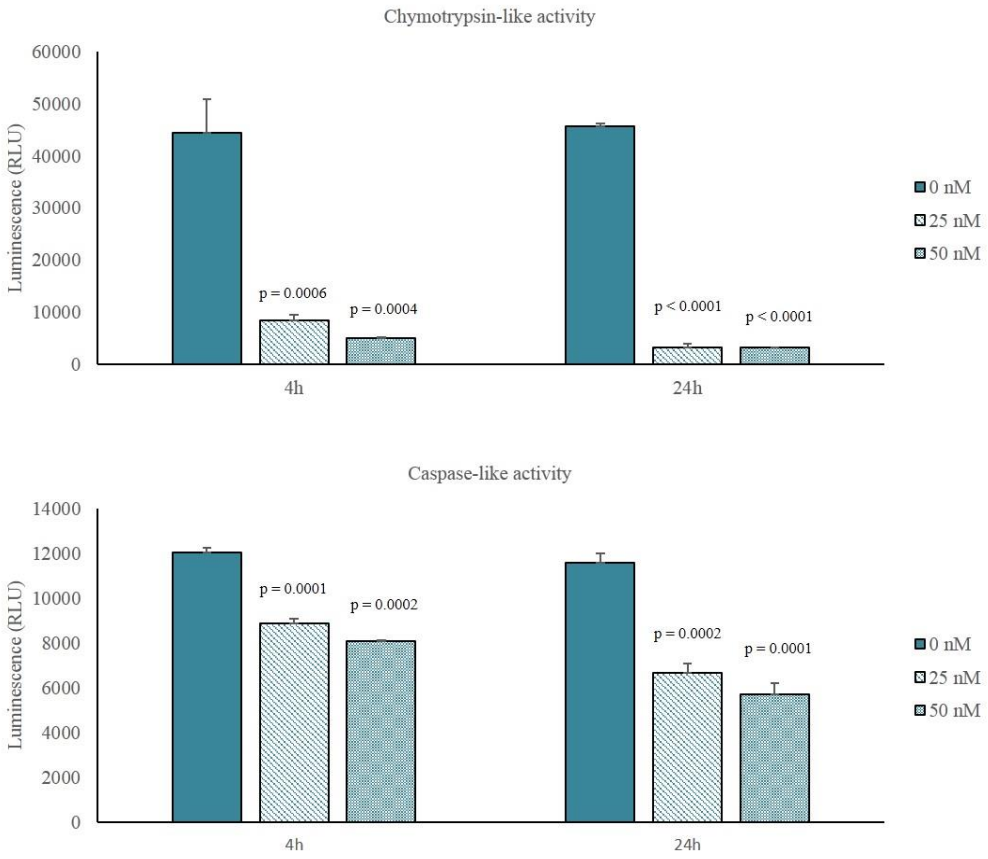

Figure 3.39. Velcade inhibits the trypsin-like, chymotrypsin-like and caspase-like peptidase activities of the proteasome. Crude extracts obtained from MKN74 cells treated with 0 – 50 nM of curcumin for 4 hours and 24 hours show reduced proteosomal activities. *p* values, as compared with untreated controls

3.45 Bortezomib promotes ER stress amplification in MKN74 cells.

It has been shown that bortezomib promotes accumulation of insoluble N-CoR in the cytoplasm of MKN74 cells (Figure 3.37). To test if accumulation of N-CoR mediated by bortezomib is linked to amplification of ER stress, protein levels of ER stress markers, GRP78, HSP60 and PDI, was determined by western blot analysis of bortezomib-treated MKN74 cells. Bortezomib induced the formation of high molecular weight (HMW) PDI in a dose-dependent manner (Fig. 3.40A). Additionally, treatment of bortezomib for different time points also indicated the upregulation of GRP78 and HMW HSP60 and PDI expression in a time-dependent manner (Fig. 3.40B). Collectively, these data suggest that bortezomib contributes to ER stress via inhibiting the degradation of misfolded N-CoR in MKN74 cells.

A

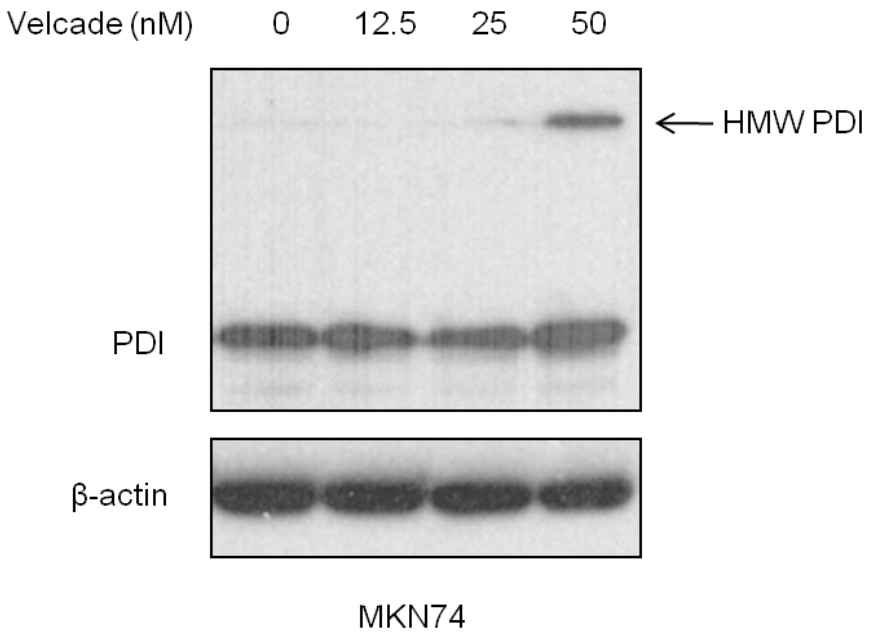

B

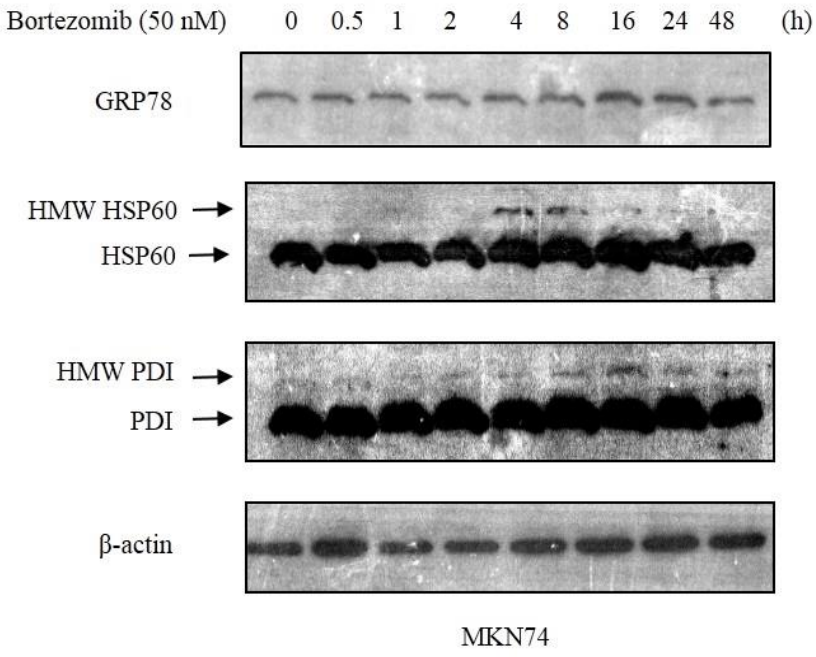

Figure 3.40. Bortezomib promotes formation of HMW ER stress markers GRP78, PDI and HSP60 in a dose- and time-dependent manner. (A) MKN74 cells were treated with bortezomib in a dose-dependent manner at the concentrations indicated for 24 hours. Western blot detection was carried out on the crude extracts using anti-PDI antibody. (B) MKN74 cells were treated with 50 nM of bortezomib in a time-dependent manner between 0-48 hours. Western blot detection was carried out on the crude extracts using anti-GRP78, anti-HSP60 and anti-PDI antibodies. Level of β-actin expression was determined as an indication of loading control.

3.46 Bortezomib induces UPR-induced apoptosis in MKN74 cells.

So far, bortezomib has been shown to induce the accumulation of misfolded N-CoR in MKN74 cells, which resulted in amplification of ER stress (Fig. 3.36, 3.37 & 3.40). Since bortezomib was also shown to activate the apoptotic pathway at similar doses (Fig. 3.34 & 3.35), it was hypothesized that the accumulation of misfolded N-CoR by bortezomib may activate unfolded protein response (UPR) in these cells, eventually leading to programmed cell death. As such, the effects of bortezomib on UPR were investigated next.

UPR involves three signaling pathways which originate in the ER, mediated by three ER transmembrane proteins – inositol-requiring enzyme 1(IRE-1), pancreatic ER kinase (PKR)-like ER kinase (PERK), and activating transcription factor 6 (ATF6). As unfolded proteins accumulate in the ER, these proximal sensors are activated by their dissociation from ER chaperone GRP78, which leads to their activation and triggers the UPR. UPR is initially triggered to reduce accumulation of unfolded proteins to restore ER homeostasis. In cases where protein accumulation and ER stress persists beyond the folding capacity of the ER, UPR signaling switches from pro-survival to pro-apoptotic.[130,137]

Westerm blot analysis of UPR signaling pathways was carried out on MKN74 cells treated with 50 nM bortezomib in a time-dependent manner, between 0-24 hours. Activation of UPR via the PERK pathway was evident by the increased expression of phospho-PERK after 8 hours of treatment, which was accompanied by phosphorylation of eukaryotic initiation factor 2 α (eIF2α). Upregulation of growth-arrest and DNA-damage-inducible gene 34

(GADD34), a pro-apoptotic protein associated with ER stress-induced apoptosis, was also observed. It is also a protein-phosphatase 1 (PP1)-interacting protein that induces PP1 to dephosphorylate eIF2α, thus relieving the translational block mediated by phosphorylated eIF2α. This explains the attenuation of eIF2α phosphorylation observed at 24 hours of treatment (Fig. 3.41). This negative feedback mechanism by GADD34 limits the translational block through phosphorylation of eiF2α by PERK, thus ensuring an efficient response to prolonged ER stress. Bortezomib treatment also activated the IRE1 pathway in MKN74 cells. After 4 hours of treatment, bortezomib induced phosphorylation of apoptosis signal regulating kinase 1 (ASK1), followed by phosphorylation of c-jun N-terminal kinase (JNK). JNK phosphorylation is accompanied by a concomitant increase in the phosphorylation of B cell lymphoma 2 (BCL2) (Fig. 3.42). The IRE1-ASK-JNK pathway has previously been implicated in ER stress-induced cell death.[192] Phosphorylation of BCL2 also inhibits its anti-apoptotic activity. That UPR was activated in bortezomib-treated MKN74 cells was further confirmed by the activation of ATF6 as seen by the detection of its cleaved, active form after 4 hours of treatment. Additonally, up-regulation of pro-apoptotic protein BAK was observed after 4 hours of treatment (Fig. 3.43). As bortezomib has earlier been shown to result in caspase activation and PARP cleavage (Fig. 3.35), the data collectively suggests that bortezomib-mediated inhibition of misfolded N-CoR degradation may elicit ER stress via the activation of the UPR pathways, ultimately promoting UPR-induced apoptosis.

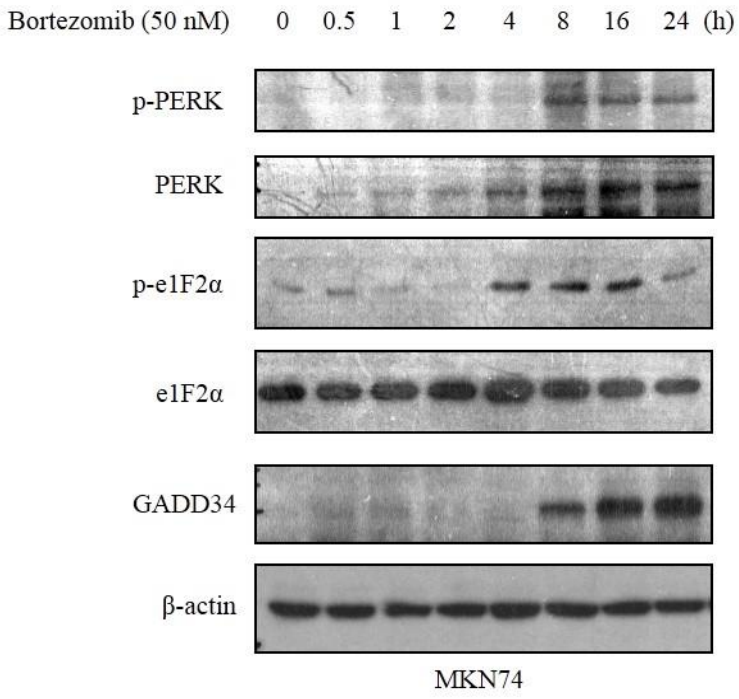

Figure 3.41. Bortezomib activates the PERK pathway in MKN74 cells. MKN74 cells were treated with 50 nM of bortezomib for 0 - 24 h. Western blot analysis was carried out using anti-phospho-PERK, anti-PERK, anti-phospho-elF2α, anti-elF2α, and anti-GADD34 antibodies. Level of β-actin expression was determined as an indication of loading control.

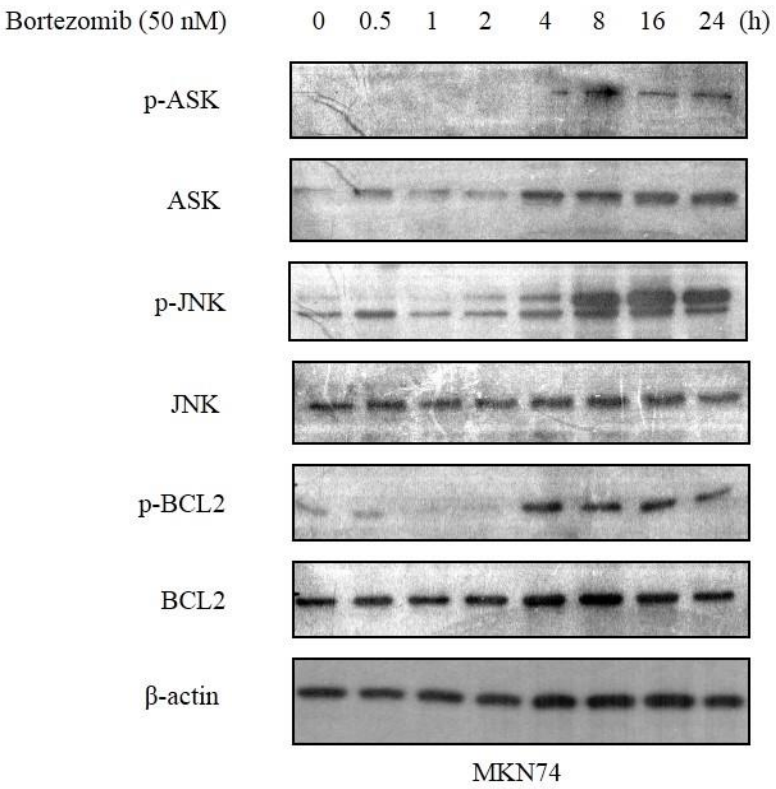

Figure 3.42. Bortezomib activates the IRE pathway in MKN74 cells. MKN74 cells were treated with 50 nM of bortezomib for 0 - 24 h. Western blot analysis was carried out using anti-phospho-ASK, anti-ASK, anti-phospho-JNK, anti-JNK, anti-phospho-BCL2, and anti-BCL2 antibodies. Level of β-actin expression was determined as an indication of loading control.

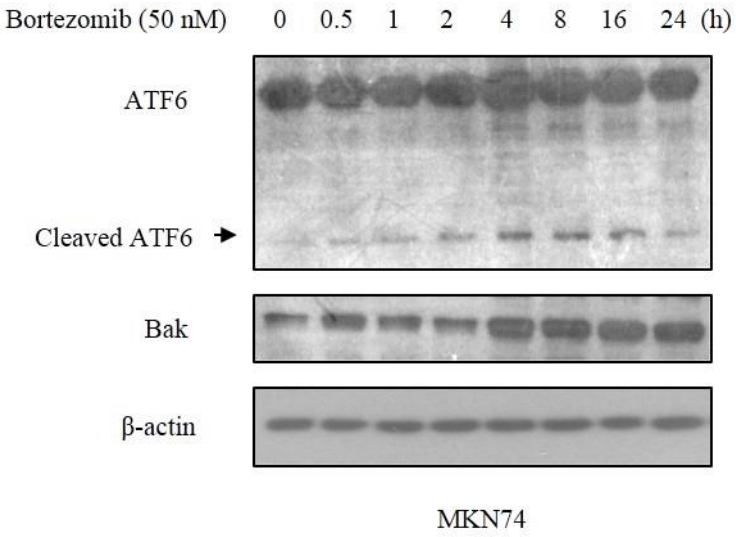

Figure 3.43. Bortezomib activates the ATF6 pathway in MKN74 cells. MKN74 cells were treated with 50 nM of bortezomib for 0 - 24 h. Western blot analysis was carried out using anti-ATF6 and anti-Bak antibodies. Level of β-actin expression was determined as an indication of loading control.

CHAPTER 4

Discussion

4.1 GC011, an artemisinin derivative with TGF-β-like activity, is a promising therapeutic candidate for TGF-β sensitive gastric cancers.

4.1.1 GC011 exhibits its potent growth inhibitory effects in TGF-β sensitive gastric cancer cells by sensitizing them to TGF-β-induced apoptosis.

Given the paucity of modalities for the clinical treatment of gastric cancer, new approaches for therapeutic development are urgent and necessary. One possibility is drug repositioning, the process of finding new uses for existing drugs, which presents a safer and more economical approach as these drugs have already been proven safe for clinical use. In this context, one such promising compound is artemisinin, which has already been FDA-approved for the treatment of malaria and is well-tolerated without adverse side effects. Antitumor activity of artemisinin has already been documented in human trials [111] and also in individual clinical cases.[109,110,193] Artemether and artesunate have been used in cancer therapy with good tolerability and lack of significant side effects. In all, a large body of in-vitro and in-vivo finding has since demonstrated the usefulness of artemisinins against tumor cells derived from various subtypes of human malignancies, but relatively little mechanistic information has been presented. Of note, only one study to date has assessed its use in gastric cancer.[180] In this report, we have presented evidence of potent growth inhibitory function of an artemisinin derivative on TGF-β sensitive gastric cancer cells. The data observed in the MTS assay showed that treatment with 5 μM of GC011 for 96 hours was capable of inhibiting almost 80% cell growth, which corresponded with a similar percentage of apoptotic cells observed at the same dose and treatment time. This suggests that the anti-proliferative effect of GC011 on SNU16 cells was mainly by the activation of

the apoptotic pathway. It is significant to note that GC011 did not demonstrate cytotoxic effects on normal gastric cancer cells, suggesting its specificity to cancer cells. As such, GC011 could be a promising cytotoxic agent for a selected group of TGF-β sensitive gastric cancers.

Although inactivation of TGF-β signaling and resistance of cells to TGF-β stimuli are linked to the carcinogenesis in several human tumors including gastric cancer, the effect of TGF-β could also be pro-oncogenic, especially in the later stages of the carcinogenic process. The pro-oncogenic role of TGF-β is mainly manifested in the form of cellular resistance to TGF-β stimuli which could indirectly result from the TGF-β-induced production of extracellular matrix, suppression of immune function, or promotion of angiogenesis. Interestingly, artemisinin has also been shown to downregulate the expression of oncogenic TGF-β target genes such as MMPs [118]. It would therefore be interesting to study if GC011 and other artemisinin derivatives could downregulate these oncogenic TGF-β target genes in gastric cancer cells as well.

In addition, TGF-β resistance could also result from the mutation or inactivation of TGF-β receptors or Smad proteins, as well as silencing of TGF-β target genes. In particular, down-regulation of Smad3 expression was associated with TGF-β resistance in a gastric cancer derived cells SNU-484, and when Smad3 was ectopically expressed in SNU-484 cells, the cells became TGF-β sensitive.[181] These findings suggest that TGF-β resistant tumors could be sensitized to the growth inhibitory effects of TGF-β through the therapeutic restoration of function of Smad-TGF-β pathway. In this study,

it was demonstrated that the selective antitumor effects of GC011 in SNU16 cells was apparently mediated by the activation of Smad-dependent up-regulation of TGF-β target genes p21 and PAI-1, suggesting that GC011 could restore the deregulated Smad-dependent TGF-β signaling in TGF-β sensitive gastric cancer cells. Additionally, it was also found that GC011 upregulated the expression of the TGF-β1 ligand (Fig. 3.11C), further suggesting that GC011 could exert its antitumor effects by activating or enhancing TGF-β growth inhibitory pathways.

Although TGF-β resistance is a universal phenomenon in most gastric cancer cells, this resistance is largely acquired during the later stage of the carcinogenic process.[194,195] Therefore, despite its lack of effectiveness against TGF-β resistant cells, GC011 could still be effective against majority of gastric cancer if used during the early stage of the carcinogenic process. Moreover, the possibility that GC011 can sensitize TGF-β resistant cells to apoptosis at higher concentration cannot be ruled out and needs to be investigated. Therefore, further investigation with GC011 and other artemisinin derivatives [103,179] will be required in order to evaluate their full therapeutic potential in gastric cancer.

4.1.2 GC011 inhibits N-CoR-mediated transcriptional repression of TGF-β target genes.

Several studies have postulated the involvement of N-CoR in the negative regulation of TGF-β signaling. In the absence of ligand stimulation, N-CoR, together with the other components of the repressor complex, such as SnoN and HDAC, is recruited to the promoter of TGF-β target genes. Upon ligand

binding, this repressive complex is removed, thus allowing transcriptional activation of the genes to proceed.[184] It was shown in this report that ligand stimulation of the TGF-β signaling pathway, whether by GC011 and TGF-β1, could induce the degradation of N-CoR and HDAC1 in TGF-β sensitive cells, similar to the ligand-induced degradation of SnoN.[184] N-CoR ablation also led to the activation of the promoter of the TGF-β responsive gene, suggesting that transcriptional activity of TGF-β target genes may be regulated by N-CoR. Further studies need to be carried out to establish the role of N-CoR on promoter activity of TGF-β target genes, and also investigate the action of GC011 on the other known components of the N-CoR transcriptional repression machinery, such as MeCP2, Ski/SnoN and other HDACs.

Of significance, N-CoR was found to be mislocalised in TGF-β resistant SNU5 cells, in contrast to its nuclear localisation in TGF-β sensitive SNU16 cells. As nuclear N-CoR appears to be sensitive to GC011-induced degradation, while cytoplasmic N-CoR is not, it is tempting to speculate if N-CoR localisation may be a good marker for the identification of the subset of gastric tumors that might be amenable to GC011 treatment.

4.1.3 Runx3 induces degradation of N-CoR via the ubiquitin-proteosome pathway and possibly regulates N-CoR-mediated repression of TGF-β target genes.

Runx3 is a tumor suppressor strongly implicated in gastric cancer and other epithelial cancers, and has been established as a downstream target of the tumor suppressive TGF-β pathway. It was found that Runx3 expression was diminished in a majority of gastric cancers due to hemizygous deletion and

hypermethylation of its promoter,[62] and its aberrant localisation in gastric cancer cell lines was also reported.[19] Consistent with these reports, this study determined that Runx3 was not expressed in most of the gastric cancer cell lines, except for TGF-β sensitive cell line SNU16. Given the role of N-CoR in DNA-dependent methylation repression,[85] initial investigations were carried out to determine if epigenetic regulation of Runx3 might be mediated by N-CoR. Instead, it was found that Runx3 induced the cytoplasmic translocation of N-CoR and its subsequent degradation via the ubiquitin-proteosome pathway. This in turn would relieve target genes from transcriptional repression. While it is currently unknown how Runx3 mediates the degradation of N-CoR through the UPP, it is possible that Runx3 is a putative E3 ubiquitin ligase. Nevertheless, these findings may be able to provide novel insights into transcriptional regulation by these two distinct classes of molecules and their possible interactions. As Runx3 has previously been found to upregulate proapoptotic Bim and p21 via the TGF-β pathway,[72,73] it is speculated that Runx3 might regulate N-CoR-mediated repression of TGF-β target genes by inducing its degradation via the UPP. Initial work in this study revealed that N-CoR overexpression abrograted Runx3-induced activation of TGF-β responsive promoter, IgCα, suggesting a mechanistic link between these two molecules in TGF-β gene transcriptional activity. Further work needs to be carried out to explore this link.

4.2 Bortezomib therapeutically targets the UPR pathway in gastric cancer by inhibiting the degradation of misfolded N-CoR.

4.2.1 Gastric cancer cells harbor an APL-like misfolded conformational dependent loss of N-CoR.

Previously, our laboratory has reported a role of misfolded conformation dependent loss (MCDL) of N-CoR in the pathogenesis of acute promyelocytic leukemia (APL).[187] Other studies in our laboratory identified an APL-like MCDL loss of N-CoR in acute monoblastic leukemia (AML-M5)[196] and non-small cell lung cancer (NSCLC)[197], and subsequently identified inhibition of N-CoR misfolding as an attractive strategy for treatment. It was therefore hypothesized that an APL-like MCDL of N-CoR might be a common feature in malignancy. Indeed, initial screening of N-CoR in gastric cancer cell lines revealed the post-transcriptional loss of N-CoR in most of the cell lines, and a down-regulation of N-CoR protein expression in most gastric tumor tissues. Subsequent experiments showed that majority of N-CoR in gastric cancer cell lines displayed characteristics of misfolded N-CoR similar to that seen in APL,[187] such as aberrant cytoplasmic localization, detergent insolubility and amplification of ER stress. A similar down-regulation and mislocalisation of N-CoR was also detected in gastric tumor tissues, indicating that MCDL of N-CoR was not exclusive to gastric cancer cell lines.

It was previously demonstrated that fusion protein PML-RAR-induced aberrant post-translational modification of N-CoR contributed to its misfolding in APL.[187] Initial investigations in this study suggested that misfolded N-CoR observed in gastric cancer may also have been an outcome of aberrant post-translational modification, specifically serine-threonine phosphorylation, although the underlying oncogenic events are currently not known. SMRT, another transcriptional corepressor closely related with N-CoR, has been reported to be regulated by several SMRT-targeting serine-threonine kinases, including IKKα and MEKK-1, leading to their cytosolic

translocation,[94,190,191] but few N-CoR-targeting kinases have been identified. It would therefore be of great interest to further investigate the role of kinases in the regulation of N-CoR stability and function, and also the underlying mechanism leading to it.

Although the question of whether MCDL of N-CoR in gastric cancer can contribute to the malignant growth and transformation of gastric cancer cells has yet to be answered, given the active involvement of N-CoR regulation in several cellular pathways, misfolding of N-CoR may have several tumor-promoting consequences. A possible consequence is the loss of normal tumor suppressive function of N-CoR due to its misfolding. As observed in TGF-β sensitive gastric cancer cell lines, N-CoR is functional and plays a role in the regulation of the tumor suppressive pathway of TGF-β signaling. It is possible that loss or misfolding of N-CoR may contribute to TGF-β resistance, thus promoting survival of early cancer cells. Misfolded N-CoR may also lead to the loss of its suppressive function on other oncogenic pathways, such as the PI3K/Akt/mTOR pathway, contributing to the survival and growth of cancer cells, such as that seen in thyroid tumor cell.[95] Another mechanism has been identified in APL, whereby autophagic degradation of misfolded N-CoR neutralized ER stress and thus protected the cells from ER stress-induced apoptosis (Fig. 4.1).[197] Further investigations on the effects of N-CoR misfolding in gastric cancer should be carried out to provide new insights into the molecular aspects of gastric cancer development and aid in development of new therapeutics.

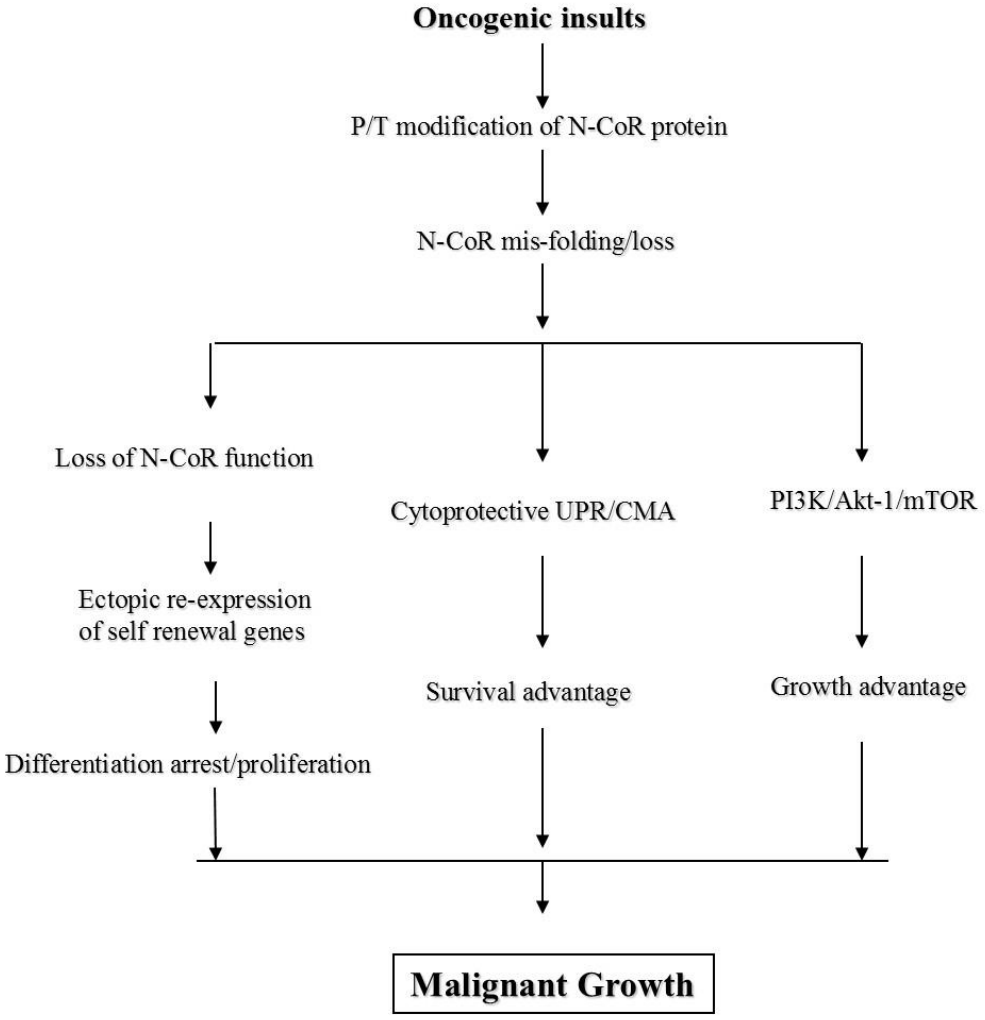

Figure 4.1. Possible contributions of misfolded N-CoR to the transformation and malignant growth of cancer cells. The misfolded conformation dependent loss of N-CoR can contribute to the malignant growth and transformation of gastric cancer cells through multiple mechanisms; such as loss of normal tumor suppressive function of N-CoR due to misfolding, neutralization of ER stress due to the degradation of misfolded N-CoR and possible activation of oncogenic pathways due to loss of its suppressive function. P/T: post-translational; N-CoR: nuclear receptor co-repressor; UPR: unfolded protein response; CMA: chaperone-mediated autophagy; PI3K: Phosphoinositide 3-kinase, mTOR: mammalian target of rapamycin.

4.2.2 Bortezomib induces cytotoxic UPR by inhibiting proteasome-mediated degradation of misfolded N-CoR in gastric cancer.

In mammalian cells, a coordinated biochemical response to the accumulation of misfolded proteins within the ER termed the unfolded protein response (UPR) exists to maintain ER homeostasis.[130] This cellular response to ER stress consists of two branches; on one hand it induces cytoprotective pathways to re-establish homeostasis, such as enhancing protein folding capacity through upregulation of ER chaperone proteins and enhancing degradation of misfolded proteins via ER-associated degradation (ERAD).[152] On the other hand, if the ER stress is prolonged and unresolved, signaling pathways that promote apoptosis are activated.[133] In tumor cells which grow under oncogenic stress conditions such as accumulation of misfolded proteins, there is a great reliance on the cytoprotective UPR for survival [154]. In contrast, most normal cells are not subject to stress, and the UPR pathways are inactive. This selective importance of UPR in the maintenance of malignancy has therefore provided a therapeutic window for agents targeting the UPR as an anticancer strategy.

In this study, gastric cancer cells harboring the misfolded N-CoR displayed high constitutive expression levels of ER resident chaperones GRP78 and PDI compared to SNU16, which expressed native N-CoR in the nucleus. The prevalent loss of N-CoR in these cells also suggested its degradation via the ERAD pathway. Although the levels of N-CoR protein in all the gastric cancer cell lines were substantially lower than that in TGF-β sensitive SNU16 cells, the gastric cancer cells displayed differential expression of N-CoR. It is possible that the cells in which some N-CoR expression was still detected

were still in the early stages of the misfolding process (Fig. 4.2), and were therefore not subjected to ERAD yet. Proteasomal degradation of misfolded proteins retrotranslocated from the ER to the cytosol represents the final step in ERAD.[152] It was therefore postulated that disruption of the ERAD pathway via proteasome inhibition may result in the accumulation of the misfolded N-CoR, thus triggering ER stress and ultimately, the induction of terminal UPR, that is, cell death. Bortezomib is the first proteasome inhibitor developed successfully for anti-cancer therapy.[163] Experiments were carried out to investigate the anticancer effects of bortezomib on gastric cancer cells and its effects on the misfolded N-CoR and the UPR pathways. As expected, bortezomib treatment significantly inhibited proliferation of gastric cancer cells. Of note, this cytotoxicity observed in gastric cancer cells was achieved at very low doses (nM) which were not cytotoxic to the normal human gastric cancer cell line, HFE-145. Although bortezomib was effective in inhibiting proliferation of most gastric cancer cell lines after 48 hours with a low dose of 50 nM, the cell lines displayed different levels of sensitivity to bortezomib at 24 hours. One reason could be that the cells are at different levels of ER stress, depending on the accumulated misfolded protein load present in each cell line.

Previous studies have shown that bortezomib induces caspase-dependent apoptotic cell death in MM cells.[172] In line with these reports, the cytotoxic effects of bortezomib in gastric cancer cells were also found to be associated with the induction of the apoptotic pathway, via the activation of caspase-9, caspase-3 and PARP cleavage. In addition, bortezomib also promoted the accumulation of misfolded N-CoR in these cells, which was accompanied by activation of ER stress reflected by the formation of high molecular weight

PDI, HSP60 and GRP78. Evidence that bortezomib sensitized gastric cancer cells to UPR-induced apoptosis, or terminal UPR, was reflected in the activation of the IRE1-ASK1-JNK pathway with bortezomib treatment, and inhibition of anti-apoptotic BCL-2, thus committing the cells to ER stress-induced cell death. Pro-apoptotic BAK and GADD34 proteins were also up-regulated by the activation of the PERK and ATF6 pathways respectively.

In addition to its proteasome inhibitory function, it is possible that bortezomib-induced apoptosis of gastric cancer cells may involve other mechanisms such as that reported in melanoma and prostate cancer cells.[177,178] This could explain in part why bortezomib was also found to promote cytotoxic effects in TGF-β sensitive cells, SNU16 and SNU620, which lack misfolded N-CoR. Alternatively, bortezomib may induce accumulation of other misfolded proteins present in gastric cancer. Although the proteasome inhibitory function of bortezomib has been well-established in MM and other cancers, it is yet to be shown in gastric cancer cells. The inhibitory effect of bortezomib on proteasome function in gastric cancer cells was therefore analysed and it was found that bortezomib significantly inhibited all three proteolytic activities of the proteasome in MKN74 cells in a dose- and time-dependent manner, further establishing its potent activity as a proteasome inhibitor in various tumors. In all, these findings suggest the therapeutic potential of bortezomib in gastric cancer cells.

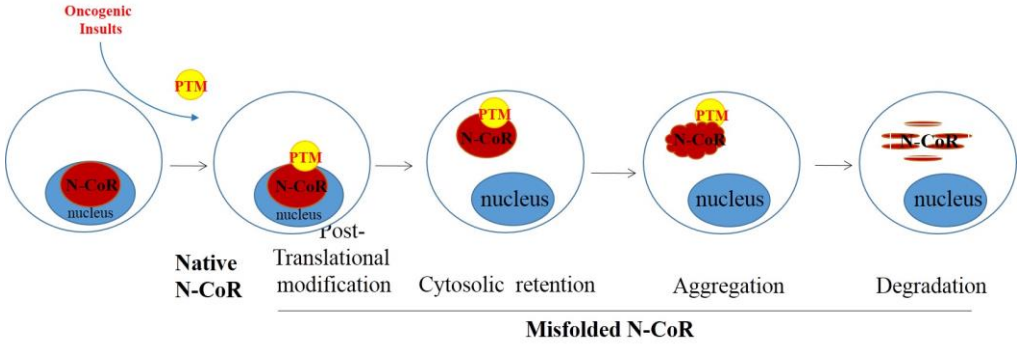

Figure 4.2. Representation of the different stages of N-CoR misfolding in gastric cancer cells. The misfolding of N-CoR in gastric cancer cells is initiated by yet to be identified oncogenic stimuli, which results in the post-translational modification of the native N-CoR in these cells, such as serine-threonine phosphorylation, leading to a conformational change in N-CoR. The misfolded N-CoR is then exported out of the nucleus, where it accumulates until it reaches threshold levels that trigger proteasome-mediated degradation in the cytoplasm. PTM: post-translational modification; N-CoR: nuclear receptor co-repressor.

4.3. Concluding remarks

Multiple signaling pathways have been implicated in gastric carcinogenesis, and it is increasingly clear that dysregulation of these intracellular signaling pathways represent a common pathogenic mechanism in gastric cancer. An important signaling pathway which has been widely implicated in gastric carcinogenesis is the transforming growth factor-β (TGF-β) pathway, which is involved in various biological processes such as cell proliferation, differentiation, migration and apoptosis. The pleiotropic effects of this pathway are regulated by its interactions with adaptor proteins, ubiquitinators and various transcriptional factors. One such factor is the nuclear receptor co-repressor (N-CoR), whose role in regulating transcriptional repression of TGF-β target genes has been postulated in several studies. Another molecule, transcription factor Runx3, is a downstream target of TGF-β signaling pathway and its tumor suppressor role in gastric cancer has been firmly established.

In this thesis, the therapeutic potential of the artemisinin derivative GC011 on various gastric cancer-derived cell lines was investigated, shedding new light into dysregulation of TGF-β signaling pathway in gastric cancer and also highlighting the therapeutic potential of GC011 in TGF-β sensitive gastric cancers. It was found that GC011 induced selective growth inhibition and promoted apoptosis in TGF-β sensitive gastric cancer cells. The pro-apoptotic effect of the GC011 was apparently mediated though the activation of Smad3-dependent up-regulation of known TGF-β target genes PAI-1 and p21. GC011 also demonstrated a stimulatory effect similar to TGF-β on the promoter of a bona fide TGF-β target gene IgCα that contains a consensus TGF-β response

element. GC011-induced activation of TGF-β targets apparently resulted from the abrogation of N-CoR meditated transcriptional repression of TGF-β promoter as GC011 promoted a selective degradation of N-CoR/HDAC1 protein in TGF-β sensitive cells. RUNX3 was found to induce the proteasome-mediated degradation of N-CoR. These findings highlight the therapeutic potential of GC011 as a putative TGF-β analogue in TGF-β sensitive gastric cancer cells. The proposed action of GC011 on TGF-β sensitive gastric cancer cells is summarized in Figure 4.3.

As GC011 is only effective in TGF-β sensitive gastric cancer cells, alternative therapeutic approaches that would be effective in a wider scope of gastric cancers are needed. Our lab has previously identified a role for misfolded conformational dependent loss (MCDL) of N-CoR in the pathogenesis of APL cells, and subsequently in AML-M5 and NSCLC cells since, suggesting that misfolded N-CoR is a general trait of malignant cells. Indeed, the findings in this thesis suggested that a similar MCDL of N-CoR is also prevalent in gastric cancer cells. As in APL cells, misfolded N-CoR in gastric cancer cells are likewise cytoplasmic, detergent-insoluble, post-translationally modified, and are associated with ER stress amplification. Given that tumor cells are heavily reliant on the UPR pathway to promote the degradation of misfolded proteins via the ERAD pathway, the current study assessed the antitumor activity of a proteasome inhibitor bortezomib in gastric cancer cells. The results showed that bortezomib inhibited the degradation of misfolded N-CoR in gastric cancer cells, resulting in its toxic accumulation, ultimately leading to the induction of terminal UPR in these cells. These findings suggest that proteasome inhibition is a promising strategy in gastric cancer, and identifies

bortezomib as a potential candidate for the treatment of gastric cancer. Also, gastric cancer cells may have a low threshold for proteosomal inihibitor-induced UPR activation and ER stress-induced apoptosis due to the presence of misfolded N-CoR. A summary of these findings is represented in Figure 4.4.

These novel findings presented in this thesis therefore not only provide mechanistic insights into the antitumor activities of artemisinin and bortezomib in gastric cancer cells, but also further delineate the underlying molecular pathways which might facilitate future strategies to enhance therapeutic efficacy in gastric cancer.

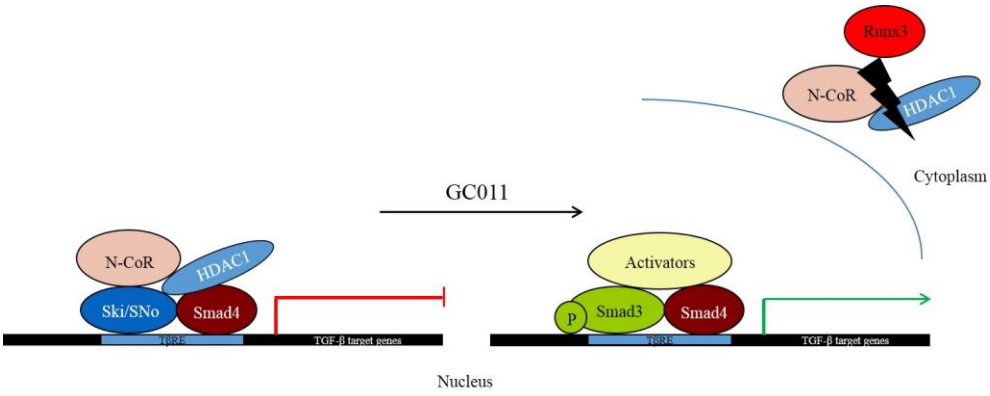

Figure 4.3. Proposed mode of action of artemisinin derivative on TGF-β target genes in TGF-β sensitive gastric cancer cells. In the nuclei of unstimulated TGF-β sensitive gastric cancer cells, transcriptional repressors Ski and SnoN binds to repeated AGAC or GTCT elements on TGF-β target gene promoters together with Smad3/4, and recruits transcriptional corepressor N-CoR and its associated repressor complex including HDAC1. In the absence of a signal, transcriptional activity of these genes are inhibited by this repressor complex. Upon GC011 treatment, the TGF-β signalling pathway is activated which induces Runx3 to mediate the cytoplasmic export of N-CoR and its subsequent proteosomal degradation, thereby displacing the N-CoR-HDAC1-repressor complex from the promoter of the TGF-β target genes. This in turn would allow activators to bind and activate transcription of target genes, and promote growth arrest and apoptosis in these cells. TβRE: TGF-β responsive element.

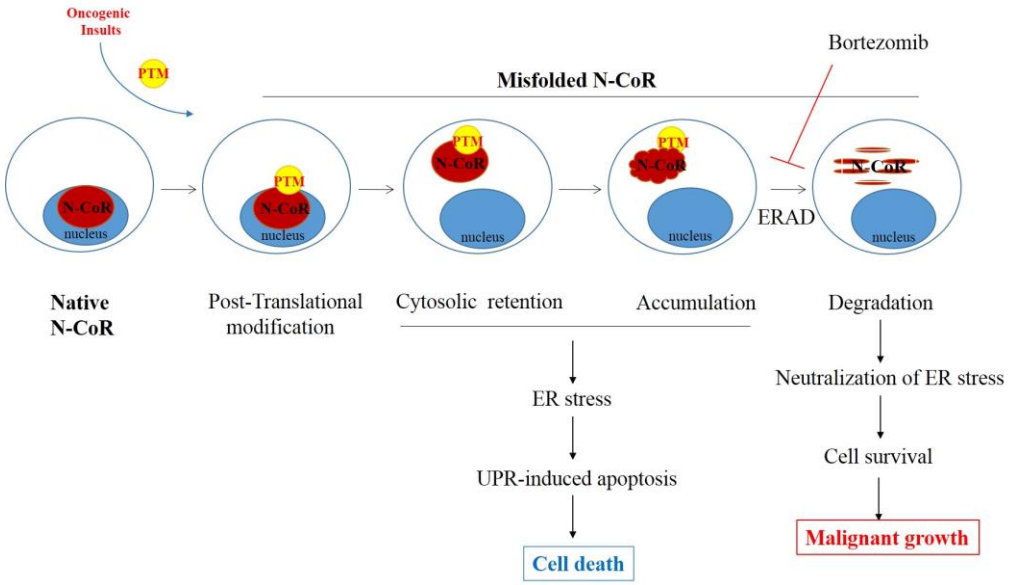

Figure 4.4. Targeting the action of ERAD pathway on misfolded N-CoR in gastric cancer cells with proteasome inhibitor, bortezomib. In response to unknown oncogenic stimuli, aberrant phosphorylation of N-CoR takes place, resulting in its misfolded conformation in gastric cancer cells. In a functioning UPR pathway, misfolded N-CoR is then exported to the cytoplasm where its accumulation eventually triggers its degradation via the ERAD pathway. Proteasome inhibition by bortezomib inhibits the ERAD pathway, thus leading to a toxic accumulation of misfolded N-CoR in gastric cancer cells. This results in the amplification of ER stress, eventually leading to the induction of ER stress-induced apoptosis. Thus, proteasome inhibition presents an attractive therapeutic approach in gastric cancer. PTM: post-translational medication; UPR: unfolded protein response; ERAD: ER-associated degradation.

REFERENCES

1 Ferlay, J. *et al.* Estimates of worldwide burden of cancer in 2008: GLOBOCAN 2008. *International journal of cancer. Journal international du cancer* **127**, 2893-2917, doi:10.1002/ijc.25516 (2010).

2 Hamilton, S. R. & Aaltonen, L. A. *Pathology and genetics of tumours of the digestive system*. (IARC press Lyon, 2000).

3 Lauren, P. THE TWO HISTOLOGICAL MAIN TYPES OF GASTRIC CARCINOMA: DIFFUSE AND SO-CALLED INTESTINAL-TYPE CARCINOMA. AN ATTEMPT AT A HISTO-CLINICAL CLASSIFICATION. *Acta pathologica et microbiologica Scandinavica* **64**, 31-49 (1965).

4 Lawson, J. D., Sicklick, J. K. & Fanta, P. T. Gastric Cancer. *Current Problems in Cancer* **35**, 97-127, doi:http://dx.doi.org/10.1016/j.currproblcancer.2011.03.001 (2011).

5 Buiatti, E. *et al.* A case-control study of gastric cancer and diet in Italy. *International journal of cancer* **44**, 611-616 (1989).

6 Kono, S., Ikeda, M., Tokudome, S. & Kuratsune, M. A case-control study of gastric cancer and diet in Northern Kyushu, Japan. *Cancer Science* **79**, 1067-1074 (1988).

7 Tsugane, S. & Sasazuki, S. Diet and the risk of gastric cancer: review of epidemiological evidence. *Gastric cancer : official journal of the International Gastric Cancer Association and the Japanese Gastric Cancer Association* **10**, 75-83, doi:10.1007/s10120-007-0420-0 (2007).

8 Uemura, N. *et al.* Helicobacter pylori infection and the development of gastric cancer. *The New England journal of medicine* **345**, 784-789, doi:10.1056/NEJMoa001999 (2001).

9 Hartgrink, H. H., Jansen, E. P. M., van Grieken, N. C. T. & van de Velde, C. J. H. Gastric cancer. *The Lancet* **374**, 477-490, doi:http://dx.doi.org/10.1016/S0140-6736(09)60617-6.

10 Canedo, P. *et al.* The interferon gamma receptor 1 (IFNGR1) -56C/T gene polymorphism is associated with increased risk of early gastric carcinoma. *Gut* **57**, 1504-1508, doi:10.1136/gut.2007.143578 (2008).

11 El-Omar, E. M. *et al.* Interleukin-1 polymorphisms associated with increased risk of gastric cancer. *Nature* **404**, 398-402, doi:10.1038/35006081 (2000).

12 Hold, G. L. *et al.* A functional polymorphism of toll-like receptor 4 gene increases risk of gastric carcinoma and its precursors. *Gastroenterology* **132**, 905-912, doi:10.1053/j.gastro.2006.12.026 (2007).

13 Machado, J. C. *et al.* A proinflammatory genetic profile increases the risk for chronic atrophic gastritis and gastric carcinoma. *Gastroenterology* **125**, 364-371 (2003).

14 Franco, A. T. *et al.* Regulation of gastric carcinogenesis by Helicobacter pylori virulence factors. *Cancer research* **68**, 379-387, doi:10.1158/0008-5472.can-07-0824 (2008).

15 Guilford, P. J. *et al.* E-cadherin germline mutations define an inherited cancer syndrome dominated by diffuse gastric cancer. *Human mutation* **14**, 249-255, doi:10.1002/(sici)1098-1004(1999)14:3<249::aid-humu8>3.0.co;2-9 (1999).

16 Pharoah, P. D., Guilford, P. & Caldas, C. Incidence of gastric cancer and breast cancer in CDH1 (E-cadherin) mutation carriers from hereditary diffuse gastric cancer families. *Gastroenterology* **121**, 1348-1353 (2001).

17 Gylling, A. *et al.* Is gastric cancer part of the tumour spectrum of hereditary non-polyposis colorectal cancer? A molecular genetic study. *Gut* **56**, 926-933, doi:10.1136/gut.2006.114876 (2007).

18 Shinmura, K. *et al.* A novel STK11 germline mutation in two siblings with Peutz-Jeghers syndrome complicated by primary gastric cancer. *Clinical genetics* **67**, 81-86, doi:10.1111/j.1399-0004.2005.00380.x (2005).

19 Ito, K. *et al.* RUNX3, a novel tumor suppressor, is frequently inactivated in gastric cancer by protein mislocalization. *Cancer research* **65**, 7743-7750, doi:10.1158/0008-5472.can-05-0743 (2005).

20 Xu, X. *et al.* Haploid loss of the tumor suppressor Smad4/Dpc4 initiates gastric polyposis and cancer in mice. *Oncogene* **19**, 1868-1874, doi:10.1038/sj.onc.1203504 (2000).

21 Kokkola, A. *et al.* Presence of high-level DNA copy number gains in gastric carcinoma and severely dysplastic adenomas but not in moderately dysplastic adenomas. *Cancer genetics and cytogenetics* **107**, 32-36 (1998).

22 Koo, S. H. *et al.* Genetic alterations of gastric cancer: comparative genomic hybridization and fluorescence In situ hybridization studies. *Cancer genetics and cytogenetics* **117**, 97-103 (2000).

23 Panani, A. D. & Roussos, C. Non-random structural chromosomal changes in primary gastric cancer. *Cancer letters* **225**, 291-295, doi:10.1016/j.canlet.2004.12.003 (2005).

24 Yamashita, Y. *et al.* Recurrent chromosomal rearrangements at bands 8q24 and 11q13 in gastric cancer as detected by multicolor spectral karyotyping. *World journal of gastroenterology : WJG* **11**, 5129-5135 (2005).

25 Aguilera, A. & Gomez-Gonzalez, B. Genome instability: a mechanistic view of its causes and consequences. *Nature reviews. Genetics* **9**, 204-217, doi:10.1038/nrg2268 (2008).

26 Bacani, J. *et al.* Tumor microsatellite instability in early onset gastric cancer. *The Journal of molecular diagnostics : JMD* **7**, 465-477, doi:10.1016/s1525-1578(10)60577-6 (2005).

27 Ottini, L. *et al.* MRE11 expression is impaired in gastric cancer with microsatellite instability. *Carcinogenesis* **25**, 2337-2343, doi:10.1093/carcin/bgh257 (2004).

28 Arai, T. *et al.* Role of methylation of the hMLH1 gene promoter in the development of gastric and colorectal carcinoma in the elderly. *Geriatrics & gerontology international* **10 Suppl 1**, S207-212, doi:10.1111/j.1447-0594.2010.00590.x (2010).

29 Lawes, D. A., SenGupta, S. & Boulos, P. B. The clinical importance and prognostic implications of microsatellite instability in sporadic cancer. *European journal of surgical oncology : the journal of the European Society of Surgical Oncology and the British Association of Surgical Oncology* **29**, 201-212 (2003).

30 Oliveira, C., Seruca, R., Seixas, M. & Sobrinho-Simoes, M. The clinicopathological features of gastric carcinomas with microsatellite instability may be mediated by mutations of different "target genes": a study of the TGFbeta RII, IGFII R, and BAX genes. *The American journal of pathology* **153**, 1211-1219 (1998).

31 Ohtsu, A., Yoshida, S. & Saijo, N. Disparities in gastric cancer chemotherapy between the East and West. *Journal of clinical oncology : official journal of the American Society of Clinical Oncology* **24**, 2188-2196, doi:10.1200/jco.2006.05.9758 (2006).

32 Roukos, D. H. Early-stage gastric cancer: a highly treatable disease. *Annals of surgical oncology* **11**, 127-129 (2004).

33 Kappas, A. M., Fatouros, M. & Roukos, D. H. Is it time to change surgical strategy for gastric cancer in the United States? *Annals of surgical oncology* **11**, 727-730, doi:10.1245/aso.2004.05.907 (2004).

34 Kim, S. H., Karpeh, M. S., Klimstra, D. S., Leung, D. & Brennan, M. F. Effect of microscopic resection line disease on gastric cancer survival. *Journal of gastrointestinal surgery : official journal of the Society for Surgery of the Alimentary Tract* **3**, 24-33 (1999).

35 Songun, I., Bonenkamp, J. J., Hermans, J., van Krieken, J. H. & van de Velde, C. J. Prognostic value of resection-line involvement in patients undergoing curative resections for gastric cancer. *European journal of cancer (Oxford, England : 1990)* **32A**, 433-437 (1996).

36 Fiorica, F. *et al.* The impact of radiotherapy on survival in resectable gastric carcinoma: a meta-analysis of literature data. *Cancer treatment reviews* **33**, 729-740, doi:10.1016/j.ctrv.2007.08.005 (2007).

37 Ilson, D. H. *et al.* Phase II trial of paclitaxel, fluorouracil, and cisplatin in patients with advanced carcinoma of the esophagus. *Journal of clinical oncology : official journal of the American Society of Clinical Oncology* **16**, 1826-1834 (1998).

38 Lai, I. R., Lee, W. J., Huang, M. T. & Lin, H. H. Comparison of serum CA72-4, CEA, TPA, CA19-9 and CA125 levels in gastric cancer patients and correlation with recurrence. *Hepato-gastroenterology* **49**, 1157-1160 (2002).

39 Lynch, H. T. *et al.* Hereditary diffuse gastric cancer: prophylactic surgical oncology implications. *The Surgical clinics of North America* **88**, 759-778, vi-vii, doi:10.1016/j.suc.2008.04.006 (2008).

40 Adelstein, D. J., Rodriguez, C. P., Rybicki, L. A., Ives, D. I. & Rice, T. W. A phase II trial of gefitinib for recurrent or metastatic cancer of the esophagus or gastroesophageal junction. *Investigational new drugs* **30**, 1684-1689, doi:10.1007/s10637-011-9736-z (2012).

41 Uronis, H. E. *et al.* A phase II study of capecitabine, oxaliplatin, and bevacizumab in the treatment of metastatic esophagogastric adenocarcinomas. *The oncologist* **18**, 271-272, doi:10.1634/theoncologist.2012-0404 (2013).

42 Rutkowski, P. *et al.* Neoadjuvant imatinib in locally advanced gastrointestinal stromal tumors (GIST): the EORTC STBSG experience. *Annals of surgical oncology* **20**, 2937-2943, doi:10.1245/s10434-013-3013-7 (2013).

43 Massague, J. TGF-beta signal transduction. *Annual review of biochemistry* **67**, 753-791, doi:10.1146/annurev.biochem.67.1.753 (1998).

44 Li, X., Zhang, Y. Y., Wang, Q. & Fu, S. B. Association between endogenous gene expression and growth regulation induced by TGF-beta1 in human gastric cancer cells. *World journal of gastroenterology : WJG* **11**, 61-68 (2005).

45 Nastiuk, K. L. *et al.* FLICE-like inhibitory protein blocks transforming growth factor beta 1-induced caspase activation and apoptosis in prostate epithelial cells. *Molecular cancer research : MCR* **6**, 231-242, doi:10.1158/1541-7786.mcr-07-0386 (2008).

46 Su, E., Han, X. & Jiang, G. The transforming growth factor beta 1/SMAD signaling pathway involved in human chronic myeloid leukemia. *Tumori* **96**, 659-666 (2010).

47 Wang, X. *et al.* TGF-beta1 inhibits the growth and metastasis of tongue squamous carcinoma cells through Smad4. *Gene* **485**, 160-166, doi:10.1016/j.gene.2011.06.023 (2011).

48 Derynck, R. & Zhang, Y. E. Smad-dependent and Smad-independent pathways in TGF-beta family signalling. *Nature* **425**, 577-584, doi:10.1038/nature02006 (2003).

49 Itoh, S., Itoh, F., Goumans, M. J. & Ten Dijke, P. Signaling of transforming growth factor-beta family members through Smad proteins. *European journal of biochemistry / FEBS* **267**, 6954-6967 (2000).

50 Massague, J. & Wotton, D. Transcriptional control by the TGF-beta/Smad signaling system. *The EMBO journal* **19**, 1745-1754, doi:10.1093/emboj/19.8.1745 (2000).

51 Miyazawa, K., Shinozaki, M., Hara, T., Furuya, T. & Miyazono, K. Two major Smad pathways in TGF-beta superfamily signalling. *Genes to cells : devoted to molecular & cellular mechanisms* **7**, 1191-1204 (2002).

52 Miyazono, K., ten Dijke, P. & Heldin, C. H. TGF-beta signaling by Smad proteins. *Advances in immunology* **75**, 115-157 (2000).

53 Hanahan, D. & Weinberg, R. A. The hallmarks of cancer. *Cell* **100**, 57-70 (2000).

54 Akhurst, R. J. & Derynck, R. TGF-beta signaling in cancer--a double-edged sword. *Trends in cell biology* **11**, S44-51 (2001).

55 Derynck, R., Akhurst, R. J. & Balmain, A. TGF-beta signaling in tumor suppression and cancer progression. *Nature genetics* **29**, 117-129, doi:10.1038/ng1001-117 (2001).

56 Pardali, K. & Moustakas, A. Actions of TGF-beta as tumor suppressor and pro-metastatic factor in human cancer. *Biochimica et biophysica acta* **1775**, 21-62, doi:10.1016/j.bbcan.2006.06.004 (2007).

57 Siegel, P. M. & Massague, J. Cytostatic and apoptotic actions of TGF-beta in homeostasis and cancer. *Nature reviews. Cancer* **3**, 807-821, doi:10.1038/nrc1208 (2003).

58 Wang, L. H. *et al.* Inactivation of SMAD4 tumor suppressor gene during gastric carcinoma progression. *Clinical cancer research : an official journal of the American Association for Cancer Research* **13**, 102-110, doi:10.1158/1078-0432.ccr-06-1467 (2007).

59 Weinstein, M., Yang, X. & Deng, C. Functions of mammalian Smad genes as revealed by targeted gene disruption in mice. *Cytokine & growth factor reviews* **11**, 49-58 (2000).

60 Takaku, K. *et al.* Gastric and duodenal polyps in Smad4 (Dpc4) knockout mice. *Cancer research* **59**, 6113-6117 (1999).

61 Tamura, G. *et al.* Allelotype of adenoma and differentiated adenocarcinoma of the stomach. *The Journal of pathology* **180**, 371-377, doi:10.1002/(sici)1096-9896(199612)180:4<371::aid-path704>3.0.co;2-2 (1996).

62 Li, Q. L. *et al.* Causal relationship between the loss of RUNX3 expression and gastric cancer. *Cell* **109**, 113-124 (2002).

63 Park, K. *et al.* Genetic changes in the transforming growth factor beta (TGF-beta) type II receptor gene in human gastric cancer cells: correlation with sensitivity to growth inhibition by TGF-beta. *Proceedings of the National Academy of Sciences of the United States of America* **91**, 8772-8776 (1994).

64 Kang, S. H. *et al.* Transcriptional repression of the transforming growth factor-beta type I receptor gene by DNA methylation results in the development of TGF-beta resistance in human gastric cancer. *Oncogene* **18**, 7280-7286, doi:10.1038/sj.onc.1203146 (1999).

65 Karsenty, G. & Wagner, E. F. Reaching a genetic and molecular understanding of skeletal development. *Developmental cell* **2**, 389-406 (2002).

66 Tracey, W. D. & Speck, N. A. Potential roles for RUNX1 and its orthologs in determining hematopoietic cell fate. *Seminars in cell & developmental biology* **11**, 337-342, doi:10.1006/scdb.2000.0186 (2000).

67 Yang, S. *et al.* In vitro and in vivo synergistic interactions between the Runx2/Cbfa1 transcription factor and bone morphogenetic protein-2 in stimulating osteoblast differentiation. *Journal of bone and mineral research : the official journal of the American Society for Bone and Mineral Research* **18**, 705-715, doi:10.1359/jbmr.2003.18.4.705 (2003).

68 Wei, D. *et al.* Loss of RUNX3 expression significantly affects the clinical outcome of gastric cancer patients and its restoration causes drastic suppression of tumor growth and metastasis. *Cancer research* **65**, 4809-4816, doi:10.1158/0008-5472.can-04-3741 (2005).

69 Hanai, J. *et al.* Interaction and functional cooperation of PEBP2/CBF with Smads. Synergistic induction of the immunoglobulin germline Calpha promoter. *The Journal of biological chemistry* **274**, 31577-31582 (1999).

70 Massague, J., Blain, S. W. & Lo, R. S. TGFbeta signaling in growth control, cancer, and heritable disorders. *Cell* **103**, 295-309 (2000).

71 Fukamachi, H. & Ito, K. Growth regulation of gastric epithelial cells by Runx3. *Oncogene* **23**, 4330-4335, doi:10.1038/sj.onc.1207121 (2004).

72 Chi, X. Z. *et al.* RUNX3 suppresses gastric epithelial cell growth by inducing p21(WAF1/Cip1) expression in cooperation with transforming growth factor {beta}-activated SMAD. *Molecular and cellular biology* **25**, 8097-8107, doi:10.1128/mcb.25.18.8097-8107.2005 (2005).

73 Yano, T. *et al.* The RUNX3 tumor suppressor upregulates Bim in gastric epithelial cells undergoing transforming growth factor beta-induced apoptosis. *Molecular and cellular biology* **26**, 4474-4488, doi:10.1128/mcb.01926-05 (2006).

74 Saeki, N. *et al.* GASDERMIN, suppressed frequently in gastric cancer, is a target of LMO1 in TGF-beta-dependent apoptotic signalling. *Oncogene* **26**, 6488-6498, doi:10.1038/sj.onc.1210475 (2007).

75 Nagy, L. & Schwabe, J. W. Mechanism of the nuclear receptor molecular switch. *Trends in biochemical sciences* **29**, 317-324, doi:10.1016/j.tibs.2004.04.006 (2004).

76 Horlein, A. J. *et al.* Ligand-independent repression by the thyroid hormone receptor mediated by a nuclear receptor co-repressor. *Nature* **377**, 397-404, doi:10.1038/377397a0 (1995).

77 Jackson, T. A. *et al.* The partial agonist activity of antagonist-occupied steroid receptors is controlled by a novel hinge domain-binding coactivator L7/SPA and the corepressors N-CoR or SMRT. *Molecular endocrinology (Baltimore, Md.)* **11**, 693-705 (1997).

78 Lavinsky, R. M. *et al.* Diverse signaling pathways modulate nuclear receptor recruitment of N-CoR and SMRT complexes. *Proceedings of the National Academy of Sciences of the United States of America* **95**, 2920-2925 (1998).

79 Li, J. *et al.* Both corepressor proteins SMRT and N-CoR exist in large protein complexes containing HDAC3. *The EMBO journal* **19**, 4342-4350, doi:10.1093/emboj/19.16.4342 (2000).

80 Heinzel, T. *et al.* A complex containing N-CoR, mSin3 and histone deacetylase mediates transcriptional repression. *Nature* **387**, 43-48, doi:10.1038/387043a0 (1997).

81 Karagianni, P. & Wong, J. HDAC3: taking the SMRT-N-CoRrect road to repression. *Oncogene* **26**, 5439-5449, doi:10.1038/sj.onc.1210612 (2007).

82 Fischle, W. *et al.* Enzymatic activity associated with class II HDACs is dependent on a multiprotein complex containing HDAC3 and SMRT/N-CoR. *Molecular cell* **9**, 45-57 (2002).

83 Nomura, T. *et al.* Ski is a component of the histone deacetylase complex required for transcriptional repression by Mad and thyroid hormone receptor. *Genes & development* **13**, 412-423 (1999).

84 Wang, J., Hoshino, T., Redner, R. L., Kajigaya, S. & Liu, J. M. ETO, fusion partner in t(8;21) acute myeloid leukemia, represses transcription by interaction with the human N-CoR/mSin3/HDAC1 complex. *Proceedings of the National Academy of Sciences of the United States of America* **95**, 10860-10865 (1998).

85 Yoon, H. G., Chan, D. W., Reynolds, A. B., Qin, J. & Wong, J. N-CoR mediates DNA methylation-dependent repression through a methyl CpG binding protein Kaiso. *Molecular cell* **12**, 723-734 (2003).

86 Ahmad, K. F. *et al.* Mechanism of SMRT corepressor recruitment by the BCL6 BTB domain. *Molecular cell* **12**, 1551-1564 (2003).

87 Parekh, S. *et al.* BCL6 programs lymphoma cells for survival and differentiation through distinct biochemical mechanisms. *Blood* **110**, 2067-2074, doi:10.1182/blood-2007-01-069575 (2007).

88 Jepsen, K. & Rosenfeld, M. G. Biological roles and mechanistic actions of co-repressor complexes. *Journal of cell science* **115**, 689-698 (2002).

89 Jepsen, K. *et al.* Combinatorial roles of the nuclear receptor corepressor in transcription and development. *Cell* **102**, 753-763 (2000).

90 Park, D. M. *et al.* N-CoR pathway targeting induces glioblastoma derived cancer stem cell differentiation. *Cell cycle (Georgetown, Tex.)* **6**, 467-470 (2007).

91 Bailey, P. *et al.* The nuclear receptor corepressor N-CoR regulates differentiation: N-CoR directly interacts with MyoD. *Molecular endocrinology (Baltimore, Md.)* **13**, 1155-1168 (1999).

92 Lin, R. J., Egan, D. A. & Evans, R. M. Molecular genetics of acute promyelocytic leukemia. *Trends in genetics : TIG* **15**, 179-184 (1999).

93 Tomita, A., Buchholz, D. R., Obata, K. & Shi, Y. B. Fusion protein of retinoic acid receptor alpha with promyelocytic leukemia protein or promyelocytic leukemia zinc finger protein recruits N-CoR-TBLR1 corepressor complex to repress transcription in vivo. *The Journal of biological chemistry* **278**, 30788-30795, doi:10.1074/jbc.M303309200 (2003).

94 Fernandez-Majada, V. *et al.* Aberrant cytoplasmic localization of N-CoR in colorectal tumors. *Cell cycle (Georgetown, Tex.)* **6**, 1748-1752 (2007).

95 Furuya, F. *et al.* Nuclear receptor corepressor is a novel regulator of phosphatidylinositol 3-kinase signaling. *Molecular and cellular biology* **27**, 6116-6126, doi:10.1128/mcb.00900-07 (2007).

96 Sun, Y. *et al.* Interaction of the Ski oncoprotein with Smad3 regulates TGF-beta signaling. *Molecular cell* **4**, 499-509 (1999).

97 Luo, K. *et al.* The Ski oncoprotein interacts with the Smad proteins to repress TGFbeta signaling. *Genes & development* **13**, 2196-2206 (1999).

98 Stroschein, S. L., Wang, W., Zhou, S., Zhou, Q. & Luo, K. Negative feedback regulation of TGF-beta signaling by the SnoN oncoprotein. *Science (New York, N.Y.)* **286**, 771-774 (1999).

99 Klayman, D. L. Qinghaosu (artemisinin): an antimalarial drug from China. *Science (New York, N.Y.)* **228**, 1049-1055 (1985).

100 Hien, T. T. & White, N. J. Qinghaosu. *Lancet* **341**, 603-608 (1993).

101 Benakis, A., Paris, M., Loutan, L., Plessas, C. T. & Plessas, S. T. Pharmacokinetics of artemisinin and artesunate after oral administration in healthy volunteers. *The American journal of tropical medicine and hygiene* **56**, 17-23 (1997).

102 Fishwick, J., McLean, W. G., Edwards, G. & Ward, S. A. The toxicity of artemisinin and related compounds on neuronal and glial cells in culture. *Chemico-biological interactions* **96**, 263-271 (1995).

103 Haynes, R. K. *et al.* Artemisone--a highly active antimalarial drug of the artemisinin class. *Angewandte Chemie (International ed. in English)* **45**, 2082-2088, doi:10.1002/anie.200503071 (2006).

104 Singh, N. P. & Lai, H. Selective toxicity of dihydroartemisinin and holotransferrin toward human breast cancer cells. *Life sciences* **70**, 49-56 (2001).

105 Dell'Eva, R. *et al.* Inhibition of angiogenesis in vivo and growth of Kaposi's sarcoma xenograft tumors by the anti-malarial artesunate. *Biochemical pharmacology* **68**, 2359-2366, doi:10.1016/j.bcp.2004.08.021 (2004).

106 Chen, H. H., Zhou, H. J. & Fang, X. Inhibition of human cancer cell line growth and human umbilical vein endothelial cell angiogenesis by artemisinin derivatives in vitro. *Pharmacological research : the official journal of the Italian Pharmacological Society* **48**, 231-236 (2003).

107 Li, L. N. *et al.* Artesunate attenuates the growth of human colorectal carcinoma and inhibits hyperactive Wnt/beta-catenin pathway. *International journal of cancer. Journal international du cancer* **121**, 1360-1365, doi:10.1002/ijc.22804 (2007).

108 Efferth, T., Dunstan, H., Sauerbrey, A., Miyachi, H. & Chitambar, C. R. The anti-malarial artesunate is also active against cancer. *International journal of oncology* **18**, 767-773 (2001).

109 Berger, T. G. *et al.* Artesunate in the treatment of metastatic uveal melanoma--first experiences. *Oncology reports* **14**, 1599-1603 (2005).

110 Singh, N. P. & Panwar, V. K. Case report of a pituitary macroadenoma treated with artemether. *Integrative cancer therapies* **5**, 391-394, doi:10.1177/1534735406295311 (2006).

111 Zhang, Z. Y. *et al.* [Artesunate combined with vinorelbine plus cisplatin in treatment of advanced non-small cell lung cancer: a randomized controlled trial]. *Zhong xi yi jie he xue bao = Journal of Chinese integrative medicine* **6**, 134-138 (2008).

112 Hou, J., Wang, D., Zhang, R. & Wang, H. Experimental therapy of hepatoma with artemisinin and its derivatives: in vitro and in vivo activity, chemosensitization, and mechanisms of action. *Clinical cancer research : an official journal of the American Association for Cancer Research* **14**, 5519-5530, doi:10.1158/1078-0432.ccr-08-0197 (2008).

113 Singh, N. P. & Lai, H. C. Artemisinin induces apoptosis in human cancer cells. *Anticancer research* **24**, 2277-2280 (2004).

114 Zhou, H. J., Wang, Z. & Li, A. Dihydroartemisinin induces apoptosis in human leukemia cells HL60 via downregulation of transferrin receptor expression. *Anti-cancer drugs* **19**, 247-255 (2008).

115 Handrick, R. *et al.* Dihydroartemisinin induces apoptosis by a Bak-dependent intrinsic pathway. *Molecular cancer therapeutics* **9**, 2497-2510, doi:10.1158/1535-7163.mct-10-0051 (2010).

116 Chen, H. H., Zhou, H. J., Wang, W. Q. & Wu, G. D. Antimalarial dihydroartemisinin also inhibits angiogenesis. *Cancer chemotherapy and pharmacology* **53**, 423-432, doi:10.1007/s00280-003-0751-4 (2004).

117 Wang, S. J. *et al.* Dihydroartemisinin inhibits angiogenesis in pancreatic cancer by targeting the NF-kappaB pathway. *Cancer chemotherapy and pharmacology* **68**, 1421-1430, doi:10.1007/s00280-011-1643-7 (2011).

118 Buommino, E. *et al.* Artemisinin reduces human melanoma cell migration by down-regulating alpha V beta 3 integrin and reducing metalloproteinase 2 production. *Investigational new drugs* **27**, 412-418, doi:10.1007/s10637-008-9188-2 (2009).

119 Galal, A. M. *et al.* Deoxyartemisinin derivatives from photooxygenation of anhydrodeoxydihydroartemisinin and their cytotoxic evaluation. *Journal of natural products* **65**, 184-188 (2002).

120 Gaut, J. R. & Hendershot, L. M. The modification and assembly of proteins in the endoplasmic reticulum. *Current opinion in cell biology* **5**, 589-595 (1993).

121 Braakman, I. & Bulleid, N. J. Protein folding and modification in the mammalian endoplasmic reticulum. *Annual review of biochemistry* **80**, 71-99, doi:10.1146/annurev-biochem-062209-093836 (2011).

122 Swanton, E. & Bulleid, N. J. Protein folding and translocation across the endoplasmic reticulum membrane. *Molecular membrane biology* **20**, 99-104, doi:10.1080/0968768031000069241 (2003).

123 Wu, J. & Kaufman, R. J. From acute ER stress to physiological roles of the Unfolded Protein Response. *Cell death and differentiation* **13**, 374-384, doi:10.1038/sj.cdd.4401840 (2006).

124 Coe, H. & Michalak, M. ERp57, a multifunctional endoplasmic reticulum resident oxidoreductase. *The international journal of biochemistry & cell biology* **42**, 796-799, doi:10.1016/j.biocel.2010.01.009 (2010).

125 Gillece, P., Luz, J. M., Lennarz, W. J., de La Cruz, F. J. & Romisch, K. Export of a cysteine-free misfolded secretory protein from the endoplasmic reticulum for degradation requires interaction with protein disulfide isomerase. *The Journal of cell biology* **147**, 1443-1456 (1999).

126 Liberek, K., Lewandowska, A. & Zietkiewicz, S. Chaperones in control of protein disaggregation. *The EMBO journal* **27**, 328-335, doi:10.1038/sj.emboj.7601970 (2008).

127 Feldman, D. E. & Frydman, J. Protein folding in vivo: the importance of molecular chaperones. *Current opinion in structural biology* **10**, 26-33 (2000).

128 Young, J. C., Agashe, V. R., Siegers, K. & Hartl, F. U. Pathways of chaperone-mediated protein folding in the cytosol. *Nature reviews. Molecular cell biology* **5**, 781-791, doi:10.1038/nrm1492 (2004).

129 Kaufman, R. J. Stress signaling from the lumen of the endoplasmic reticulum: coordination of gene transcriptional and translational controls. *Genes & development* **13**, 1211-1233 (1999).

130 Schroder, M. & Kaufman, R. J. The mammalian unfolded protein response. *Annual review of biochemistry* **74**, 739-789, doi:10.1146/annurev.biochem.73.011303.074134 (2005).

131 Ogata, M. *et al.* Autophagy is activated for cell survival after endoplasmic reticulum stress. *Molecular and cellular biology* **26**, 9220-9231, doi:10.1128/mcb.01453-06 (2006).

132 Ding, W. X. *et al.* Differential effects of endoplasmic reticulum stress-induced autophagy on cell survival. *The Journal of biological chemistry* **282**, 4702-4710, doi:10.1074/jbc.M609267200 (2007).

133 Fribley, A., Zhang, K. & Kaufman, R. J. Regulation of apoptosis by the unfolded protein response. *Methods in molecular biology (Clifton, N.J.)* **559**, 191-204, doi:10.1007/978-1-60327-017-5_14 (2009).

134 Bertolotti, A., Zhang, Y., Hendershot, L. M., Harding, H. P. & Ron, D. Dynamic interaction of BiP and ER stress transducers in the unfolded-protein response. *Nature cell biology* **2**, 326-332, doi:10.1038/35014014 (2000).

135 Tsai, Y. C. & Weissman, A. M. The Unfolded Protein Response, Degradation from Endoplasmic Reticulum and Cancer. *Genes & cancer* **1**, 764-778, doi:10.1177/1947601910383011 (2010).

136 Diehl, J. A., Fuchs, S. Y. & Koumenis, C. The cell biology of the unfolded protein response. *Gastroenterology* **141**, 38-41, 41 e31-32, doi:10.1053/j.gastro.2011.05.018 (2011).

137 Szegezdi, E., Logue, S. E., Gorman, A. M. & Samali, A. Mediators of endoplasmic reticulum stress-induced apoptosis. *EMBO reports* **7**, 880-885, doi:10.1038/sj.embor.7400779 (2006).

138 McCullough, K. D., Martindale, J. L., Klotz, L. O., Aw, T. Y. & Holbrook, N. J. Gadd153 sensitizes cells to endoplasmic reticulum stress by down-regulating Bcl2 and perturbing the cellular redox state. *Molecular and cellular biology* **21**, 1249-1259, doi:10.1128/mcb.21.4.1249-1259.2001 (2001).

139 Puthalakath, H. *et al.* ER stress triggers apoptosis by activating BH3-only protein Bim. *Cell* **129**, 1337-1349, doi:10.1016/j.cell.2007.04.027 (2007).

140 Rutkowski, D. T. & Kaufman, R. J. A trip to the ER: coping with stress. *Trends in cell biology* **14**, 20-28 (2004).

141 Healy, S. J., Gorman, A. M., Mousavi-Shafaei, P., Gupta, S. & Samali, A. Targeting the endoplasmic reticulum-stress response as an anticancer strategy. *European journal of pharmacology* **625**, 234-246, doi:10.1016/j.ejphar.2009.06.064 (2009).

142 Hsiao, J. R. *et al.* Endoplasmic reticulum stress triggers XBP-1-mediated up-regulation of an EBV oncoprotein in nasopharyngeal carcinoma. *Cancer research* **69**, 4461-4467, doi:10.1158/0008-5472.can-09-0277 (2009).

143 Wang, G., Yang, Z. Q. & Zhang, K. Endoplasmic reticulum stress response in cancer: molecular mechanism and therapeutic potential. *American journal of translational research* **2**, 65-74 (2010).

144 Boelens, J., Lust, S., Offner, F., Bracke, M. E. & Vanhoecke, B. W. Review. The endoplasmic reticulum: a target for new anticancer drugs. *In vivo (Athens, Greece)* **21**, 215-226 (2007).

145 Ciechanover, A. The ubiquitin-proteasome proteolytic pathway. *Cell* **79**, 13-21 (1994).

146 Blagosklonny, M. V., Wu, G. S., Omura, S. & el-Deiry, W. S. Proteasome-dependent regulation of p21WAF1/CIP1 expression. *Biochemical and biophysical research communications* **227**, 564-569, doi:10.1006/bbrc.1996.1546 (1996).

147 Li, B. & Dou, Q. P. Bax degradation by the ubiquitin/proteasome-dependent pathway: involvement in tumor survival and progression. *Proceedings of the National Academy of Sciences of the United States of America* **97**, 3850-3855, doi:10.1073/pnas.070047997 (2000).

148 Breitschopf, K., Zeiher, A. M. & Dimmeler, S. Ubiquitin-mediated degradation of the proapoptotic active form of bid. A functional consequence on apoptosis induction. *The Journal of biological chemistry* **275**, 21648-21652, doi:10.1074/jbc.M001083200 (2000).

149 Rock, K. L. *et al.* Inhibitors of the proteasome block the degradation of most cell proteins and the generation of peptides presented on MHC class I molecules. *Cell* **78**, 761-771 (1994).

150 Groll, M. *et al.* The catalytic sites of 20S proteasomes and their role in subunit maturation: a mutational and crystallographic study. *Proceedings of the National Academy of Sciences of the United States of America* **96**, 10976-10983 (1999).

151 Adams, J. The proteasome: structure, function, and role in the cell. *Cancer treatment reviews* **29 Suppl 1**, 3-9 (2003).

152 Tsai, B., Ye, Y. & Rapoport, T. A. Retro-translocation of proteins from the endoplasmic reticulum into the cytosol. *Nature reviews. Molecular cell biology* **3**, 246-255, doi:10.1038/nrm780 (2002).

153 Obeng, E. A. *et al.* Proteasome inhibitors induce a terminal unfolded protein response in multiple myeloma cells. *Blood* **107**, 4907-4916, doi:10.1182/blood-2005-08-3531 (2006).

154 Masdehors, P. *et al.* Increased sensitivity of CLL-derived lymphocytes to apoptotic death activation by the proteasome-specific inhibitor lactacystin. *British journal of haematology* **105**, 752-757 (1999).

155 Drexler, H. C., Risau, W. & Konerding, M. A. Inhibition of proteasome function induces programmed cell death in proliferating endothelial cells. *FASEB journal : official publication of the Federation of American Societies for Experimental Biology* **14**, 65-77 (2000).

156 Schenkein, D. Proteasome inhibitors in the treatment of B-cell malignancies. *Clinical lymphoma* **3**, 49-55 (2002).

157 Adams, J. *et al.* Proteasome inhibitors: a novel class of potent and effective antitumor agents. *Cancer research* **59**, 2615-2622 (1999).

158 Kisselev, A. F. & Goldberg, A. L. Proteasome inhibitors: from research tools to drug candidates. *Chemistry & biology* **8**, 739-758 (2001).

159 Almond, J. B. & Cohen, G. M. The proteasome: a novel target for cancer chemotherapy. *Leukemia* **16**, 433-443, doi:10.1038/sj.leu.2402417 (2002).

160 Groll, M., Berkers, C. R., Ploegh, H. L. & Ovaa, H. Crystal structure of the boronic acid-based proteasome inhibitor bortezomib in complex with the yeast 20S proteasome. *Structure (London, England : 1993)* **14**, 451-456, doi:10.1016/j.str.2005.11.019 (2006).

161 Kane, R. C., Bross, P. F., Farrell, A. T. & Pazdur, R. Velcade: U.S. FDA approval for the treatment of multiple myeloma progressing on prior therapy. *The oncologist* **8**, 508-513 (2003).

162 Kane, R. C. *et al.* Bortezomib for the treatment of mantle cell lymphoma. *Clinical cancer research : an official journal of the American Association for Cancer Research* **13**, 5291-5294, doi:10.1158/1078-0432.ccr-07-0871 (2007).

163 Kane, R. C., Farrell, A. T., Sridhara, R. & Pazdur, R. United States Food and Drug Administration approval summary: bortezomib for the treatment of progressive multiple myeloma after one prior therapy. *Clinical cancer research : an official journal of the American Association for Cancer Research* **12**, 2955-2960, doi:10.1158/1078-0432.ccr-06-0170 (2006).

164 Jagannath, S. *et al.* Bortezomib therapy alone and in combination with dexamethasone for previously untreated symptomatic multiple myeloma. *British journal of haematology* **129**, 776-783, doi:10.1111/j.1365-2141.2005.05540.x (2005).

165 Oakervee, H. E. *et al.* PAD combination therapy (PS-341/bortezomib, doxorubicin and dexamethasone) for previously untreated patients with multiple myeloma. *British journal of haematology* **129**, 755-762, doi:10.1111/j.1365-2141.2005.05519.x (2005).

166 Adams, J. Preclinical and clinical evaluation of proteasome inhibitor PS-341 for the treatment of cancer. *Current opinion in chemical biology* **6**, 493-500 (2002).

167 Kondagunta, G. V. *et al.* Phase II trial of bortezomib for patients with advanced renal cell carcinoma. *Journal of clinical oncology : official*

journal of the American Society of Clinical Oncology **22**, 3720-3725, doi:10.1200/jco.2004.10.155 (2004).

168 Richardson, P. G. *et al.* Bortezomib or high-dose dexamethasone for relapsed multiple myeloma. *The New England journal of medicine* **352**, 2487-2498, doi:10.1056/NEJMoa043445 (2005).

169 Shah, S. A. *et al.* 26S proteasome inhibition induces apoptosis and limits growth of human pancreatic cancer. *Journal of cellular biochemistry* **82**, 110-122 (2001).

170 Bae, S. H. *et al.* Effects of the proteasome inhibitor bortezomib alone and in combination with chemotherapeutic agents in gastric cancer cell lines. *Oncology reports* **19**, 1027-1032 (2008).

171 Landowski, T. H., Megli, C. J., Nullmeyer, K. D., Lynch, R. M. & Dorr, R. T. Mitochondrial-mediated disregulation of Ca2+ is a critical determinant of Velcade (PS-341/bortezomib) cytotoxicity in myeloma cell lines. *Cancer research* **65**, 3828-3836, doi:10.1158/0008-5472.can-04-3684 (2005).

172 Gu, H., Chen, X., Gao, G. & Dong, H. Caspase-2 functions upstream of mitochondria in endoplasmic reticulum stress-induced apoptosis by bortezomib in human myeloma cells. *Molecular cancer therapeutics* **7**, 2298-2307, doi:10.1158/1535-7163.mct-08-0186 (2008).

173 Adams, J. The development of proteasome inhibitors as anticancer drugs. *Cancer cell* **5**, 417-421 (2004).

174 Cusack, J. C., Jr. *et al.* Enhanced chemosensitivity to CPT-11 with proteasome inhibitor PS-341: implications for systemic nuclear factor-kappaB inhibition. *Cancer research* **61**, 3535-3540 (2001).

175 Mitsiades, N. *et al.* Molecular sequelae of proteasome inhibition in human multiple myeloma cells. *Proceedings of the National Academy of Sciences of the United States of America* **99**, 14374-14379, doi:10.1073/pnas.202445099 (2002).

176 Meister, S. *et al.* Extensive immunoglobulin production sensitizes myeloma cells for proteasome inhibition. *Cancer research* **67**, 1783-1792, doi:10.1158/0008-5472.can-06-2258 (2007).

177 Qin, J. Z. *et al.* Proteasome inhibitors trigger NOXA-mediated apoptosis in melanoma and myeloma cells. *Cancer research* **65**, 6282-6293, doi:10.1158/0008-5472.can-05-0676 (2005).

178 Befani, C. D. *et al.* Bortezomib represses HIF-1alpha protein expression and nuclear accumulation by inhibiting both PI3K/Akt/TOR and MAPK pathways in prostate cancer cells. *Journal of molecular medicine (Berlin, Germany)* **90**, 45-54, doi:10.1007/s00109-011-0805-8 (2012).

179 Haynes, R. K. *et al.* Highly antimalaria-active artemisinin derivatives: biological activity does not correlate with chemical reactivity. *Angewandte Chemie (International ed. in English)* **43**, 1381-1385, doi:10.1002/anie.200352343 (2004).

180 Alcantara, D. D. *et al.* In vitro evaluation of the cytotoxic and genotoxic effects of artemether, an antimalarial drug, in a gastric cancer cell line (PG100). *Journal of applied toxicology : JAT* **33**, 151-156, doi:10.1002/jat.1734 (2013).

181 Han, S. U. *et al.* Loss of the Smad3 expression increases susceptibility to tumorigenicity in human gastric cancer. *Oncogene* **23**, 1333-1341, doi:10.1038/sj.onc.1207259 (2004).

182 Han, S. U. *et al.* CEACAM5 and CEACAM6 are major target genes for Smad3-mediated TGF-beta signaling. *Oncogene* **27**, 675-683, doi:10.1038/sj.onc.1210686 (2008).

183 Kang, S. H. *et al.* Rapid induction of p21WAF1 but delayed down-regulation of Cdc25A in the TGF-beta-induced cell cycle arrest of gastric carcinoma cells. *British journal of cancer* **80**, 1144-1149, doi:10.1038/sj.bjc.6690478 (1999).

184 Levy, L. *et al.* Arkadia activates Smad3/Smad4-dependent transcription by triggering signal-induced SnoN degradation. *Molecular and cellular biology* **27**, 6068-6083, doi:10.1128/mcb.00664-07 (2007).

185 Ku, J. L. & Park, J. G. Biology of SNU cell lines. *Cancer research and treatment : official journal of Korean Cancer Association* **37**, 1-19, doi:10.4143/crt.2005.37.1.1 (2005).

186 Luo, K. Ski and SnoN: negative regulators of TGF-beta signaling. *Current opinion in genetics & development* **14**, 65-70, doi:10.1016/j.gde.2003.11.003 (2004).

187 Ng, A. P. *et al.* Therapeutic targeting of nuclear receptor corepressor misfolding in acute promyelocytic leukemia cells with genistein. *Molecular cancer therapeutics* **6**, 2240-2248, doi:10.1158/1535-7163.mct-06-0705 (2007).

188 Ng, A. P., Chng, W. J. & Khan, M. Curcumin sensitizes acute promyelocytic leukemia cells to unfolded protein response-induced apoptosis by blocking the loss of misfolded N-CoR protein. *Molecular cancer research : MCR* **9**, 878-888, doi:10.1158/1541-7786.mcr-10-0545 (2011).

189 Chauhan, D., Hideshima, T., Mitsiades, C., Richardson, P. & Anderson, K. C. Proteasome inhibitor therapy in multiple myeloma. *Molecular cancer therapeutics* **4**, 686-692, doi:10.1158/1535-7163.mct-04-0338 (2005).

190 Hoberg, J. E., Yeung, F. & Mayo, M. W. SMRT derepression by the IkappaB kinase alpha: a prerequisite to NF-kappaB transcription and survival. *Molecular cell* **16**, 245-255, doi:10.1016/j.molcel.2004.10.010 (2004).

191 Hong, S. H. & Privalsky, M. L. The SMRT corepressor is regulated by a MEK-1 kinase pathway: inhibition of corepressor function is associated with SMRT phosphorylation and nuclear export. *Molecular and cellular biology* **20**, 6612-6625 (2000).

192 Yang, W., Tiffany-Castiglioni, E., Koh, H. C. & Son, I. H. Paraquat activates the IRE1/ASK1/JNK cascade associated with apoptosis in human neuroblastoma SH-SY5Y cells. *Toxicology letters* **191**, 203-210, doi:10.1016/j.toxlet.2009.08.024 (2009).

193 Singh, N. P. & Verma, K. B. Case report of a laryngeal squamous cell carcinoma treated with artesunate. *Archive of Oncology* **10**, 279-280 (2002).

194 Miyazono, K., Suzuki, H. & Imamura, T. Regulation of TGF-beta signaling and its roles in progression of tumors. *Cancer Sci* **94**, 230-234 (2003).

195 Mishra, L., Derynck, R. & Mishra, B. Transforming growth factor-beta signaling in stem cells and cancer. *Science (New York, N.Y.)* **310**, 68-71, doi:10.1126/science.1118389 (2005).

196 Nin, D. S. *et al.* Role of misfolded N-CoR mediated transcriptional deregulation of Flt3 in acute monocytic leukemia (AML)-M5 subtype. *PloS one* **7**, e34501, doi:10.1371/journal.pone.0034501 (2012).

197 Ali, A. B., Nin, D. S., Tam, J. & Khan, M. Role of chaperone mediated autophagy (CMA) in the degradation of misfolded N-CoR protein in non-small cell lung cancer (NSCLC) cells. *PloS one* **6**, e25268, doi:10.1371/journal.pone.0025268 (2011).